KINETIC ANALYSES ON TWO TRANSLATIONAL GTPASES;

LEPA AND EF-TU

Evelina Ines De Laurentiis
B.Sc. University of Lethbridge, 2007
M.Sc. University of Lethbridge, 2010

A Thesis
Submitted to the School of Graduate Studies
of the University of Lethbridge
in Partial Fulfillment of the
Requirements for the Degree

DOCTOR OF PHILOSOPHY

IN

BIOMOLECULAR SCIENCE

Department of Chemistry and Biochemistry
University of Lethbridge
LETHBRIDGE, ALBERTA, CANADA

Abstract

Protein synthesis is an essential process for all living organisms and is an effective major target for current antibiotics. Elongation factor Tu (EF-Tu) is a highly conserved and essential protein that functions during protein synthesis. EF-Ts interacts with EF-Tu to help maintain a functionally active state of EF-Tu required for cell growth. Although EF-Ts is essential for *Escherichia coli*, its sequence is poorly conserved. LepA is a highly conserved protein within bacteria and has a similar structure to EF-Tu. In spite of this, LepA has been shown to be non-essential under ideal conditions and the function of LepA still remains elusive. An analysis on the structurally unique aspects of LepA, EF-Tu and EF-Ts was performed here in an effort to gain an understanding on the functions of these proteins. This knowledge, in combination with their unique structural components will provide important tools in developing new and effective antibiotics.

Acknowledgements

Thank you to my supervisor Dr. Hans-Joachim Wieden for having me as a student and allowing me to learn something new every day.

I would like to thank my committee members Dr. Ute Kothe-Wieden, Dr. Marc Roussel and Dr. James Thomas for taking the time to read and critically analyze this thesis.

Thanks to all the members in the lab over the years especially Fan Mo, Kate Greeff, Valerie Hurdle, Luc Roberts and Dominic Mudiayi. For the friendships and memories (Christmer) that will not be forgotten.

Special thanks to Susan Hill who supplied me with paper towels and laughs.

Thank you to my mom, dad and sister for helping me when I needed it and supporting me all the time.

Thank you to Evan Mercier who supported me every day and helped me get through some bad ones. I am glad you decided to do graduate studies here in Lethbridge because this would not have been as much fun without you here.

Table of Contents

ABSTRACT **III**

ACKNOWLEDGEMENTS **IV**

TABLE OF CONTENTS **V**

LIST OF TABLES **IX**

LIST OF FIGURES **X**

LIST OF BUFFERS **XI**

LIST OF ABBREVIATIONS **XII**

CHAPTER 1 **1**

TRANSLATION **1**
1.1a The Bacterial Ribosome 1
1.1b GTPases 4
1.1c Protein Synthesis 6
1.1d Translation Elongation in Bacteria 8
1.1e Objectives 15

CHAPTER 2. **20**

IDENTIFICATION OF TWO STRUCTURAL ELEMENTS IN LEPA IMPORTANT FOR ITS RIBOSOME STIMULATED GTPASE ACTIVITY. **20**

2.1 INTRODUCTION **20**
2.1a Identification and Initial Characterisation of LepA 20
2.1b Analysis of LepA Under Stress Conditions 21
2.1c Histidine as a Catalytic Residue 22
2.1d Structural Analysis of LepA 23
2.1e LepA Interaction with the Ribosome 26
2.1f Cellular Function of LepA 27

2.2 MATERIALS AND METHODS 29
2.2a Molecular Biology 29
2.2b Mutagenesis 30
2.2c Expression and Purification of LepA Proteins 31
2.2d Purification of E. coli Ribosomes 33
2.2e Fluorescence Titrations 35
2.2f Stopped-Flow Fluorescence 36
2.2g LepA Proteins Binding to the Ribosome 38
2.2h GTP Hydrolysis 38

2.3 RESULTS 41
2.3a Structure Prediction of the C-Terminal Domain of LepA 41
2.3b LepA Interaction with Guanine Nucleotides (GDP/GDPNP/GTP). 42
2.3c LepA Interaction with the Ribosome 50
2.3d GTPase Activity of LepA 53
2.3e Catalytic Histidine in LepA 56

2.4 DISCUSSION 57
2.4a LepA and Guanine Nucleotides 57
2.4b The C-Terminal Domain of LepA is Involved in GTPase Activation on the Ribosome 60
2.4c H81 is the Catalytic Histidine in LepA 64

2.5 FUTURE DIRECTIONS 65

CHAPTER 3 68

A TAIL OF TWO PROTEINS; THE C-TERMINAL MODULE OF EF-TS ALTERS NUCLEOTIDE EXCHANGE IN EF-TU. 68

3.1 INTRODUCTION 68
3.1a The Function of EF-Tu 68
3.1b Nucleotide Exchange in EF-Tu 73
3.1c Divergence of EF-Ts 75

3.2 MATERIALS AND METHODS 76
3.2a Molecular Biology 76
3.2b Mutagenesis 77
3.2c Protein Expression and Purification 79
3.2d Preparation of EF-Tu•mant-GDP, EF-Tu•mant-GTP 82

3.2e Rapid Kinetic Measurements 82
3.2f Sequence alignment 85

3.3 RESULTS 87
3.3a Interaction of GDP/GTP with EF-Tu (k_1, k_{-1}, k_5, k_{-5}) 88
3.3b Interaction of EF-Tu with EF-Ts in the presence of GTP 90
3.3c Interaction of EF-Tu with EF-Ts in the presence of GDP 93
3.3d Interaction of EF-Tu with EF-Ts (k_2, k_{-2}) 95
3.3e Interaction of EF-Tu with EF-Ts Variants 98

3.4 DISCUSSION 103
3.4a Guanine Nucleotide Exchange in E. coli and P. aeruginosa EF-Tu. 103
3.4b Variation in the C-terminal module of EF-Ts 105

3.5 FUTURE DIRECTIONS 111

CHAPTER 4 113

CONSTRUCTION OF A FULLY ACTIVE CYS-LESS ELONGATION FACTOR TU: FUNCTIONAL ROLE OF CONSERVED CYSTEINE 81. 113

4.1 INTRODUCTION 113

4.2 MATERIALS AND METHODS 118
4.2a Cloning and Site-Directed Mutagenesis 118
4.2b Protein Expression and Purification 119
4.2c Preparation of Nucleotide-Free EF-Tu 120
4.2d Preparation of EF-Tu•mant-GDP, EF-Tu•mant-GTP 120
4.2e Rapid Kinetic Measurements 120
4.2f Components of the Translation Machinery 122
4.2g Hydrolysis Protection Assay 122
4.2h Dipeptide formation 123

4.3 RESULTS 124
4.3a Evolution-Based Construction of a Cysteine-Free Variant of EF-Tu 124
4.3b Interaction with Guanine Nucleotides (GDP/GTP) 125
4.3c EF-Ts Stimulated Guanine Nucleotide Dissociation 128
4.3d Interaction of aa-tRNA with EF-Tu 129
4.3e EF-Tu Dependent Dipeptide Formation 131

4.4 DISCUSSION **133**
4.4a Evolution-Based Design and Previous Studies 133
4.4b Functional Role of Cysteine 81 136

4.5 FUTURE DIRECTIONS **139**

CHAPTER 5 CONCLUSION **140**

REFERENCES **142**

APPENDIX **150**

A.1 LEPA **150**
A.1a Cysteine residues in LepA 151
A.1b Alignment of LepA Primary Sequence within Bacteria 152

A.2 EF-TU AND EF-TS **158**
A.2a Alignment of EF-Ts Primary Sequence within Bacteria 159
A.2b Alignment of EF-Tu Primary Sequence within Bacteria 165

A.3 FLUORESCENT LABELLING OF EF-TU **171**
A.3a Fluorescently Labelling EF-Tu Containing a Single Cysteine (L264C) 171
A.3b Intramolecular Hetero-Fluorescent Labelling of EF-Tu Containing Two Cysteine Residues 172
A.3c Intramolecular Hetero-Fluorescent Labelling of EF-Tu Containing Two Cysteine Residues using a “Shotgun” Method 174
A.3d Absorbance and Fluorescence Emission Analysis 175

List of Tables

Table 2.1.	Dissociation Constants (K_D) Governing the Interaction Between LepA Variants and Mant-GDP.	45
Table 2.2.	Dissociation Constants (K_D) Governing the Interaction Between LepA Variants and Mant-GDPNP.	45
Table 2.3.	Rate of Mant-Guanine Nucleotide Dissociation from LepA Variants.	47
Table 2.4.	Rate of Association Between LepA Variants and Mant-Guanine Nucleotides.	50
Table 2.5.	Dissociation Constants (K_D) Between LepA Variants and Mant-GDP/GTP Determined by Pre-Steady State Kinetics.	50
Table 2.6.	Intrinsic GTPase Activity of LepA Variants.	54
Table 2.7.	70S Stimulated GTPase Activity of LepA Variants.	55
Table 3.1.	Kinetic Parameters Governing the Nucleotide Interaction with EF-Tu.	89
Table 3.2.	EF-Ts Induced Dissociation of GDP and GTP from EF-Tu	96
Table 3.3.	Determined Rate Constants for the Kinetic Mechanism of Nucleotide Exchange in EF-$Tu_{E.c.}$.	97
Table 3.4	Determined Rate Constants for the Interaction between EF-Tu, EF-Ts Variants and Guanine Nucleotides.	102
Table 4.1.	Kinetic Constants Governing the Interactions Between EF-Tu and Guanine Nucleotides.	127
Table 4.2.	EF-Ts Induced Dissociation of mant-Nucleotides from EF-Tu.	129
Table 4.3.	EF-Tu Mediated Protection of Phe-$tRNA^{Phe}$ against Spontaneous Hydrolysis.	131
Table A.1.	Identity of Cysteine Composition within Bacterial LepA.	150
Table A.2.	Accession Numbers and Organisms used to Align LepA Primary Sequence.	151
Table A.3.	Accession Numbers and Organisms used to Align EF-Ts Primary Sequence.	158-159
Table A.4.	Accession Numbers and Organisms used to Align EF-Tu Primary Sequence.	164-165
Table A.5.	Protein Yield Following Fluorescently Labelling of a Single Cysteine Containing EF-Tu.	171
Table A.6.	Protein Yield Following Intramolecular Double-Labelling an EF-Tu Containing Two Cysteine Residues.	173
Table A.7.	Protein Yield Following Intramolecular Double-Labelling an EF-Tu Containing Two Cysteine Residues via “Shotgun” Method.	174

List of Figures

Figure 1.1.	The bacterial ribosome with three tRNA binding sites.	2
Figure 1.2.	General cycle of a GTPase.	5
Figure 1.3.	The cyclic process of translation in bacteria.	8
Figure 1.4.	Structure of tRNA.	10
Figure 1.5.	EF-Tu-dependent A site binding.	11
Figure 1.6.	The functional cycle of EF-Tu.	12
Figure 1.7.	Translocation in the presence of EF-G.	14
Figure 2.1.	Structural comparison of LepA and EF-G.	24
Figure 2.2.	Structure prediction of the CTD of LepA.	41
Figure 2.3.	CTD truncation variants constructed.	42
Figure 2.4.	Equilibrium fluorescence titration of LepA with guanine nucleotides.	44
Figure 2.5.	Dissociation of guanine nucleotides from LepA.	47
Figure 2.6.	Association kinetics for guanine nucleotides and LepA.	49
Figure 2.7.	Immunodetection of LepA bound to the ribosome following ultracentrifugation.	52
Figure 2.8.	Michaelis-Menten titration of the intrinsic GTPase activity of LepA.	54
Figure 2.9.	Michaelis-Menten titration of the ribosome stimulated GTPase activity of LepA.	55
Figure 2.10.	Model of LepA interacting with guanine nucleotides.	59
Figure 3.1.	Structures of EF-Tu bound to GTP and GDP.	69
Figure 3.2.	Structure of EF-Tu bound to aa-tRNA.	70
Figure 3.3.	Structure of EF-Tu bound to EF-Ts.	72
Figure 3.4.	Structures of the eEF1A•eEF1Bα and the $EF\text{-}Tu_{mt}$•$EF\text{-}Ts_{mt}$ complex.	74
Figure 3.5.	Kinetic mechanism of nucleotide exchange in EF-Tu catalyzed by EF-Ts	87
Figure 3.6.	Dissociation of mant-GTP and mant-GDP from EF-Tu.	88
Figure 3.7.	Association of mant-GDP and mant-GTP to EF-Tu.	90
Figure 3.8.	Interaction of EF-Tu with GTP and EF-Ts.	92
Figure 3.9.	Interaction of EF-Tu with GDP and EF-Ts.	95
Figure 3.10.	Interaction of EF-Tu with EF-Ts (k_2).	96
Figure 3.11.	EF-Ts variants constructed.	99
Figure 3.12.	Catalyzed dissociation of guanine nucleotides from EF-Tu with EF-Ts variants.	101
Figure 3.13.	Variance in EF-Tu•EF-Ts Contacts.	108
Figure 4.1.	Overview of cysteine residues present in the EF-Tu•GTP complex.	116
Figure 4.2.	Determination of nucleotide association rate constants.	126
Figure 4.3.	Determination of nucleotide dissociation rate constants.	128
Figure 4.4.	EF-Tu•GTP•aa-tRNA ternary complex stability.	130
Figure 4.5.	Peptide bond formation.	132
Figure A.1.	LepA Protein Preparations.	149
Figure A.2.	Overview of cysteine residues in *E. coli* LepA.	150
Figure A.3.	Primary sequence alignment of LepA within bacteria.	152-155
Figure A.4.	Phylogenetic Tree of bacterial LepA aligned above.	156
Figure A.5.	EF-Tu preparations.	157
Figure A.6.	EF-Ts preparations.	157
Figure A.7.	Primary sequence alignment of EF-Ts within bacteria.	160-162
Figure A.8.	Phylogenetic Tree of bacterial EF-Ts species aligned above.	163
Figure A.9.	Primary sequence alignment of EF-Tu within bacteria.	166-168
Figure A.10.	Phylogenetic Tree of bacterial EF-Tu species aligned above.	169
Figure A.11.	Structures of thiol reactive fluorescent dyes.	170
Figure A.12.	Fluorescence emission scans of single labelled EF-Tu.	175
Figure A.13.	Emission scans of EF-Tu fluorescently labelled with two different dyes.	175
Figure A.14.	EF-Tu labelled with F5M and RRM.	176

List of Buffers

2.1: 50 mM Tris-Cl pH 7.5 (20 °C), 70 mM NH_4Cl, 30 mM KCl and 7 mM $MgCl_2$
2.2: 50 mM Tris-Cl pH 8.0 (4 °C), 60 mM NH_4Cl, 7 mM $MgCl_2$, 300 mM KCl, 7 mM BME, 1 mM PMSF, 10 mM imidazole and 15% glycerol
2.3: Buffer 2.2, 20 mM imidazole
2.4: Buffer 2.2, 250 mM imidazole
2.5: 50 mM Tris-Cl pH 7.5 (4°C), 70 mM NH_4Cl, 300 mM KCl, 7 mM $MgCl_2$ and 15% glycerol
2.6: 20 mM Tris-Cl pH 7.6 (4°C), 100 mM NH_4Cl, 10.5 mM $MgCl_2$, 0.5 mM EDTA and 3 mM BME
2.7: 20 mM Tris-Cl pH 7.6 (4°C), 500 mM NH_4Cl, 10.5 $MgCl_2$, 0.5 mM EDTA, 1.1 M sucrose, 3 mM BME
2.8: 20 mM Tris-Cl pH 7.6 (4°C), 500 mM NH_4Cl, 10.5 mM $MgCl_2$, 0.5 mM EDTA and 7 mM BME
2.9: 20 mM Tris-Cl pH 7.6 (4°C), 60 mM NH_4Cl, 5.25 mM Mg acetate, 0.25 mM EDTA, and 3 mM BME
2.10: 20 mM Tris-Cl pH 7.6 (4°C), 50 mM NH_4Cl and 5 mM $MgCl_2$
2.11: 20 mM Tris-HCl pH7.6 (4°C), 60 mM NH_4Cl, 5.25 mM Mg acetate, 0.25 mM EDTA, 10% sucrose, 3 mM BME
2.12: 1 M $HClO_4$, 3 mM potassium phosphate
3.1: Buffer 2.1
3.2: 50 mM Tris-Cl pH 8.0 (4°C), 60 mM NH_4Cl, 7 mM $MgCl_2$, 300 mM KCl, 7 mM BME, 1 mM PMSF, 10 mM imidazole, 15% glycerol and 50 µM GDP
3.3: Buffer 3.2, 20 mM imidazole
3.4: Buffer 3.2, 250 mM imidazole
3.5: 25 mM Tris-Cl pH 7.5 (4°C), 50 mM NH_4Cl, 10 mM $MgCl_2$, 0.1% PMSF, and 50 µM GDP
3.6: 20 mM Tris-Cl pH 8.0 (4°C), 50 mM NH_4Cl, 0.1 mM EDTA and 50 µM GDP
3.7: 20 mM Tris-Cl pH 8.0 (4°C), 50 mM NH_4Cl, 0.1 mM EDTA, 60 mM DTT, 400 mM KCl
3.8: 20 mM Tris-Cl pH 8.0 (4°C), 50 mM NH_4Cl, 0.1 mM EDTA, 400 mM KCl, 50 µM GDP
3.9: 25 mM Tris-Cl, pH 7.5 (20°C), 50 mM NH_4Cl, 10 mM EDTA
3.10: 25 mM Tris-Cl pH 7.5 (4°C), 50 mM NH_4Cl
4.1: Buffer 2.1/3.1
4.2: 25 mM Tris-acetate (OAc) pH 7.5 (20°C), 8 mM $Mg(OAc)_2$, 3 mM ATP, 100 mM NH_4OAc, 30 mM KOAc, 1 mM DTT
4.3: 20 mM NH_4OAc pH 5, 10 mM $Mg(OAc)_2$, 400 mM NaCl
4.4: Buffer 4.3, 30% ethanol
4.5: 50 mM Tris-Cl pH 7.5 (4°C), 70 mM NH_4Cl, 30 mM KCl, 10 mM $MgCl_2$
4.7: 0.1% Trifluoroacetic acid
4.8: 0.1% TFA, 65% Acetonitrile
A.1: 25 mM Tris-Cl pH 7.5 (4 °C), 7 mM $MgCl_2$, 30 mM KCl, 20% glycerol
A.2: 25 mM Tris-Cl pH 7.5 (4 °C), 7 mM $MgCl_2$, 30 mM KCl
A.3: Buffer A.1, 100 mM DTT

List of Abbreviations

1,5-IAEDANS	5-((((2-Iodoacetyl)amino)ethyl)amino)Naphthalene-1-Sulfonic Acid
apo	Free of a bound cofactor
A site	Aminoacyl-tRNA binding site
aa-tRNA	aminoacyl-transfer ribonucleic acid
BipA	Bvg-intermediate phase protein A
BME	β-mercaptoethanol
Cp	Chloroplast
CPM	7-diethylamino-3-(4'-maleimidylphenyl)-4-methylcoumarin
Cryo-EM	Cryogenic electron microscopy
CTD	C-Terminal Domain
DTT	Dithiothreitol
EDTA	Ethylenediaminetetraacetic acid
EF	Elongation Factor
E site	tRNA exit site
F5M	Fluorescein-5-maleimide
FRET	Förster resonance energy transfer
GAP	GTPase activating protein
GEF	Guanine nucleotide exchange factor
GDP	Guanosine diphosphate
GDPNP	Guanosine 5′-[β,γ-imido]triphosphate
GTP	Guanosine triphosphate
Guf	GTPase of Unknown Function
IF	Initiation Factor
IPTG	Isopropyl β-D-1-thiogalactopyranoside
k_{app}	Apparent rate
k_{cat}	Catalytic constant
K_D	Dissociation constant
kDa	kilodaltons
K_M	Michaelis constant
k_{off}	Rate of dissociation
k_{on}	Rate of association
lep	Leader Peptidase
Mant	2'-/3'-O-N'-Methylanthraniloyl
mRNA	Messenger RNA
MWCO	Molecular Weight cutoff
OD_{600}	Optical Density at 600 nm
ORF	Open reading frame
PDB ID	Protein data bank identification code
PEP	Phosphoenolpyruvate
P_i	Phosphate
PK	Pyruvate Kinase
PMSF	Phenylmethanesulfonylfluoride
P site	Peptidyl-tRNA binding site
PTC	Peptidyl transferase centre
PTI	Photon Technology International
RF	Release Factor
RNA	Ribonucleic acid
RNP	Ribonucleoprotein
RRF	Ribosome recycling factor
RRM	Rhodamine Red Maleimide
SDS-PAGE	Sodium dodecyl sulfate polyacrylamide gel electrophoresis
SEC	Size exclusion chromatography
sm	single molecule
TCA	Trichloroacetic acid

TFA	Trifluoroacetic acid
TPCK	*N*-tosyl-L-phenylalanylchloromethane
Ts	Thermal stable
Tu	Thermal unstable
v_{max}	Maximum rate
X-Gal	5-bromo-4-chloro-3-indolyl-β-D-galactopyranoside

Chapter 1

Translation

The process of gene expression is the process in which genetic information is utilized towards the synthesis of a functional cellular product, such as an essential protein. In all living organisms gene expression is a highly complex and regulated process. It involves a large number of intermediate steps and many molecular interaction partners that facilitate the necessary speed and accuracy of this process. In bacteria, gene expression can be simplified into two main stages which are the processes of transcription and translation. During the process of transcription, DNA is used as a template for the synthesis of messenger RNA (mRNA). Messenger RNA is subsequently utilized during translation to direct the synthesis of proteins (1). In bacteria the transcribed mRNA is used directly as a message for protein synthesis. This process utilizes triplet nucleotide codons, encoded within the mRNA, which specify the sequence of amino acids needed to build a specific polypeptide chain.

Proteins are ubiquitous macromolecules as they are found in all domains of life and fulfill diverse roles such as cellular signalling, transporting molecules and catalyzing metabolic processes (2). As proteins are essential to all forms of life, it is not surprising that protein synthesis occurs in all domains of life.

1.1a The Bacterial Ribosome

The process of protein synthesis takes place on the ribosome, which is a ribocucleoprotein (RNP) comprised of a large and a small subunit (Figure 1.1). Each

ribosomal subunit is made up of approximately two-thirds ribosomal RNA (rRNA) and one-third protein. The ribosome encompasses 30% of the cellular mass of a bacterial cell and approximately 5% of a eukaryotic cell (3). In *Escherichia coli*, the ribosome has a mass of 2.5 MDa and a sedimentation coefficient of 70S.

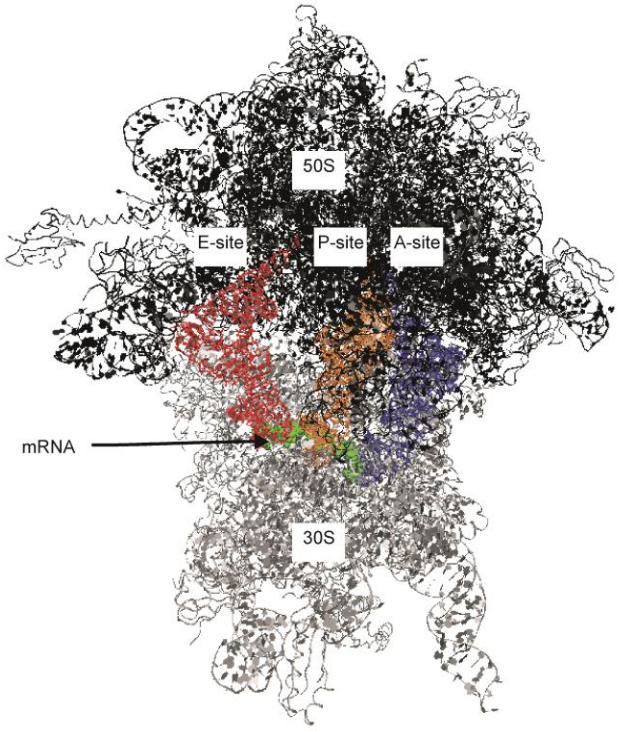

Figure 1.1. The bacterial ribosome with three tRNA binding sites occupied. Structure of the 70S ribosome from *Thermus Thermophilus* represented in ribbon, in complex with mRNA (spacefill and coloured in green), A- P- and E-site bound tRNA (shown in licorice and coloured blue, orange and red, respectively). The 50S is coloured in black and the 30S is coloured in grey. Structure was obtained by X-ray crystallography to 3.6 Å resolution (PDB ID 2WDK, 2WDL (4)).

In bacteria, the large ribosomal subunit, or the 50S subunit, contains a 2904 nucleotide 23S rRNA and a 115 nucleotide 5S rRNA and 34 (L1-L34) ribosomal proteins (5), while the small ribosomal subunit, the 30S subunit, consists of a 1542 nucleotide 16S rRNA and 21 (S1-S21) ribosomal proteins (6). The ribosome contains 3 tRNA binding sites

(Figure 1.1), the aminoacyl (A) site, the peptidyl (P) site and the exit (E) site (7), which straddle both the 50S and 30S subunits.

Prior to ribosome assembly 16S and 23S rRNA are processed by RNase III (8), RNase E, RNase G (9) and RNase T (10), to form a mature 16S and 23S rRNA. Following maturation of the 16S and 23S rRNA, all rRNA and ribosomal proteins must assemble in the correct manner to form an active ribosomal complex (11). Self-assembly has been shown to occur in the absence of co-factors *in vitro* (12). However, the conditions utilized to observe self-assembly are not physiologically relevant and the rate observed for self-assembly is too slow to sustain life. Further evidence suggests that several additional ribosomal biogenesis factors monitor the assembly of the ribosome, which are required for the fast and efficient assembly observed *in vivo*.

Numerous biochemical and structural studies on the ribosome have facilitated the overall understanding of what parts within the ribosome contribute to its overall function. Electron microscopic studies on the structure of the ribosome have been available since the 1970s; however, it was not until 1999 that high resolution X-Ray crystallographic structures of the ribosome became available. The overall structure of the small ribosomal subunit is largely determined by the 16S rRNA. There are three main domains within the 30S (5' domain, central domain and 3' major domain) which form the body, platform and head of the 30S subunit (13). The 30S subunit harbours the site of decoding (the decoding centre), which is involved in the selection of the correct aminoacylated-tRNA (aa-tRNA) corresponding to the mRNA codon presented in the A site of the translating ribosome (14). Nucleotides A1492, A1493 and G530 of the 16S rRNA interact with the codon-anticodon helix in the ribosomal A site (14). Cognate Watson-Crick base pairing results

in a short double helix which is stabilized by the conserved nucleotides A1492, A1493 and G530 (14). Stabilization of a cognate Watson-Crick base pair is critical during the decoding process, as this is utilized to discriminate cognate codon-anticodon interactions against near-cognate and non-cognate interactions.

Similar to the small ribosomal subunit, the large subunit structure is mainly determined by its large rRNA (23S rRNA). The 50S ribosomal subunit contains the peptidyl transferase centre (PTC), which catalyzes peptide-bond formation (15). In addition, the 50S subunit also contains the so called L7/L12 stalk, which has been shown to stimulate the activity of guanine nucleotide triphosphatases (GTPases) such as EF-Tu and EF-G interacting with the ribosomal A site (16,17).

1.1b GTPases

GTPases are molecular switches that function in a variety of cellular processes and are regulated by guanine nucleotide binding (Figure 1.2). When bound to GTP, these proteins are active, which means that they can efficiently interact with their downstream effectors in this state. This interaction is maintained until GTP hydrolysis occurs. Typically, the intrinsic rate of GTP hydrolysis by GTPases is slow and occurs with rates on the order of $10^{-4}s^{-1}$ (18). This slow rate of GTP hydrolysis by the GTPase is likely to maintain an active state of the protein until its function is carried out. However, GTPases which are constantly in an active state have been shown to have toxic effects on a cell (19). Therefore, GTPase activating proteins or factors (GAP/GAF) are utilized within a cell to stimulate the rate of GTP hydrolysis. For GTPases EF-G and EF-Tu, the ribosome acts as

a GAF and has been shown to stimulate the intrinsic rate of GTP hydrolysis by 10^6-fold (20). Following GTP hydrolysis, the protein is bound to GDP in an inactive state, such that it cannot interact efficiently with its downstream effector (21). GDP must dissociate from the protein before GTP can bind so that the protein can return to an active state. Guanine nucleotide exchange factors (GEFs) are utilized to catalyze the dissociation of GDP from the protein if dissociation is slower than the rate needed to regenerate an active state of the protein for further function. In this way GEFs promote the regeneration of an active GTP-bound GTPase.

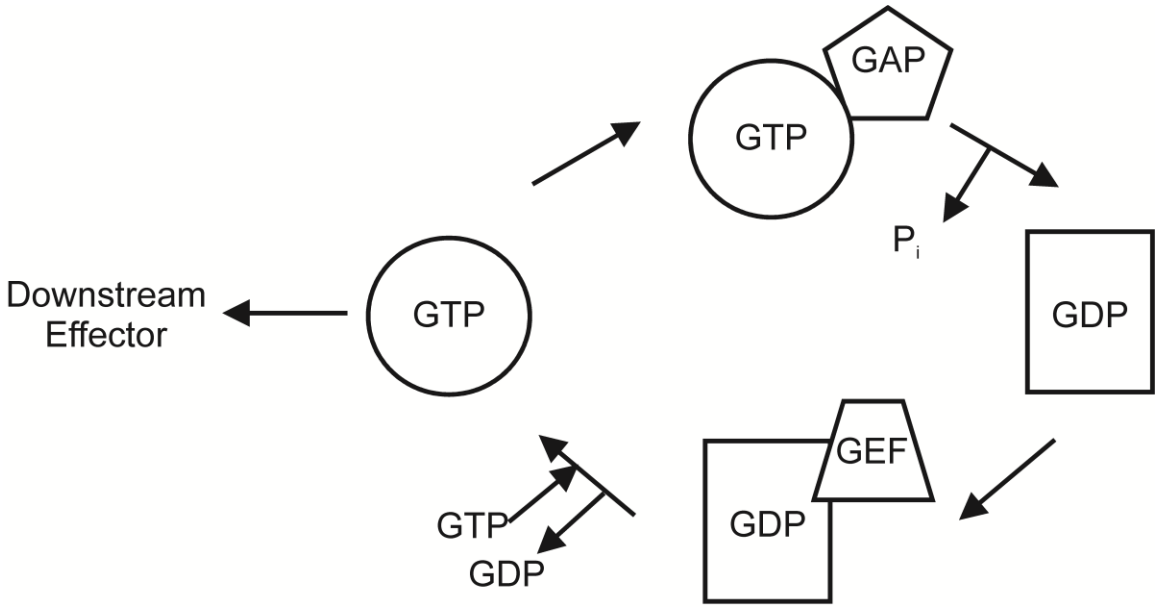

Figure 1.2. General cycle of a GTPase. A GTPase bound to GTP adopts an active state that may interact with a downstream effector for further function until GTP hydrolysis occurs. This is often stimulated by a GTPase activating protein/factor (GAP/GAF). The GTPase, now bound to GDP, is in an inactive state. GDP dissociation can be catalyzed by a guanine nucleotide exchange factor (GEF). GTP can subsequently bind and the process may continue.

1.1c Protein Synthesis

The process of mRNA directed protein synthesis is catalyzed by the ribosome and can be divided into four distinct steps, initiation, elongation, termination and recycling (Figure 1.3).

Initiation involves the assembly of a pre-initiation complex containing mRNA, as well as an initiator tRNA onto the small ribosomal subunit, followed by the subsequent association of the large subunit to form an initiation complex that can be used in the process of elongation (22). Initiation in bacteria is catalyzed by three initiation factors IF1, IF2 and IF3 (22), which promote the correct positioning of the start codon as well as the initiator tRNA. In eukaryotes and archaea the process of initiation is far more complex than in bacteria as several other initiation factors are required. In eukaryotes, proper positioning of the mRNA initiation codon in the P site of the ribosome is facilitated by initiation factors in combination with scanning of the mRNA (23). Binding of the mRNA to the small subunit in bacteria does not require initiation factors to assist in recruitment or scanning for positioning of the mRNA. Correct positioning of the mRNA in bacteria is facilitated by the interaction of the Shine-Dalgarno sequence in the mRNA with the complementary anti-Shine-Dalgarno sequence on the 16S rRNA (24). Initiator tRNA in eukaryotes is delivered to the small subunit with the help of initiation factors. Although binding of initiator tRNA in bacteria can be accelerated by the presence of initiation factors, it is not delivered to the small subunit by initiation factors (25).

Following initiation, elongation of the polypeptide chain encoded by the mRNA can occur. Elongation is the only process in translation that is universally conserved and consists of three main steps (i) decoding of the mRNA, (ii) peptide-bond formation and

(iii) translocation (26). This process is catalyzed by the universally conserved elongation factors (EF), EF-Tu, EF-Ts and EF-G in bacteria and eEF1A, eEF1Bα and eEF2 in eukaryotes (21).

Once a stop-codon is encountered in the A site of the ribosome, release factors (RF1 and RF2) in bacteria recognize and bind to the ribosome and catalyze peptide release (27). RF1 and RF3 contain a conserved GGQ motif that is essential for peptide release through positioning of the hydrolytic water (28). Although RF3 accelerates the dissociation of RF1 and RF2 from the ribosome, it is not essential in bacteria (29). Similar to bacteria, eukaryotes contain a release factor (eRF1) which recognizes termination codons (26). However, eRF1 is able to recognize all the termination codons and binds to release factor 3 (eRF3) before binding to the ribosome (30). Furthermore, unlike RF3, eRF3 is essential for peptide release (31).

Following termination the ribosome is recycled to prepare for catalysis of a new round of protein synthesis. In this process ribosome recycling factor (RRF) and EF-G catalyze the dissociation of the 70S ribosome into the 50S and 30S ribosomal subunits (32). IF3 binds to the 30S subunit still containing mRNA and tRNA and promotes their dissociation (26). With the ribosomal subunits now separated, initiation can occur once again and the process of protein synthesis can restart. Interestingly, no RRF homologue is found in eukaryotes, and this process is poorly understood in eukaryotes. Recently, it has been shown that ABCE1 in eukaryotes can promote ribosome recycling (33). Although recycling in eukaryotes is not well understood, it is clear that it is different than the prokaryote process.

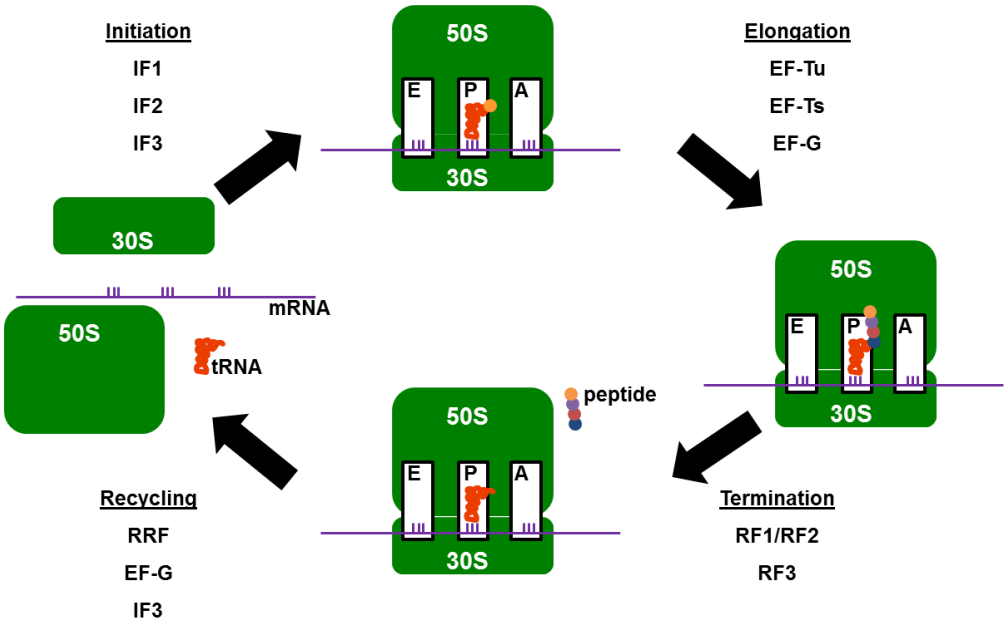

Figure 1.3. The cyclic process of translation in bacteria. Protein synthesis in bacteria occurs by four main steps, initiation, elongation, termination and recycling. The factors involved in each process, as well as a snapshot of the end product for each step is represented**.**

1.1d Translation Elongation in Bacteria

The process of elongation can be broken down into three main steps, decoding of the mRNA, peptide-bond formation and translocation (26).

Decoding of the mRNA codon occurs by the cognate aa-tRNA (1). Transfer RNA (tRNA) is an adaptor molecule that bridges the gap between the mRNA and the growing polypeptide chain. Through mRNA codon – tRNA anticodon interactions, aa-tRNA is able to recognize mRNA codons that correspond to a specific amino acid attached to the tRNA (1). In turn, this amino acid can be utilized in building a polypeptide chain on the ribosome (34). There are approximately 30 different tRNAs within prokaryotes (35) which are amino acid specific and have been studied extensively over the last 50 years in terms of processing, dynamics and structure.

Each tRNA contains between 75 to 90 RNA nucleotides and forms a cloverleaf secondary structure (36) (Figure 1.4). While diverse in sequence, all tRNAs share a similar secondary and tertiary structure (Figure 1.4). All tRNAs consist of a phosphorylated 5' end, a dihydro uracil loop (D-loop) which contains a modified dihydrouridine base, an anticodon loop that can base pair with the mRNA triplet codon, a variable loop which differs in length between tRNAs, a TΨC loop (T-loop) that contains a pseudouridine and an acceptor stem comprised of the 3' end for amino acid attachment (36). The elements of the secondary structure fold into an L-shaped tertiary conformation (36), where the anticodon loop and the acceptor stem are at opposite ends and approximately 76 Å apart. The D and T-loops of the tRNA form the elbow region in the tertiary structure (Figure 1.4). This L-shape formed by all tRNAs facilitates the contacts made during protein synthesis. For example, the anticodon loop of the tRNA can interact with the mRNA, while the amino acid on the acceptor stem can make contacts near the polypeptide chain.

Even though all aa-tRNAs are very similar with respect to their general structure, each tRNA is charged with a specific amino acid. This specificity is critical for maintaining the genetic code. To help maintain specificity there are discriminator bases within tRNAs which are utilized in distinguishing them from each other during aminoacylation (37). Aa-tRNA synthetases use a double-sieve mechanism to help prevent errors which may propagate into the synthesis of errant proteins. The strategy of the double-sieve mechanism is to combine the use of a restricted binding pocket for the specific amino acid with proofreading. Following the aminoacylation of tRNA, EF-Tu binds to the formed aa-tRNA and facilitates its delivery to the translating ribosome (38).

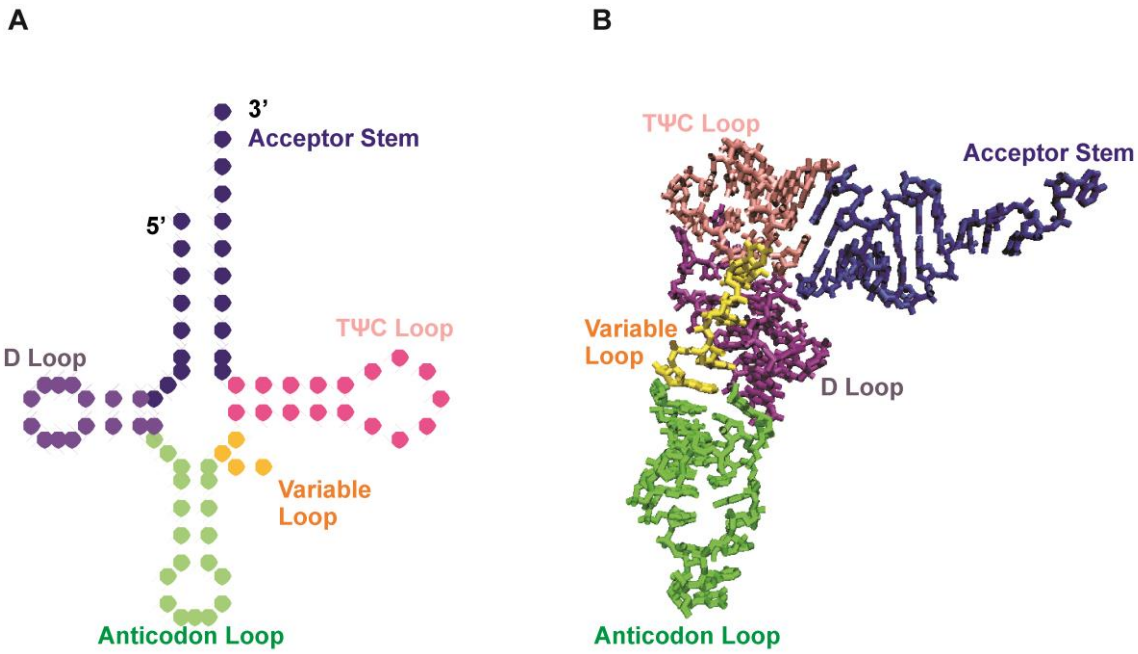

Figure 1.4. Structure of tRNA. (A) Secondary structure of the cloverleaf tRNA showing the acceptor stem coloured in blue, the TΨC loop coloured in pink, the anticodon loop coloured in green, the D loop coloured in purple and the variable loop coloured in yellow. (B) The crystal structure of yeast tRNA is coloured as in A. (PDB ID 6TNA was used (36)).

EF-Tu in *E. coli* is a 43 kilodalton (kDa) (39) GTPase involved in the delivery of aa-tRNA to the A site of an actively translating ribosome (40). In the active GTP-bound state of EF-Tu, a ternary complex (EF-Tu•GTP•aa-tRNA) is formed and rapidly binds to the ribosome (Figure 1.5). The laboratory of Dr. Marina Rodnina has performed a detailed analysis of the many steps during EF-Tu facilitated delivery of aa-tRNA to the translating ribosome (41). Following initial binding and correct codon-anticodon recognition, GTPase activation of EF-Tu occurs (42). This stimulation by the ribosome results in a 10^6-fold increase in the GTPase activity of EF-Tu (20). Furthermore, this stimulation is required to maintain the rapid and accurate rate of protein synthesis.

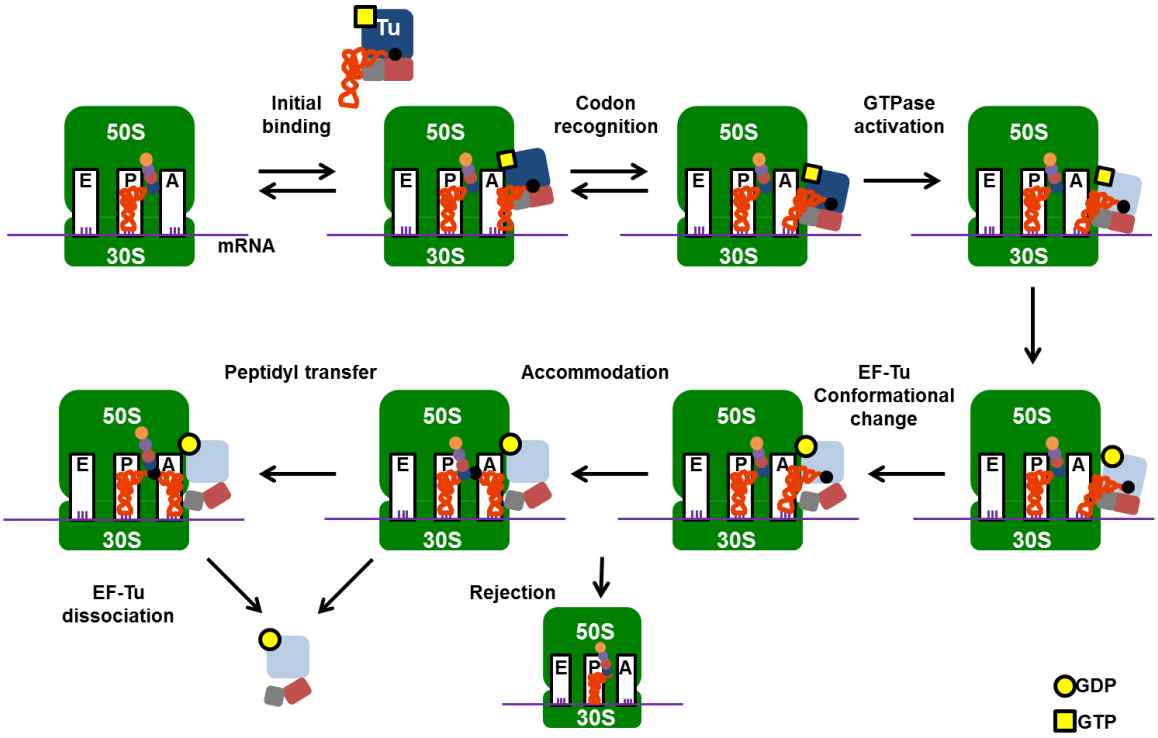

Figure 1.5. EF-Tu-dependent A site binding. During initial binding, the ternary complex binds to the ribosome, followed by codon recognition, triggering GTPase activation of EF-Tu (light blue). Subsequently GTP hydrolysis and P_i release occur, inducing a conformational change in EF-Tu leading to the release and accommodation of the aa-tRNA and peptidyl transfer. EF-Tu•GDP can dissociate before, during or after accommodation of aa-tRNA.

Following GTP hydrolysis and P_i release (43), EF-Tu undergoes a large conformational change (44) which results in the inactive EF-Tu•GDP complex. As EF-Tu•GDP has a 2-fold decreased affinity for aa-tRNA compared to EF-Tu•GTP, aa-tRNA is subsequently released from EF-Tu•GDP (41). EF-Tu•GDP dissociates from the ribosome, however the exact timing - whether it occurs before, during, or after tRNA accomodation into the ribosomal A site is not known. EF-Tu•GDP must be recycled to EF-Tu•GTP to enable efficient protein synthesis *in vivo*. EF-Tu has a higher binding affinity for GDP than for GTP (45) and the rate of GDP dissociation from EF-Tu is extremely slow, therefore nucleotide exchange is catalyzed by the guanine nucleotide exchange factor (GEF) EF-Ts

(Figure 1.6) (46,47). The high cellular concentration of GTP (10 mM) relative to GDP (1 mM) (48) allows EF-Tu to be recycled to its active GTP-bound form, enabling binding of a new aa-tRNA to continue the cycle of elongation.

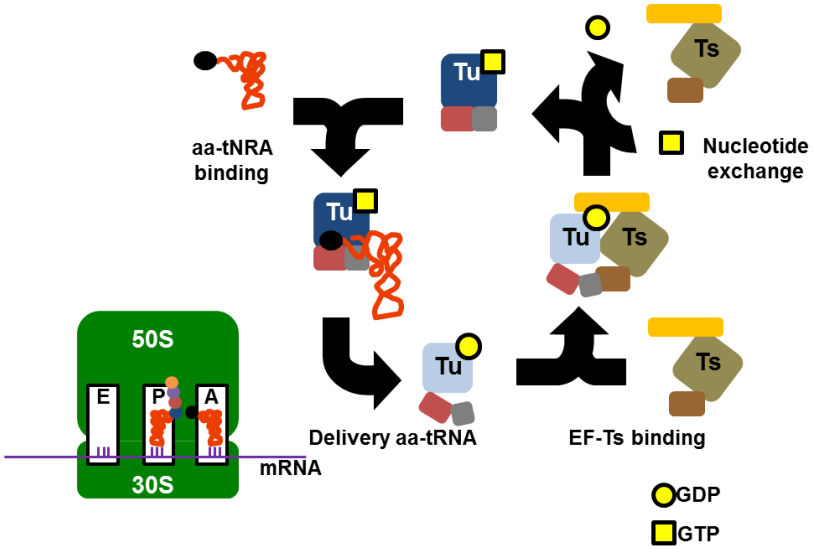

Figure 1.6. The functional cycle of EF-Tu. The cyclic process of EF-Tu catalyzing the delivery of aa-tRNA to the ribosome starts with the formation of the EF-Tu•GTP•aa-tRNA complex. Following accommodation of aa-tRNA, EF-Tu bound to GDP dissociates from the ribosome. EF-Ts facilitates the recycling of EF-Tu•GDP to EF-Tu•GTP complex.

Following aa-tRNA accommodation into the ribosomal A site, peptide-bond formation occurs between the incoming aa-tRNA and the peptidyl-tRNA in the P site (49). The PTC is composed of highly conserved rRNA and the mechanism of peptide-bond formation is conserved between eukaryotes and prokaryotes (26). The A and P-site tRNAs are positioned by interactions made with the 23S rRNA. Nucleotides of the 23S rRNA within the peptidyl-transferase center seem to have a role in positioning peptidyl-tRNA rather than in catalyzing peptide-bond formation. Proper positioning allows the α-amino group of the A-site bound aa-tRNA to attack the carbonyl carbon of the ester in the

peptidyl-tRNA in the P site. Although the ribosome is not involved in chemical catalysis it can modulate peptide-bond formation by conformational changes in the PTC (50).

In order for elongation to continue, the P and A-site tRNAs, along with the mRNA, must move to the E and P sites respectively. The translational GTPase EF-G, binds to the Pre-translocation ribosome complex in its GTP-bound active state and catalyzes translocation of the tRNAs and the mRNA (Figure 1.7) (51). Structural studies have revealed that EFG binding to the ribosome induces a so-called ratcheted state of the ribosome (52), which is critical to promote translocation. Furthermore, domain IV of EF-G protrudes into the ribosomal A site and prevents the backwards movement of the tRNAs into their original P and A site positions respectively (52). Following tRNA movement and P_i release, the ribosome can return to a non-ratcheted state (51). EF-G, now bound to GDP, dissociates from the ribosome, and the deacyl-tRNA occupying the E site quickly dissociates from the ribosome (51). The P site is occupied with the now one amino acid longer peptidyl-tRNA and the A site is empty, exposing the next codon specifying the next aa-tRNA to be incorporated into the growing polypeptide chain.

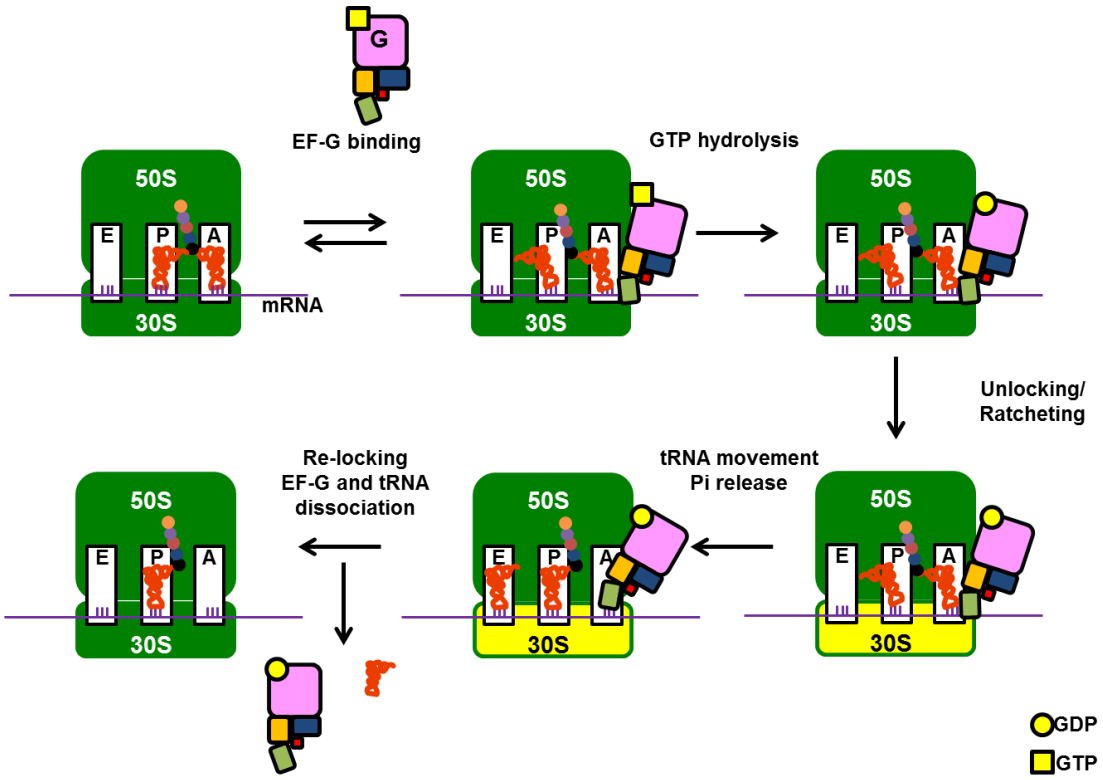

Figure 1.7. Translocation in the presence of EF-G. EF-G•GTP catalyzes translocation of A- and P-site tRNAs to the P and E sites of the ribosome by binding to the ribosome in a GTP-bound state and inducing an unlocked state of the ribosome (yellow) following GTP hydrolysis. Following translocation, EF-G•GDP and deacyl-tRNA dissociate from the ribosome. An empty A site with a new mRNA codon is left for the next round of elongation.

Forward translocation of tRNA and mRNA can occur intrinsically as peptidyl-tRNA has a higher affinity for the P site than for the A site of the ribosome (53). Therefore, peptide-bond formation promotes the movement of the A-site peptidyl-tRNA to the P site as this is thermodynamically favoured. Furthermore, in the absence of EF-G, the process of translocation can be facilitated by thiol-reactive reagents or by the omission of ribosomal proteins S12 and S13 (54).

Interestingly, it has been shown that back-translocation can occur spontaneously within the ribosome just as forward translocation can (55). Deacyl-tRNA has a higher affinity

for the P site than the E site (53). Therefore, the movement of the deacyl-tRNA, occupying the P-site, towards the ribosomal E site is not favoured. It has been shown that in the absence of all factors all tRNAs have the highest affinity for the ribosomal P site over any of other site. However, depending on the tRNAs occupying the E, P and or A-sites of the ribosome, the rate and extent of spontaneous tRNA movement within the ribosome is dependent upon the affinity of the peptidyl-tRNA and tRNA for the respective ribosomal sites (55). Movement of the tRNAs within the ribosome will reflect their most thermodynamically favoured state (55). This supports the idea that interactions made within the ribosome modulate the process and speed of translation. Translational GTPases, such as EF-G, have evolved to interact with the ribosome in such a way that the forward movement of translation is supported.

EF-G not only promotes forward translocation but prevents back-translocation by inserting its domain IV into the ribosomal A site. A translational GTPase in bacteria, LepA, has been shown to have a similar structure to EF-G, however, it has been demonstrated to catalyze back-translocation (56). Although back-translocation can occur spontaneously and can be catalyzed by LepA, the functional importance of this process is currently not understood.

1.1e Objectives

The process of elongation in protein synthesis is the only universally conserved step in translation. Therefore, knowledge obtained of this process within bacteria can be transferred to other domains of life. Elongation in protein synthesis is an essential process

and is an effective antibiotic target (57). Currently, there are several biochemical studies and structures that have elucidated the overall process of elongation and how antibiotics inhibit it. However, there are still some questions regarding events that occur during this process that need to be addressed. Knowledge obtained on the mechanism of elongation and interaction between elongation related translational GTPases and the ribosome can be utilized in the development of novel antibiotics.

Objective 1: LepA is a translational GTPase found in bacteria and eukaryotic mitochondria and chloroplasts. LepA is poorly understood in terms of its cellular and mechanistic function. It has a structure similar to EF-G and the EF-Tu•GTP•aa-tRNA ternary complex (58), however, its role or function *in vivo* is not understood. Although LepA is highly conserved throughout bacteria, it has been shown to be dispensable to the cell under optimal (culture) conditions (59).

Despite its similarity in structure to EF-G and EF-Tu•GTP•aa-tRNA, LepA contains a unique C-terminal domain (CTD) which resembles a truncated version of domain IV in EF-G (58). This domain has been demonstrated to contact the ribosome (60) and may be important for the function of LepA, as domain IV is important for the function of EF-G. It has been shown that the contacts made between the ribosome and translational GTPases EF-G and EF-Tu modulate the interaction of these proteins with guanine nucleotides as well as their GTPase activity. Information obtained on whether LepAs CTD is important for the interaction between LepA, guanine nucleotides and the ribosome may give insight into the function of this protein. **The emphasis of the first objective** will be to address the role of the unique CTD in LepA. Analysis on the role of this domain and the interaction between LepA and the ribosome, which may affect its

function as a translational GTPase, will be performed. Furthermore, a comparison of the interaction between LepA, guanine nucleotides and the ribosome to other known GTPases, such as EF-G, may give insight into the function of this protein and its role in the cell.

Objective2: EF-Tu is an essential GTPase in all living cells. In order to maintain the speed of translation observed *in vivo*, EF-Ts binds to EF-Tu and catalyzes the dissociation of GDP from EF-Tu, which allows GTP to bind. In spite of this, EF-Ts is highly divergent in sequence among bacterial species. The majority of residues involved in forming contacts with EF-Tu are conserved within EF-Ts, however, contacts made with the C-terminus of EF-Ts are poorly conserved. Furthermore, the interaction between the EF-Tu and EF-Ts homologues in eukaryotes are different than those seen in bacteria. Given the divergence of EF-Ts, it is questionable whether the contacts made between EF-Tu and EF-Ts need to be conserved to maintain function or whether this divergence results in differences in the catalytic ability of EF-Ts to act as a GEF. Understanding the variability and structural requirements within EF-Ts in bacteria might be an important tool in the design of antibiotics.

E. coli and *P. aeruginosa* are two gram-negative bacterial species which share 55% sequence identity in EF-Ts. In spite of this relatively high sequence identity within EF-Ts, these two species are extremely divergent in the sequence of the C-terminal module within EF-Ts which contacts the G-domain of EF-Tu. **The emphasis of the second objective** will be to compare the ability of EF-Ts from these two organisms to catalyze the dissociation of guanine nucleotides from EF-Tu and to determine if the

divergence observed in their C-terminal module causes any differences in their catalytic ability.

Objective 3: Comparisons of GTP and GDP-bound states of EF-Tu have revealed major domain rearrangements within EF-Tu (44). Little is known however about the mechanisms underlying these conformational changes. Furthermore, it is not understood when EF-Tu dissociates from the ribosome relative to the accommodation of aa-tRNA. Currently, the means of directly measuring these events has not been developed. By developing a real-time fluorescence-based assay for measuring the conformational dynamics of EF-Tu on and off the ribosome, the above can be investigated.

The thiol group of cysteine is often used to attach a fluorescent dye to a protein. However, cysteine residues are not always located in positions optimal for the analysis of interactions or conformational changes. **The emphasis of the third objective** will be on the construction of a cysteine-free (Cys-less) EF-Tu that can be used for the subsequent site-specific integration of cysteines located in optimal positions for fluorescent labelling and analysis. This will be a powerful tool for further understanding the dynamic movement of EF-Tu on and off the ribosome.

Significance

Analysis of all three objectives will not only help gain a better understanding of how these proteins function individually, but will also assist in understanding elongation during translation as a whole. GTPases that function during elongation have evolved to facilitate the speed and accuracy of this process through interactions with the ribosome that help ensure the directionality of translation and in this way they are essential for the

cell. A lot is known about this process, however, there are still details in this process that is not understood and will be addressed in the objectives listed above. Furthermore, given that elongation is a current target for antibiotics, addressing the above objectives may inform the development of new and unique targets.

Chapter 2.

Identification of Two Structural Elements in LepA Important for its Ribosome Stimulated GTPase Activity.

2.1 Introduction

2.1a Identification and Initial Characterisation of LepA

Deletion studies of regions flanking the gene encoding for leader (signal) peptidase I (*lep)* in *Escherichia coli* revealed that a stretch of 2 kilobases (kb) upstream of the *lep* gene is required for signal peptidase expression (61). Further studies by the lab of Masayori Inouye on the DNA sequence surrounding the *lep* gene demonstrated that the *lep* promoter is located 2 kb upstream of the gene (62). Interestingly, an open reading frame (ORF) located between the *lep* promoter and the *lep* gene was identified to encode for a 598 amino acid polypeptide and annotated as *lepA.*

The primary sequence of LepA indicates that there are no long stretches of hydrophobic regions in LepA, however localization studies of the LepA protein identified that it was mainly found in the membrane and the periplasm (62). Additionally, the mitochondrial counterpart of LepA, Guf1, was also found in the mitochondrial matrix and associated with the inner mitochondrial membrane (63). Given that LepA localizes in the cytoplasmic membrane of *E. coli*, it was originally proposed that like signal peptidase I, LepA may be involved in catalyzing the passage of proteins across the membrane (62). However, initial knockout studies of the *lepA* gene in *E. coli* under optimal growth conditions did not affect cell growth (59) indicating that, unlike signal peptidase I, LepA is not essential for the growth of *E. coli* and that LepA is not involved in protein export (59).

Further analysis by the lab of Masayori Inouye demonstrated that the amino-terminus of LepA has homology to EF-G and EF-Tu as well as IF2 (64). The sequence of the *lepA* gene revealed that LepA contains all four G motifs: G1 (P-loop; consensus $GX_4GK(S/T)$), G2 (effector loop, or switch I; DX_nT), G3 (switch II; DX_2G), and G4 (NKXD) which are responsible for interacting with a guanine nucleotide (21). GTP binding studies performed by Masayori Inouye and coworkers confirmed the presence of a guanine nucleotide binding domain and that LepA is indeed a GTP-binding protein like EF-G, EF-Tu and IF2 (64). Structural prediction tools support the idea that LepA likely has a similar secondary structure to these proteins (56). However the cellular function of LepA remains elusive.

2.1b Analysis of LepA Under Stress Conditions

In order to identify the cellular function of LepA, the effect of deleting the *lepA* gene was analyzed under various cellular growth conditions in *E. coli* (59). Although no effect of the *lepA* knockout was observed in *E. coli*, a later study in *Helicobacter pylori*, where over 1000 random gene knockouts were tested with respect to effects on growth at pH 4.8 revealed *lepA* as one of ten genes essential for growth under these conditions (65). Studies on the mitochondrial homologue of LepA (Guf1) in yeast, show that Guf1 is dispensable under optimal growth conditions in rich media (63). However, at low temperatures (15°C), *in vivo* protein synthesis in the mitochondria of cells lacking *guf1* is significantly lower than in wild type cells (63). This study also revealed that Guf1 is upregulated in mitochondria at low temperatures (15°C) as well as higher temperatures

(37°C) (63). A recent study of the chloroplast LepA homolog (CpLepA) showed that growth of *Arabidopsis thaliana* is reduced in the absence of *cplepa* (66). These studies indicate that although LepA may not be essential under ideal conditions, it may be required for cellular growth under stress conditions.

Growth of cells under different magnesium concentrations in the absence and presence of *lepA* revealed a significant reduction in cellular growth under high magnesium concentrations (100 mM) in the absence of *lepA* (67). In addition, work showed that at 14 mM Mg^{2+}, LepA is able to increase the rate of poly(Phe) synthesis *in vitro* (67). However, how LepA is activated in the cell and what the mechanism or function of LepA is remains unknown.

2.1c Histidine as a Catalytic Residue

In Ras-like G-proteins, a glutamine typically acts as a base by abstracting a proton from water, activating it for a nucleophilic attack on the gamma-phosphate of GTP ultimately triggering the efficient hydrolysis of the bound GTP (18). Interestingly, EF-Tu contains a histidine residue (His 84) in the switch II region, which has been shown to be important for GTPase activity of EF-Tu (68). Using mutagenesis in combination with rapid kinetics it was shown that substitution of His 84 in EF-Tu with an alanine residue significantly reduces the rate of ribosome stimulated GTP hydrolysis by EF-Tu, indicating that His 84 is important for catalysis of GTP hydrolysis (68). Structures of EF-Tu bound to GTP and GDP (44,69) illustrate that a conformational change occurs within the switch II region following GTP hydrolysis. A structure of EF-Tu bound to a non-hydrolyzable analogue of GTP (GMPPNP) revealed that there is a hydrophobic gate formed by Val 20 and Ile 60

within the G-domain of EF-Tu that prevents His 84 from activating a water molecule for GTP hydrolysis. Structural studies of EF-Tu on the ribosome demonstrate that the hydrophobic gate within EF-Tu opens following ribosome binding (70,71). This allows His 84, which interacts with A2662 of the 23S rRNA, to reposition and potentially activate water for GTP hydrolysis. Other translational GTPases, such as EF-G and LepA, contain a histidine that is 100% conserved in a similar location as found in EF-Tu, suggesting a similar catalytic role for this residue in all translational GTPases.

2.1d Structural Analysis of LepA

In 2008 the structure of LepA from *E. coli* was determined using X-ray crystallography (58) and confirmed that LepA is similar in structure to EF-G (Figure 2.1). LepA contains 5 domains with domains I, II, III and V of LepA corresponding closely to domains I, II, III and V of EF-G. However, LepA does not contain a domain that corresponds to domain IV of EF-G, but does contain a unique C-terminal domain (CTD) that occupies a similar position as domain IV in EF-G (Figure 2.1).

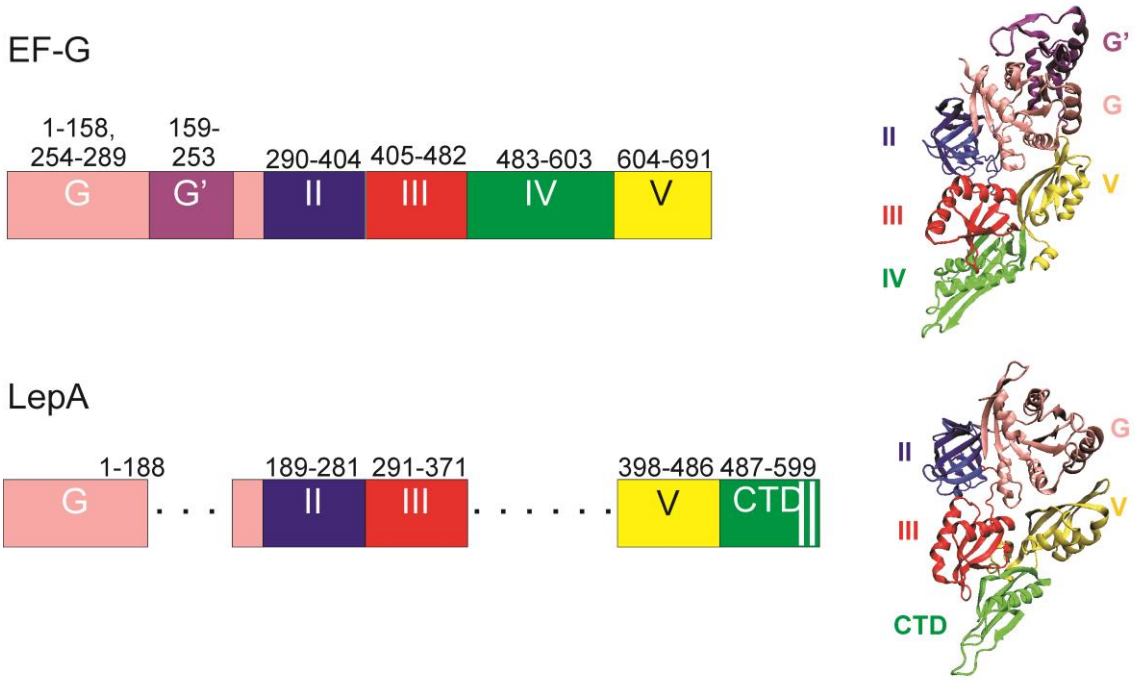

Figure 2.1. Structural comparison of LepA and EF-G. The domain arrangement is represented on the left, the corresponding residues within the domain are indicated above the respective domain. Cartoon representations of EF-G from *Thermus thermophilus* (PDB ID 1FNM (72)) and LepA from *Escherichia coli* (PDB ID 3CB4 (58)) are shown on the right. Domains are coloured according to the domain arrangement with the G-domain coloured pink, G' domain coloured purple, domain II coloured blue, domain III coloured red, domain IV coloured green and domain V coloured yellow. Residues 556 – 599 of LepA were not resolved in the structure and their position in the CTD is indicated by white lines in the alignment.

Domain I of LepA is a guanine nucleotide-binding domain (G-domain) with a Rossmann fold typical for G-proteins. Domain II in LepA has a 6-stranded β-barrel structure and domains III and V consist of a β-α-β fold, which is similar to domains III and V in EF-G. Although domains III and V in LepA have a similar fold as these domains in EF-G, they are oriented differently than in EF-G. In LepA, domain V is rotated and shifted upwards relative to domain I, allowing for a larger interface between domains I and V. The CTD of LepA is composed of a long α-helix between 4 β-sheets and is very basic giving it a net positive charge. However, as only part of the CTD is resolved in the available X-ray crystal structure of LepA (58), it is not clear what the entire structure of this domain is.

Interestingly, LepA is not the only GTP-binding protein in the prokaryotic cell with a three dimensional structure similar to that of EF-G. GTPases BipA and Tet(M)/Tet(O) also have a structure similar to that of EF-G (73-75). BipA is a 65 kDa protein that is encoded by the gene *bipA* and similar to LepA, BipA has been shown to be essential under stress conditions such as low temperature and low pH (76). However, unlike LepA, BipA has been shown to function as a virulence regulator (73). No full-length structure of BipA is currently available. However, a crystal structure of the C-terminal half (domains III, V and the CTD) of BipA from *Vibrio parahaemolyticus* (77) has been determined and shows structural similarity to domains III and V of EF-G. Furthermore, like EF-G and LepA, BipA has five domains, where the N-terminal G-domain and domains II, III and V are predicted to be similar in structure to EF-G and LepA. Also similar to LepA, BipA contains a unique CTD that has been shown, through deletion studies, to be required for BipA-ribosome interaction (78).

Tet(M) and Tet(O) are two bacterial ribosome protection proteins which have GTPase activity and mediate tetracycline resistance. They are both approximately 68 kDa in size and have been shown to be similar in structure to EF-G (74,75). Structural alignment of Tet(M) and Tet(O) reveals a high level of structural conservation with all five domains of EF-G (74).

It is interesting that the cell has evolved proteins with extremely similar structures but different functions. In spite of their functions being different, they all engage with the 70S ribosome in a similar fashion. This raises the questions as to how these interactions are regulated and timed in order to facilitate (or not inhibit) efficient protein synthesis.

2.1e LepA Interaction with the Ribosome

Structures of EF-G, LepA, Tet(O) and Tet(M) bound to the ribosome have been determined (52,60,79,80). All proteins bind to the ribosome below the L7/L12 stalk base. This binding site is shared with other translational GTPases that bind to the ribosome, such as EF-Tu (70). The available structures of factors on the ribosome have revealed that domains I, II, III and V of all three proteins contact the ribosome in a very similar fashion. Domain I, or the G-domain, contacts helix 95 of the 23S rRNA, domain II interacts with helix 5 of the 16S rRNA, domain III interacts with S12 of the 30S subunit and domain V interacts with helices 43, 44 and L11 of the 50S subunit. The largest difference in the interactions between LepA, EF-G, Tet(O) and Tet(M) and the ribosome is between the contacts made between the ribosome and domain IV of EF-G/Tet(O)/Tet(M) and the CTD of LepA. Domain IV of EF-G has been shown to be essential for EF-G's multiple turnover GTPase activity and the catalysis of translocation (81,82). Domain IV of EF-G also inserts into the A site of the ribosome and contacts P-site tRNA and mRNA. Domain IV of Tet(O) and Tet(M) extends into the ribosome in the same direction as domain IV in EF-G, however, it does not extend as far into the ribosome as EF-G and contacts helices 18 and 34 of the 16S rRNA (79,80).

Considering that the CTD of LepA is unique, it is not surprising that it makes contacts with the ribosome which are different from that of domain IV in EF-G (60). The cryo-EM structure of LepA bound to the 70S ribosome shows that the CTD of LepA makes contacts with A-site tRNA as well as helix 89 of the 23S rRNA. However, since not all of LepAs CTD is resolved in this structure, it is unknown what contacts are made between LepAs last 50 residues and the ribosome.

A recently resolved structure of the ribosome with EF-G bound, solved using X-ray crystallography, showed that the ribosome induces a conformational change in EF-G (52). The most prominent conformational change exhibited by EF-G upon binding to the ribosome is within domain IV. Not only can conformational changes within EF-G be observed upon ribosome binding, but EF-G also causes conformational changes within the ribosome itself, such as ratcheting of the two subunits and movement of the ribosomal stalk (52). A cryo-EM structure of Tet(O) bound to the ribosome revealed that similar to EF-G, Tet(O) binding leads to a movement in the ribosomal stalk (83). However, no movement between the ribosomal subunits can be observed upon Tet(O) binding. Interestingly, recent footprinting studies with LepA on the 70S ribosome indicate that LepA binds and stabilizes a ratcheted conformation of the 70S ribosome (84). However, given the lack of X-ray crystallographic structures and the poor resolution of available cryo-EM three-dimensional reconstructions for Tet(O), Tet(M), LepA and BipA bound to the ribosome, it is difficult to compare the conformational changes that may occur within the ribosome upon protein binding.

2.1f Cellular Function of LepA

LepA is a highly conserved protein within bacteria, where EF-Tu is the only translational GTPase more conserved than LepA (56). In spite of this, LepA is expressed in low amounts in the cell (85) whereas EF-Tu is a highly abundant protein.

In 2006, it was shown by Knud Nierhaus and colleagues that LepA is capable of catalyzing back-translocation, the movement of the E and P-site mRNA and tRNAs back

to the P and A sites respectively (56). However, the same study also demonstrated that back-translocation cannot reverse antibiotic induced misincorporations within translation and therefore the purpose of LepA catalyzed back-translocation in the cell is still unclear. Given the structural similarity between LepA and EF-G, the ability of LepA to catalyze forward translocation was analyzed, as well as its ability to compete with EF-G for binding to the ribosome (86). Not only is LepA able to compete with EF-G for ribosome binding, but it is also able to catalyze forward translocation. Given the cellular concentration of LepA (10-fold less than EF-G (85)), it is unlikely that LepA competes or inhibits the ability of EF-G to function in the cell. Therefore a particular functional state of the ribosome must exist that is specific for LepA and not EF-G.

LepA is the only protein similar in structure to EF-G that has been shown to promote forward translocation (86). Preliminary antibiotic studies have shown that thiostrepton, which prevents stable binding of EF-G to the ribosome, also inhibits LepA with a similar inhibitory concentration (84). These data suggest that LepA could function as EF-G in the cell, however, the lack of domain IV in LepA prevents it from inhibiting spontaneous back-translocation of the tRNAs and mRNA. LepA does contain a CTD which contacts the ribosome in a different manner than domain IV of EF-G. These contacts may be important for the overall function of LepA or may give insight into the function of LepA. The fact that the entire CTD has not been fully resolved indicates that it is a highly flexible domain. The flexibility of this domain may contribute to contacts made between LepA and the ribosome, which in turn could regulate or contribute to the function of LepA. To gain an understanding of the function of LepA, the CTD in LepA has been analyzed here in terms of its effect on known interaction partners of LepA.

2.2 Materials and Methods

2.2a Molecular Biology

The ORF for *lepA* was PCR-amplified from *E. coli* genomic DNA in a reaction catalyzed by *Pfu* DNA polymerase (Fermentas) using primers obtained from Invitrogen (5'-AATCATACCATATGAAGAATATACG-3' and 5'-CTCCTAAGCTTTATTTGTTGTCTT-3'; underlined nucleotides denote the restriction sites for *Nde*I and *Hind*III enzymes. All restriction enzymes were purchased from Fermentas and PCR reactions were carried out in a $T_{Gradient}$ thermocycler (Biometra): 25 μL of the reaction mixture contains 0.2 ng of template DNA, 1 μM of primer pair, 0.3 μM of each dNTP and 7.5 units of DNA polymerase. The reaction was carried out by pre-heating the reaction mixture to 95°C for 3 min followed by 30 cycles of 95°C for 1 min, 65°C for 1 min and 72°C for 14 min. This was followed by a final elongation step at 72°C for 15 min. PCR products were evaluated by 1% agarose gel electrophoresis at 80 V for 80 min. The resulting 3.1 kb PCR product was ligated (T4 DNA ligase, Invitrogen) into *Sma*I digested pUC19. 1.5 μL of the resulting product was transformed into 15 μL of *E. coli* DH5α competent cells (New England Biolabs) grown on Luria-Bertani (LB) agar plates supplemented with 100 μg/mL of ampicillin. Plasmids were isolated from selected colonies using a mini-prep purification kit (EZ-10 spin column plasmid DNA kit, BioBasic). Ligated plasmids were identified by restriction digestion with *Nde*I and *Hind*III. The *lepA* ORF was excised from pUC19-*lepA* with *Hind*III and *Nde*I and ligated into similarly digested pET28a. Sequence and orientation was confirmed by sequencing (Macrogen DNA Sequencing Services).

2.2b Mutagenesis

CTD truncation variants were generated based on a secondary structure prediction using Jpred (87). Truncated variants of LepA (ΔA494, ΔP520, ΔG555) were constructed via PCR using pET28a-*lepA* as a template. A single primer (5'-TAAGGCTTGCGGCCGCACTCGA-3' (Invitrogen)) was used for the construction of all three CTD truncation variants. The forward primers were obtained from Invitrogen and were used in construction of the truncation variants ΔA494, ΔP520 and ΔG555, respectively.

ΔA494-f 5'-**CGC**ATCAACACGTTCACCGTTGATTA-3'

ΔP520-f 5'-**TGG**GATCAGATCTTTCATCTTCTCCA-3'

ΔG555-f 5'-**GCC**ATAACATTTAGCCAGTACGTTTT-3'

The bold region of the primers corresponds to the codon encoding the terminal amino acid in the resulting truncation variant.

Reactions were carried out under the following conditions: 25 μL of the reaction mixture contained 80 ng of template, 13 pM of each primer, 200 μM of each dNTP and 0.4 units of DNA polymerase (Phusion, New England Biolabs). The reactions were carried out by pre-heating the reaction mixture to 98°C for 3 min followed by 35 cycles of 98°C for 1 min, 60°C for 45 sec and 72°C for 5 min followed by a final incubation at 72°C for 5 min. The PCR-amplification products were evaluated by a 1% agarose gel as described above. Blunt-end ligations of the products produced circular plasmids encoding LepA truncation variants in pET28a vectors. Products were ligated with T4 ligase (Fermentas)

and transformed into *E. coli* DH5α (New England Biolabs) competent cells for propagation and *E. coli* BL21-DE3 (New England Biolabs) competent cells for expression.

LepA H81A was constructed via site-directed mutagenesis carried out on the pET28a-*lepA* template using the Quickchange™ method (Stratagene). Primers (forward primer 5'-TATCGACACCCCAGGC**GCC**GTAGACTTCTCCTATG-3' and reverse primer 5'-CATAGGAGAAGTCTAC**GGC**GCCTGGGGTGTCGATA-3') were obtained from Invitrogen. The position of mutagenesis is denoted in bold; underlined nucleotides denote the *Sma*I restriction site (5'-CCCGGG-3') which was removed via a silent mutation. Reactions were carried out under the following conditions: 25 μL of the reaction mixture contained 80 ng of template, 1 μM of primer pair, 0.3 μM of each dNTP and 0.4 units of DNA polymerase (*Pfu,* Fermentas). The reaction was initiated by pre-heating the reaction mixture to 95°C for 3 min followed by 18 cycles of 95°C for 45 s, 65°C for 1 min, 72°C for 12 min and subsequent incubation at 72°C for 20 min. The PCR-amplified products were analyzed on a 1% agarose gel as described above. Products were ligated with T4 ligase (Fermentas) and transformed into *E. coli* DH5α (New England Biolabs) competent cells for propagation and *E. coli* BL21-DE3 (New England Biolabs) for expression. The mutation was confirmed by sequencing as described above.

2.2c Expression and Purification of LepA Proteins

All buffers were filtered through 0.45 μm Whatman nitrocellulose membranes and degassed prior to use. *E. coli* BL21-DE3 competent cells were grown in LB media

supplemented with 50 μg/mL kanamycin. For protein overexpression of LepA wild type and H81A, cells were grown at 37°C to mid-log phase (OD_{600} = ~ 0.6) and induced with isopropyl-β-D-thiogalactopyranoside (IPTG, BioBasic) to a final concentration of 1 mM. Cells were grown for an additional 3 hrs at 37°C, harvested by centrifugation (5000 x *g* for 10 min at 4°C), flash frozen and stored at -80°C. For protein overexpression of the LepA CTD truncation variants, cells were grown at 37°C to mid-log phase (OD_{600} = ~ 0.6) and induced with IPTG to a final concentration of 0.5 mM. Cells were grown for an additional 16 hrs at 16°C, harvested by centrifugation (5000 x *g* for 10 min at 4°C), flash frozen and stored at -80°C. To analyze LepA expression, samples of equal amounts of cells were taken every 30 min, lysed with 8 M urea in buffer 2.1 (50 mM Tris-Cl pH 7.5 (20 °C), 70 mM NH_4Cl, 30 mM KCl and 7 mM $MgCl_2$) and analyzed by 10% sodium dodecyl sulfate-polyacrylamide gel electrophoresis (SDS-PAGE) at 80 V for 20 min followed by 180 V for 60 min (BioRad Mini Protean 3 System). Gels were stained with Coomassie Brilliant blue; all other SDS-PAGEs were performed in a similar manner.

For purification of all LepA proteins, cell pellets (approximately 8 g) were resuspended in 7 mL of buffer 2.2 (50 mM Tris-Cl pH 8.0 (4 °C), 60 mM NH_4Cl, 7 mM $MgCl_2$, 300 mM KCl, 7 mM β-mercaptoethanol (BME), 1 mM phenylmethanesulfonylfluoride (PMSF), 10 mM imidazole and 15% glycerol) per gram of cells and lysed with 0.1 mg/mL lysozyme. Cellular debris were removed through centrifugation at 30 000 x *g* for 45 min using a JA-16 rotor (Beckman) yielding a S30 extract. LepA was purified from the S30 extract using affinity chromatography (7 mL Ni^{2+}-Sepharose resin (GE Healthcare)) equilibrated with buffer 2.2. The resin was washed three times with 50 mL

of buffer 2.2 and four times with 50 mL of buffer 2.3 (buffer 2.2 with 20 mM imidazole). The protein was eluted in 10 washes of 7 mL buffer 2.4 (buffer 2.2 with 250 mM imidazole). His_6-tagged LepA protein was concentrated to 60-100 µM via ultrafiltration (Vivaspin 20, 30000 MWCO (Sartorius)) and further purified using size exclusion chromatography (SEC) (XK26/100 column; Superdex 75 prep grade (GE healthcare)) equilibrated in buffer 2.5 (50 mM Tris-Cl pH 7.5 (4°C), 70 mM NH_4Cl, 300 mM KCl, 7 mM $MgCl_2$ and 15% glycerol). Fractions were analyzed by SDS-PAGE, and those containing LepA (of >90% pure) were pooled and concentrated via ultrafiltration (*vide supra*) and stored at -80°C. The final protein concentration was determined spectrophotometrically at 280 nm using a molar extinction coefficient (39 935 M^{-1} cm^{-1} for wild type, LepA H81A and LepA ΔG555, 38 320 M^{-1} cm^{-1} for LepA ΔP520 and LepA ΔA494; calculated using ProtParam (88)) and confirmed using the Bradford Protein Assay (BioRad). Final protein preparation purity is shown by SDS-PAGE (Appendix Figure A.1).

2.2d Purification of E. coli Ribosomes

Vacant ribosomes were purified as previously described (89) from 50g of *E. coli* MRE600 cells. Alumina was used to open the cells with a mortar and pestle for 30 min at 4°C. DNase I was added and the mixture was ground for an additional 30 min. Buffer 2.6 (20 mM Tris-Cl pH 7.6 (4°C), 100 mM NH_4Cl, 10.5 mM $MgCl_2$, 0.5 mM ethylenediaminetetraacetic acid (EDTA) and 3 mM BME) was added and the mixture was centrifuged at 1 000 x *g* for 10 min followed by 10 000 x *g* for 30 min in a Beckman

JA-14 rotor. The supernatant was filtered and centrifuged at 30 000 x *g* in a Beckman Ti-45 rotor for 30 min. This resulting supernatant (S30, approximately 40 mL) was overlayed on 20 mL of buffer 2.7 (20 mM Tris-Cl pH 7.6 (4°C), 500 mM NH_4Cl, 10.5 mM $MgCl_2$, 0.5 mM EDTA, 1.1 M sucrose, 3 mM BME) and spun at 200 000 x *g* for 17 hrs in a Ti-45 rotor. Pellets were dissolved in buffer 2.8 (20 mM Tris-Cl pH 7.6 (4°C), 500 mM NH_4Cl, 10.5 mM $MgCl_2$, 0.5 mM EDTA and 7 mM BME) with the help of a glass rod to a final volume of 100 mL. This solution was overlayed on 4 mL of buffer 2.7 and spun in a Ti-45 rotor at 200 000 x *g* for 16 hrs at 4°C. The above pellets were dissolved in buffer 2.8 as described above to a final volume of 60 mL. The solution was overlayed on 1.5 mL of buffer 2.7 and centrifuged in a Beckman SW28 at 140 000 x *g* for 13 hrs at 4°C. The resulting pellets were dissolved in 10 mL of buffer 2.9 (20 mM Tris-Cl pH 7.6 (4°C), 60 mM NH_4Cl, 5.25 mM Mg acetate, 0.25 mM EDTA, and 3 mM BME) supplemented with 5% sucrose. The concentration of ribosomes was determined by the absorbance at 260 nm, flash frozen and stored at -80°C.

70S, 50S and 30S ribosomal subunits were separated using zonal centrifugation. 400 mL of buffer 2.9 was loaded into a Beckman Ti-15 at a flow rate 8 mL/min spinning at 2000 rpm. Approximately 12 500 OD of ribosome solution (approximately 20 mL) was loaded into the spinning rotor followed by a 10-40% sucrose gradient (approximately 1370 mL) (20 mM Tris-Cl pH7.6 (4°C), 60 mM NH_4Cl, 5.25 mM Mg acetate, 0.25 mM EDTA, 3 mM BME and the corresponding percent of sucrose). Subsequently, 150 mL of 50% sucrose was loaded into the spinning rotor. This was centrifuged for 19 hrs at 28 000 rpm at 4°C. The rotor was slowed down to 2000 rpm and unloaded in 50 mL fractions with 50% sucrose at a flow rate of ~8 mL/min. The absorbance of the fractions

was monitored at a wavelength of 260 nm and fractions containing 30S, 50S subunits and 70S ribosomes were pooled and centrifuged for 48 hrs at 200 000 x *g* in a Ti-45 rotor at 4°C. Pellets were dissolved in buffer 2.10 (20 mM Tris-Cl pH 7.6 (4°C), 50 mM NH_4Cl and 5 mM $MgCl_2$) to a final concentration of approximately 10 μM, flash frozen and stored at -80°C for further use.

2.2e Fluorescence Titrations

To determine guanine nucleotide binding affinities of LepA and its variants, fluorescence measurements were performed using a Photon Technology International (PTI) QuantaMaster Spectrofluorometer. Intrinsic tryptophan fluorescence of LepA was excited at 280 nm in a 0.3 x 0.3 cm quartz cuvette (Starna) at room temperature. Förster resonance energy transfer (FRET) between the tryptophans in LepA and 2'-/3'-O-N'-Methylanthraniloyl (mant) modified guanine nucleotides was utilized to determine the equilibrium dissociation constants (K_D) for mant-GTP/GDP/GDPNP to LepA. The resulting fluorescence emission was monitored from 300 nm to 500 nm, with a slit width of 3 nm. The background fluorescence signals due to the presence of protein and nucleotide were subtracted from the overall fluorescence of the system. Measurements were carried out using 2 μM LepA in buffer 2.1 and adding increasing amounts of the respective mant-guanine nucleotide (Invitrogen). Fluorescence changes (F) in the corrected tryptophan fluorescence emission at 325 nm and mant at 440 nm were plotted as a function of nucleotide concentration and subsequently fit with a hyperbolic function (Equation 2.1), where B_{max} is the final fluorescence and X is the guanine nucleotide

concentration. From this, the dissociation constant (K_D) for each nucleotide derivative was obtained.

$$F = B_{max} \times X / (K_D + X) \quad \text{(Equation 2.1)}$$

2.2f Stopped-Flow Fluorescence

Fluorescence stopped-flow measurements were performed using a KinTek SF-2004 stopped-flow apparatus (KinTek Corporation). Measurements were performed in a manner similar to that previously described (90). In brief, mant-nucleotides were excited via FRET from the tryptophan residues (λ_{ex} = 280 nm) present in LepA and the resulting fluorescent emission was detected after passing through LG-400-F cut off filters (NewPort).

Dissociation rate constants were determined by pre-incubating 200 µM mant-GDP with 2 µM LepA in buffer 2.1 at 37°C for 15 min, or 200 µM mant-GTP / 100 µM mant-GDPNP with 2 µM LepA, 3 mM phosphoenolpyruvate (PEP) and 0.1 mg/mL pyruvate kinase (PK) in buffer 2.1 at 37°C for 15 min. These mixtures were rapidly mixed with 2 mM of corresponding guanine nucleotide in similar buffer conditions. Dissociation time courses were fit with a one-exponential function (Equation 2.2):

$$F = F_{\infty} + A \times \exp(-k_{-1} \times t) \quad \text{(Equation 2.2)}$$

where F is the fluorescence at time t, F_∞ is the fluorescence at equilibrium, and k_{-1} is the dissociation rate constant.

The apparent rate for the bimolecular association of mant-nucleotides to LepA was determined by rapidly mixing 25 μL of LepA (1 μM after mixing) with 25 μL of varying concentrations of mant-nucleotides (ranging from 3 to 50 μM after mixing) at 20°C in buffer 2.1. Mant-GTP association experiments were supplemented with 3 mM PEP and 0.1 mg/mL PK. Fluorescence time courses were best fit with a two exponential equation (Equation 2.3):

$$F = F_\infty + A \times \exp(-k_{app1} \times t) + B \times \exp(-k_{app2} \times t) \quad \text{(Equation 2.3)}$$

where F is the fluorescence at time t, F_∞ is the fluorescence at equilibrium, k_{app1} is the first apparent rate constant and k_{app2} is the second apparent rate constant. The apparent rate constants were plotted as a function of nucleotide concentration. k_{app1} was linearly dependent on nucleotide concentration and the slope of this plot represents an association rate constant ($k_{1(LepA \cdot GTP)}$ for GTP and $k_{1(LepA \cdot GDP)}$ for GDP). k_{app2} was not dependent on nucleotide concentration. Calculations were performed using TableCurve (Jandel Scientific) and Prism (GraphPad Software).

2.2g LepA Proteins Binding to the Ribosome

Binding of LepA to the ribosome was assessed using ultracentrifugation in a TLA-100.3 rotor (Beckman Coulter). Reactions containing 2 µM LepA were added to either 0.1 µM 70S, 50S or 30S ribosomal particles in the presence of 0.1 mM guanine nucleotides in a total volume of 400 µL in buffer 2.1. Reactions were incubated for 15 min at 37°C and layered onto 1700 µL of buffer 2.11 (20 mM Tris-HCl pH7.6 (4°C), 60 mM NH_4Cl, 5.25 mM Mg acetate, 0.25 mM EDTA, 10% sucrose, 3 mM BME) and centrifuged at 65 000 x *g* for 18 hrs. Pellets were resuspended in 40 µL of buffer 2.1, and 20 pmol of each sample was loaded into an immunoblot (slot-blot apparatus, BioRad Biodot SF). The presence of LepA in the pellet was detected through the use of the N-terminal His_6-tag on LepA using a monoclonal anti-polyhistidine antibody from mouse (Sigma) and anti-mouse IgG (Fab specific) peroxidase conjugate from goat (Sigma). Chemiluminescence was used for detection where 50 mL of 200 µM *p*-coumeric acid (Sigma) and 2.5 µM luminol (Sigma) in 0.1 M Tris-Cl pH 8.5 was added to 0.06% H_2O_2 in 10 mL of 0.1M Tris-Cl pH 8.5. Chemiluminescence was detected using a Typhoon 9400 imager from GE healthcare.

2.2h GTP Hydrolysis

To measure the intrinsic GTPase activity of LepA and its variants, liberation of $^{32}P_i$ from [γ^{32}P]-GTP (Perkin Elmer) was utilized. Guanine nucleotide charging solution (radioactive nucleotide at 100 dpm/pmol, 3 mM PEP, 0.1 mg/mL PK) was incubated at 37°C for 15 min to catalyze nucleotide triphosphate formation from the diphosphate form

to prevent inhibition of the GTPase by diphosphates in multiple turnover experiments. Hydrolysis assays were carried out in buffer 2.1. Reaction mixtures contained 5 μM LepA protein and 0 to 350 μM [γ^{32}P]-GTP. 10 μL samples were removed at 40 min and quenched in 50 μL buffer 2.12 (1 M $HClO_4$ with 3 mM potassium phosphate). The inorganic phosphate was extracted using 300 μL of 20 mM Na_2Mo_4 and 750 μL of isopropyl acetate. Samples were vortexed for 10 min (Eppendorf MixMate) and centrifuged at 15 800 x *g* for 5 min (Labnet Hermle Z180M Micro Centrifuge). The extracted $^{32}P_i$ phosphate-molybdate complex in the organic phase was added to 2 mL of EcoLite scintillation cocktail (EcoLite, MP Biomedicals), and counted in a Perkin-Elmer Tri-Carb 2800TR liquid scintillation analyzer. Background radioactivity was subtracted and the amount of GTP hydrolyzed as a function of time was calculated and plotted against increasing GTP concentration. Data was fit with equation 2.4.

$$Y = v_{max} \times X/ (K_M + X) \qquad \text{(Equation 2.4)}$$

where Y is equal to the concentration of GTP hydrolyzed over time, v_{max} is the maximum rate of GTP hydrolyzed over time, K_M is the substrate concentration needed to achieve a half-maximum enzyme velocity and X is the substrate (GTP) concentration.

To measure ribosome stimulated GTP hydrolysis of LepA, liberation of $^{32}P_i$ from [γ^{32}P]-GTP (Perkin Elmer) in the presence of LepA and 70S ribosomes was assessed. Guanine nucleotide charging solution was incubated as described above. Hydrolysis assays were carried out in buffer 2.1. Reaction mixtures contained 0.01 μM protein,

100 μM [γ^{32}P]-GTP and 0 to 8 μM 70S ribosomes. 10 μL samples were removed at various time points (10 to 40 min) and quenched, then $^{32}P_i$ was extracted and analysed as described above. Background radioactivity was subtracted and the concentration of GTP hydrolyzed was calculated as a function of time and plotted against increasing 70S ribosome concentration and fit with equation 2.4 where X is equal to 70S ribosome concentration.

2.3 Results

2.3a Structure Prediction of the C-Terminal Domain of LepA

Many proteins and complexes that interact with the A site of the bacterial ribosome have similar structures. The most recent structure of *E. coli* LepA illustrates how similar in structure LepA is to EF-G (Figure 2.1) (58); however, the complete structure of LepA is still unknown. To gain insight into the function of the unresolved part of the CTD of LepA, a secondary structure prediction was performed (Figure 2.2) using Jpred (87). This prediction is in good agreement with the secondary structure elements found in the structure derived from X-ray crystallography. The unresolved C-terminal amino acids (43) are predicted to form two alpha helices (Figure 2.2).

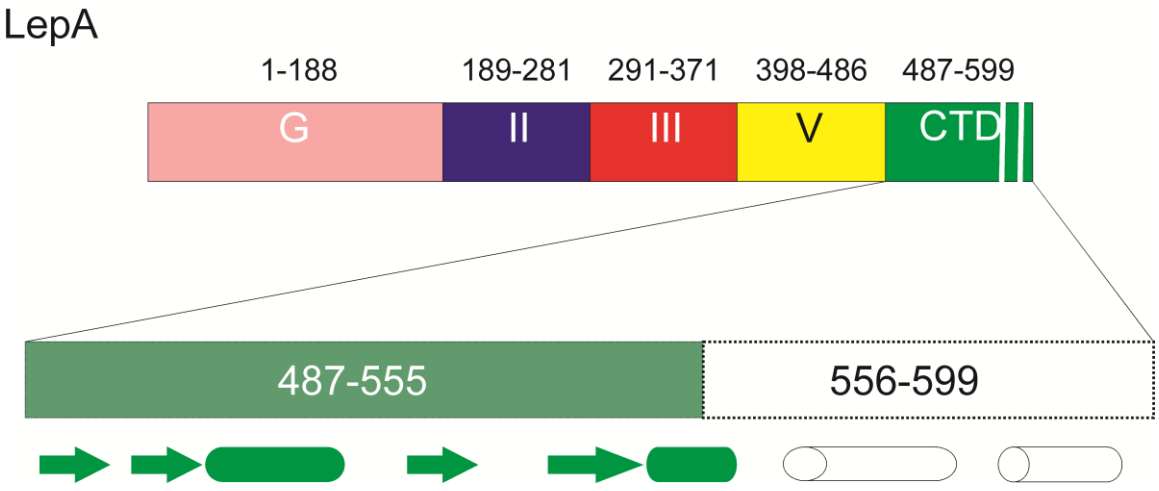

Figure 2.2. Structure prediction of the CTD of LepA. The structure of LepAs CTD was predicted using Jpred. Beta-sheets are represented as arrows and alpha-helices as cylinders. Solid green shapes are predicted structural components that are also found in the structure of LepA determined by X-ray crystallography.

From this, three CTD truncation variants were designed (Figure 2.3) in which this domain was sequentially truncated from the CTD of LepA.

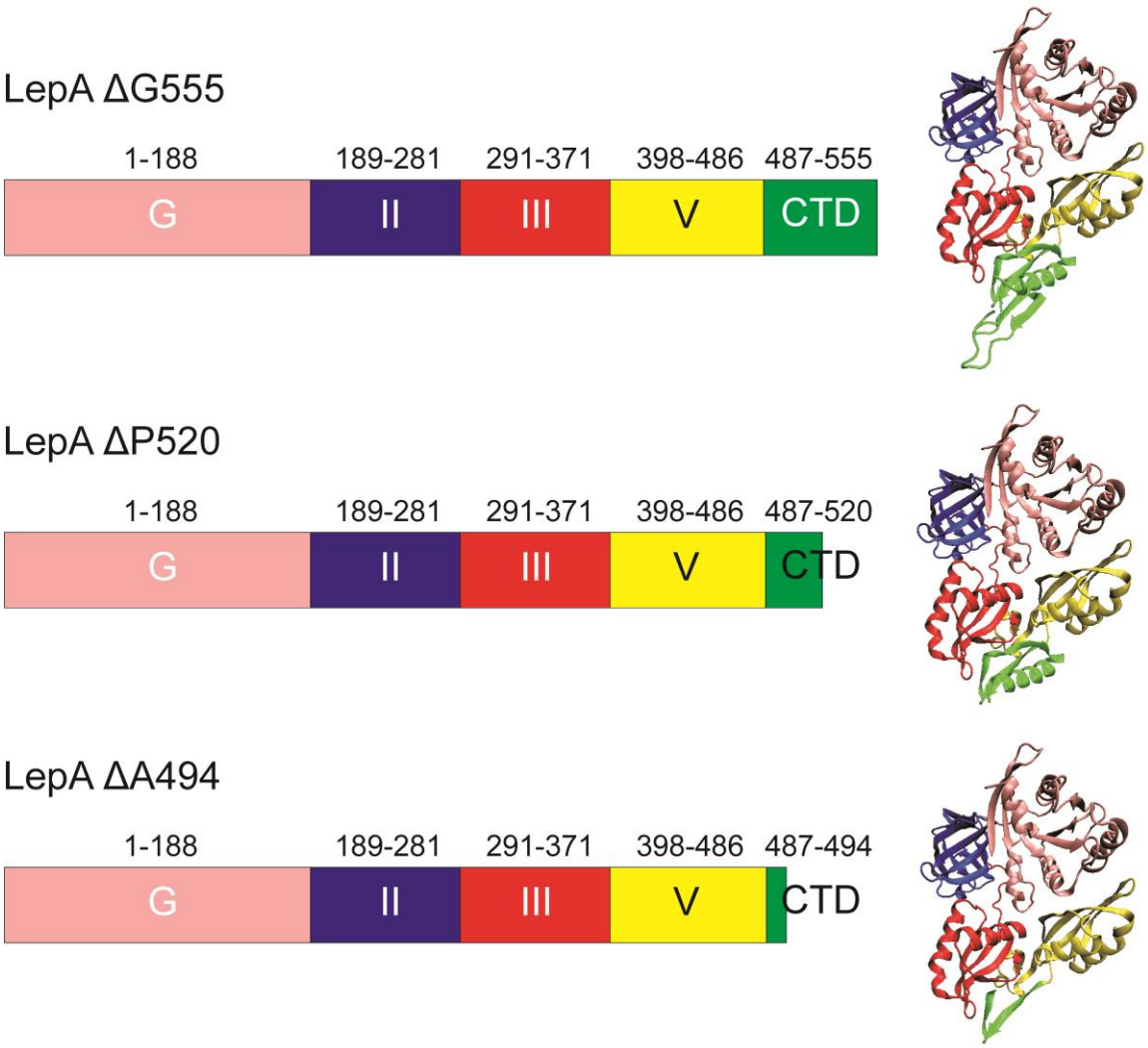

Figure 2.3. CTD truncation variants constructed. LepA ΔG555, ΔP520 and ΔA494 are illustrated respectively. The corresponding protein designation is written above the domain representation and the amino acids corresponding to these domains are written above the respective domain. All structures are represented in cartoon on the right and coloured as in figure 2.1.

2.3b LepA Interaction with Guanine Nucleotides (GDP/GDPNP/GTP).

The interaction of LepA with guanine nucleotides has not been determined so far, preventing an understanding of the cellular state of the protein. Most GTPases, such as EF-Tu and EF-G, cycle between their active GTP-bound form and their inactive GDP-bound form. To elucidate the binding affinities of LepA for guanine nucleotides,

the interaction between purified *E. coli* LepA and guanine nucleotides has been analyzed using equilibrium fluorescence spectroscopy measurements (Materials and Methods). A potential effect of the CTD on the interaction between LepA and the respective guanine nucleotides was also analyzed to elucidate a role of this unique domain within LepA. To this end, FRET between the intrinsic tryptophan residues in LepA as a donor fluorophore and the mant group on mant-labelled guanine nucleotides as an acceptor fluorophore was utilized. Upon excitation of the tryptophan residues in LepA, a decrease in tryptophan fluorescence ($\lambda_{emission\ max} \approx 325nm$) as well as an increase in mant fluorescence ($\lambda_{emission\ max} \approx 440nm$) was observed (Figure 2.4). Changes in the relative fluorescence were fit with a hyperbolic function (Eq. 2.1) and reveal a comparable affinity for mant-GDP and mant-GDPNP (a non-hydrolysable analogue of GTP) for wild type LepA ($K_{D(LepA \bullet GDP)} = 110 \pm 50\ \mu M$ and $K_{D(LepA \bullet GDPNP)} = 30 \pm 10\ \mu M$) and the LepA CTD truncation variants ΔA494 ($K_{D(\Delta A494 \bullet GDP)} = 90 \pm 45\ \mu M$ and $K_{D(\Delta A494 \bullet GDPNP)} = 60 \pm 40\ \mu M$), ΔP520 ($K_{D(\Delta P520 \bullet GDP)} = 90 \pm 70\ \mu M$ and $K_{D(\Delta P520 \bullet GDPNP)} = 55 \pm 20\ \mu M$) and ΔG555 ($K_{D(\Delta G555 \bullet GDP} = 130 \pm 120\ \mu M$ and $K_{D(\Delta G555 \bullet GDPNP)} = 50 \pm 16\ \mu M$) (Table 2.1 and 2.2). These data show that LepA has a micro-molar affinity for guanine nucleotides, which is consistent with results shown for EF-G ($K_{D(EF\text{-}G \bullet GDP)} \approx 17\ \mu M$ and $K_{D(EF\text{-}G \bullet GTP)} \approx 7\ \mu M$) (91). Furthermore, these results indicate that the CTD truncation variants constructed bind to guanine nucleotides with a similar affinity as wild type LepA.

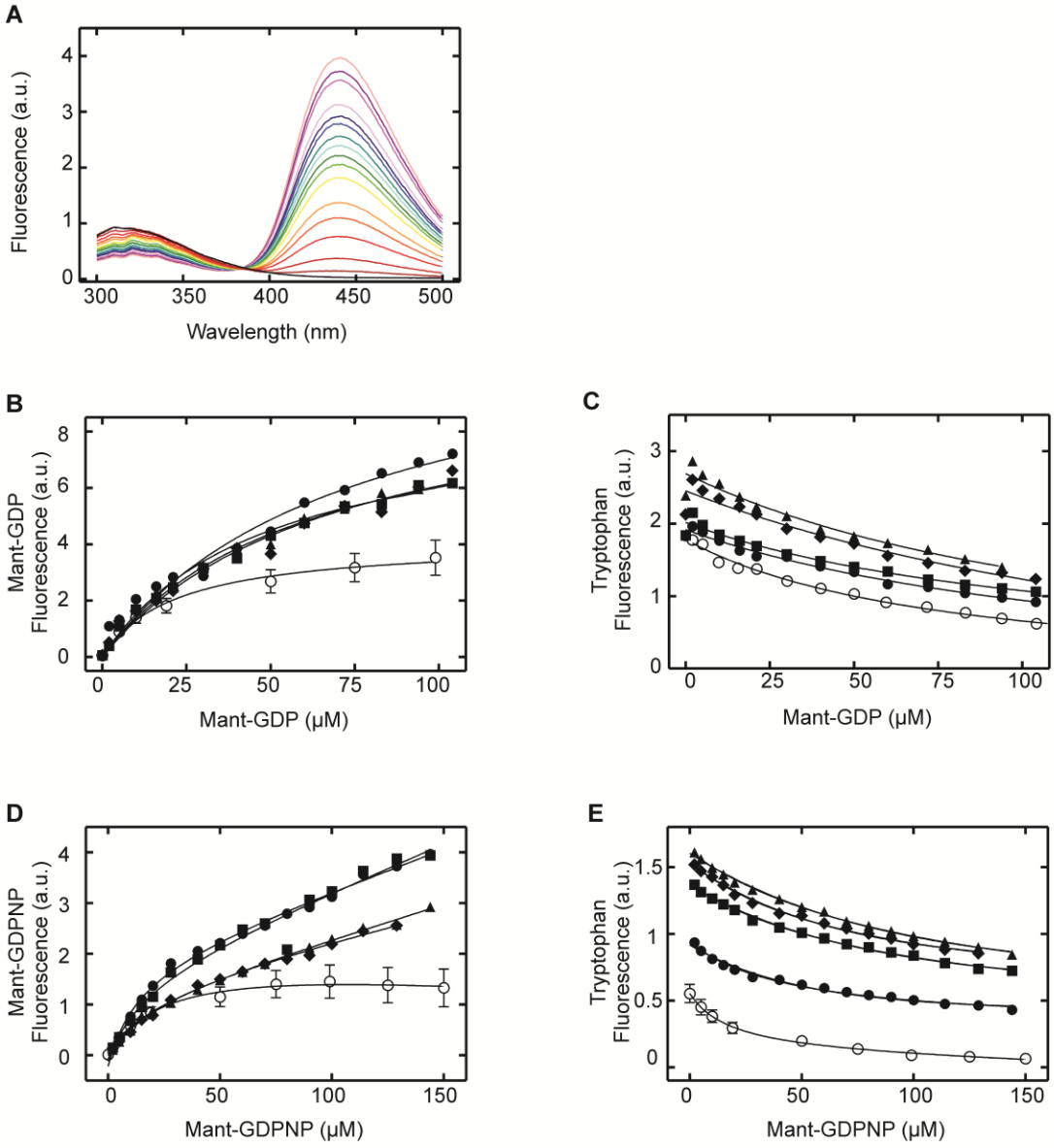

Figure 2.4. Equilibrium fluorescence titration of LepA with guanine nucleotides. (A) LepA titrated with increasing concentrations of guanine nucleotide from 0 (black) to 150 μM (pink). Fluorescence emission was monitored from 300 to 500 nm. (B) Mant-GDP or (D) Mant-GDPNP emission at 440nm and (C and E) LepA Trp emission at 325 nm was plotted as a function of increasing Mant-GDP/GDPNP concentration. Nucleotide concentration dependence of the fluorescence emission was used to determine K_D values for LepA wild type (filled circles), LepA ΔA494 (squares), LepA ΔP520 (triangles), LepA ΔG555 (diamonds) and LepA H81A (open circles).

Table 2.1. Dissociation Constants (K_D) Governing the Interaction Between LepA Variants and Mant-GDP.

LepA	K_D μM (Trp decay)	K_D μM (Mant Increase)	K_D μM average
Wild Type	140 ± 50	75 ± 20	110 ± 50
ΔA494	110 ± 60	60 ± 10	90 ± 45
ΔP520	140 ± 110	50 ± 10	90 ± 70
ΔG555	200 ± 175	70 ± 15	130 ± 120
H81A	80 ± 10	20 ± 5	50 ± 10

Table 2.2. Dissociation Constants (K_D) Governing the Interaction Between LepA Variants and Mant-GDPNP.

LepA	K_D μM (Trp decay)	K_D μM (Mant Increase)	K_D μM average
Wild Type	50 ± 10	10 ± 5	30 ± 10
ΔA494	90 ± 10	16 ± 20	60 ± 40
ΔP520	110 ± 10	15 ± 5	55 ± 20
ΔG555	80 ± 10	30 ± 10	50 ± 16
H81A	20 ± 6	30 ± 20	20 ± 10

All translational GTPases contain a conserved histidine residue that may be essential for efficient GTP hydrolysis. Based on LepAs structural similarity to EF-Tu, a sequence alignment revealed that His 81 of LepA is found in a similar position as His 84 in EF-Tu, which has been shown to be essential for GTP hydrolysis in EF-Tu (68). To confirm that substitution of His 81 in LepA provides a GTPase inactive variant of LepA which can be subsequently used as a tool for further studies on the role of GTP hydrolysis by LepA, a H81A substitution of LepA was constructed. LepA-guanine nucleotide equilibrium binding studies reveal that the final fluorescence emission of mant-GDPNP/GDP plateaus at a lower level than in the presence of the other LepA proteins. However, guanine

nucleotide binding is not affected by this substitution (Table 2.1 and 2.2) as the calculated K_D for mant-GDP and mant-GDPNP are 50 ± 13 µM and 20 ± 10 µM, respectively.

To further analyze the interaction of LepA with guanine nucleotides, rate constants for nucleotide association ($k_{1(LepA•GDP/GTP)}$) and dissociation ($k_{-1(LepA•GDP/GTP/GDPNP)}$) were determined using the stopped-flow technique based on the FRET system described above, but only monitoring the fluorescence of mant-guanine nucleotides. To measure the rate of mant-guanine nucleotide dissociation, LepA was incubated with 50 to 100-fold excess of mant-guanine nucleotide (Materials and Methods) and rapidly mixed with a 1000-fold excess of non-fluorescent guanine nucleotide to prevent rebinding of the labelled nucleotide. A rapid decrease in fluorescence was observed upon mixing, representing mant-guanine nucleotide dissociation from LepA (Figure 2.5). The k_{-1} was determined for mant-GDP, mant-GTP and mant-GDPNP from LepA proteins by fitting the obtained time courses with a one-exponential function (Eq. 2.2). The obtained values for the respective rate constants show that dissociation of mant-guanine nucleotides from all LepA proteins are similar to each other (Table 2.3). Interestingly, the rate of mant-GTP dissociation is almost 10-fold faster than mant-GDP dissociation from LepA. Furthermore, mant-GDPNP dissociation is approximately 100-fold faster than mant-GDP dissociation from LepA.

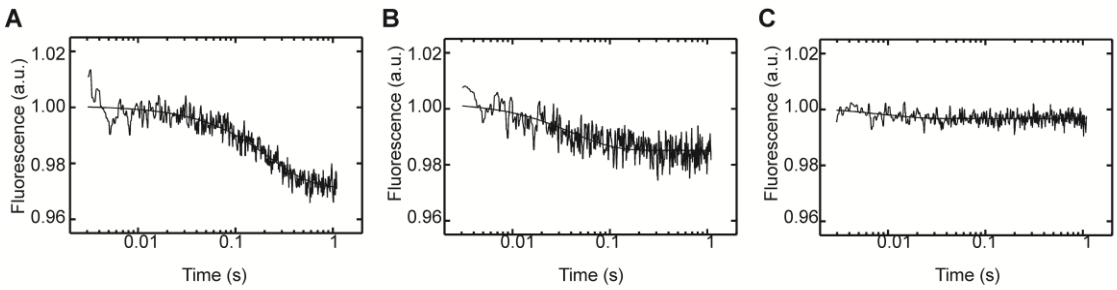

Figure 2.5. Dissociation of guanine nucleotides from LepA. (A) Time course of (A) mant-GDP (200 µM) (B) mant-GTP (200 µM) (C) mant-GDPNP (40 µM) dissociation from LepA (2 µM) measured by FRET excitation of mant-GDP/GTP/GDPNP.

Table 2.3. Rate of Mant-Guanine Nucleotide Dissociation from LepA Variants.

Protein	$k_{-1(LepA \bullet GDP)}$ (s^{-1})	$k_{-1(LepA \bullet GTP)}$ (s^{-1})	$k_{-1(LepA \bullet GDPNP)}$ (s^{-1})
LepA	4.2 ± 0.3	21 ± 4	127 ± 9
ΔA494	2.9 ± 0.5	28 ± 5	229 ± 14
ΔP520	3.4 ± 0.1	34 ± 12	417 ± 23
ΔG555	4.9 ± 0.9	14 ± 4	371 ± 76
H81A	2.8 ± 0.3	29 ± 1	185 ± 25
EF-G*	300*	7*	200*

*Data previously published (91)

In order to determine the association rate constants between LepA and guanine nucleotides, LepA was rapidly mixed with increasing concentrations of the respective mant-guanine nucleotide (Figure 2.6). All time courses showed a biphasic behaviour where the first phase was dependent on the concentration of guanine nucleotides and the second slower phase was independent of the guanine nucleotide concentration present. This is indicative of a binding event that is followed by a conformational change within LepA. Data were fit with a two-exponential equation (Eq. 2.3) to determine the apparent rates for each nucleotide concentration which were subsequently plotted as a function of the nucleotide concentration. The resulting slope of the linear concentration dependent

rate gave similar $k_{1(LepA \cdot GDP)}$ values for mant-GDP association to all LepA proteins (Table 2.4). Similar results were observed for the $k_{1(LepA \cdot GTP)}$ values for mant-GTP. The previously determined value of k_1 for mant-GTP and EF-G (0.58 ± 0.04 $\mu M^{-1}s^{-1}$) (91) is similar to that obtained here for LepA and mant-GTP (0.43 ± 0.04 $\mu M^{-1}s^{-1}$) (Table 2.4). Y-intercepts obtained from the $k_{1(LepA \cdot GDP/GTP)}$ plots are in agreement with $k_{-1(LepA \cdot GDP/GTP)}$ values determined in the above described dissociation experiments (Table 2.4) where the rate of mant-GTP dissociation is almost 10-fold faster than mant-GDP dissociation. Furthermore, K_D values obtained from k_{-1} / k_1 for mant-GTP and mant-GDP give micro-molar values (Table 2.5). However, the K_D values obtained for LepA proteins and mant-GDP is an order of magnitude lower than values for LepA and mant-GTP (Table 2.5). This is in disagreement with the equilibrium values obtained for LepA proteins and mant-GDP. In spite of this, results demonstrate that the LepA CTD truncation variants bind to guanine nucleotides with a similar affinity as wild type LepA.

The values obtained for k_2 were not dependent on guanine nucleotide concentration and were similar for all LepA proteins (Table 2.4). Furthermore, k_2 values were similar for LepA interacting with mant-GDP and mant-GTP.

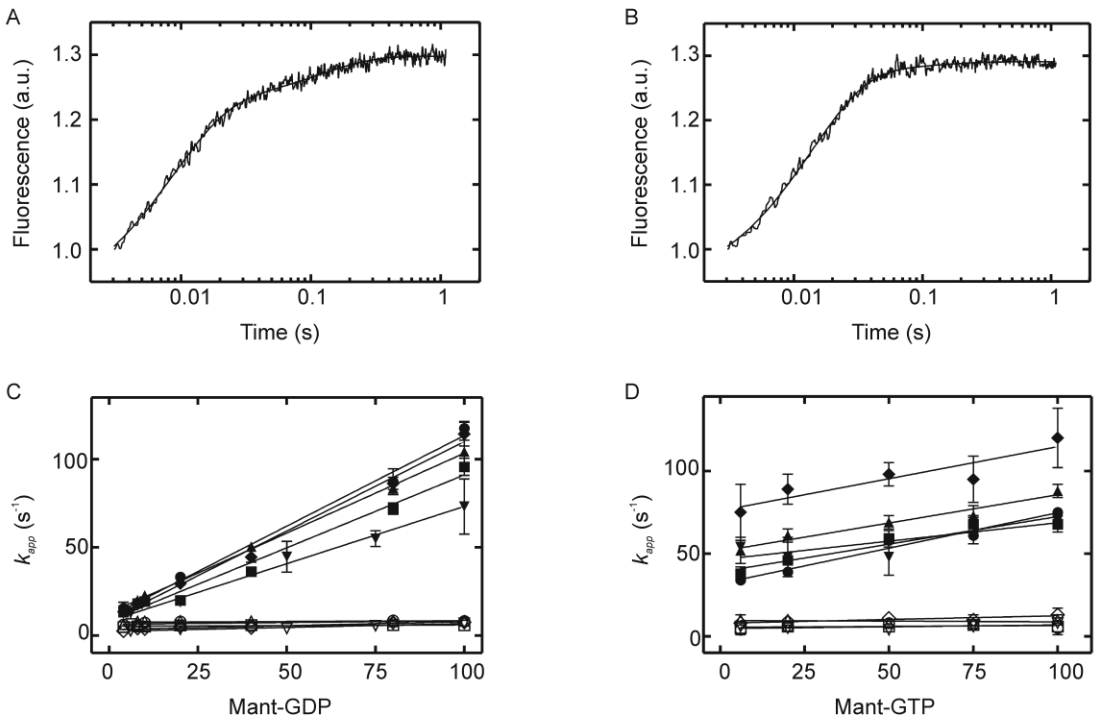

Figure 2.6. **Association kinetics for guanine nucleotides and LepA.** (A) Time course of mant-GDP (100 µM) association to LepA (2 µM) measured by FRET excitation of mant-GDP. (B) Time course of mant-GTP (100 µM) association to LepA (2 µM) measured by FRET excitation of mant-GTP. (C) Concentration dependence of k_{app} for mant-GDP and (D) mant-GTP calculated from the association time courses. LepA wild type (circles), ΔA494 (squares), ΔP520 (upright triangles), ΔG555 (diamonds) and H81A (downward triangles). Filled shapes represent k_{app1} and open are k_{app2}.

Table 2.4. Rate of Association Between LepA Variants and Mant-Guanine Nucleotides.

Protein	k_1 *(LepA•GDP)* ($\mu M^{-1}s^{-1}$)	k_{-1} *(LepA•GDP)* y-int (s^{-1})	k_2 *(LepA•GDP)* (s^{-1})	k_1 *(LepA•GTP)* ($\mu M^{-1}s^{-1}$)	k_{-1} *(LepA•GTP)* y-int (s^{-1})	k_2 *(LepA•GTP)* (s^{-1})
LepA	1.0±0.1	11±2	6.4±0.6	0.4±0.1	32±3	5.5±1.4
ΔA494	0.8±0.1	8±3	5.1±0.2	0.3±0.1	39±3	5.4±0.5
ΔP520	0.9±0.1	13±1	7.4±0.4	0.3±0.1	51±3	9.6±1.0
ΔG555	1.0±0.1	9±2	3.3±0.4	0.4±0.1	76±6	7.9±0.8
H81A	0.7±0.1	8±2	2.3±0.3	0.2±0.1	46±6	4.7±1.1
EF-G*	NA	NA	NA	0.6±0.1	NA	NA

*****Data previously published (91)

Table 2.5. Dissociation Constants (K_D) of LepA Variants and Mant-GDP/GTP Determined by Pre-Steady State Kinetics.

Protein	K_D Mant-GDP (μM)	K_D Mant-GTP (μM)
LepA	4.1 ± 0.3	50 ± 10
ΔA494	3.5 ± 0.6	85 ± 20
ΔP520	3.7 ± 0.1	100 ± 40
ΔG555	4.8 ± 0.9	40 ± 10
H81A	4.3 ± 0.5	130 ± 60

2.3c LepA Interaction with the Ribosome

The structure of LepA on the ribosome has revealed that LepAs CTD contacts the 23S rRNA (60). However, only approximately two thirds of the CTD (residues 480 – 545) have been resolved in the cryo-EM map of LepA bound to the ribosome (60). The contact between the CTD of LepA and the ribosome suggests that this domain may be involved in LepA binding to the ribosome. However, given that LepA interacts with the ribosome through other domains, the CTD may be dispensable for LepA-ribosome interaction.

Here an ultracentrifugation assay was utilized to assess whether truncating the CTD inhibits LepAs ability to bind to the 70S ribosome as well as to the individual 50S and 30S ribosomal subunits (Materials and Methods). To this end, a sucrose cushion was used to separate the ribosome/ribosome-bound LepA from the free LepA protein. Following ultracentrifugation, the presence of LepA in the ribosome pellet was assessed via immunoblotting (Materials and Methods).

The presence of all LepA proteins were detected in the 70S ribosomal pellet as well as the 50S and 30S ribosome subunit pellet, regardless of guanine nucleotide present, indicating that all CTD truncation variants of LepA are able to stably associate with the ribosome (Figure 2.7). Surprisingly, the association of LepA ΔG555 (shortest truncation) seems to be weaker than the other variants as a 5-fold higher protein concentration was needed to detect LepA ΔG555 in the ribosome pellet with comparable band intensity to the full length protein and the other truncated LepA variants (Figure 2.7d). Detection of LepA proteins in the pellet was not due to protein aggregation as LepA proteins could not be detected in the absence of the 70S ribosome or 50S or 30S ribosomal subunits. This suggests that binding of LepA to the ribosome is mainly achieved through the remaining domains of LepA interacting with the ribosome. Interestingly, a nucleotide dependence of this interaction is revealed in the differential intensity of the band corresponding to wild type LepA. Following ultracentrifugation with the 70S ribosome or 50S ribosomal subunit the LepA signal, indicative of the fraction of LepA bound, is lower in the presence of GDPNP than in the apo or GDP-bound states. This behaviour is not observed in the presence of the 30S ribosomal subunits. A similar nucleotide dependence is not

observed for the LepA variants including LepA H81A (Figure 2.7), suggesting a role for the CTD in nucleotide-dependent regulation of ribosome binding.

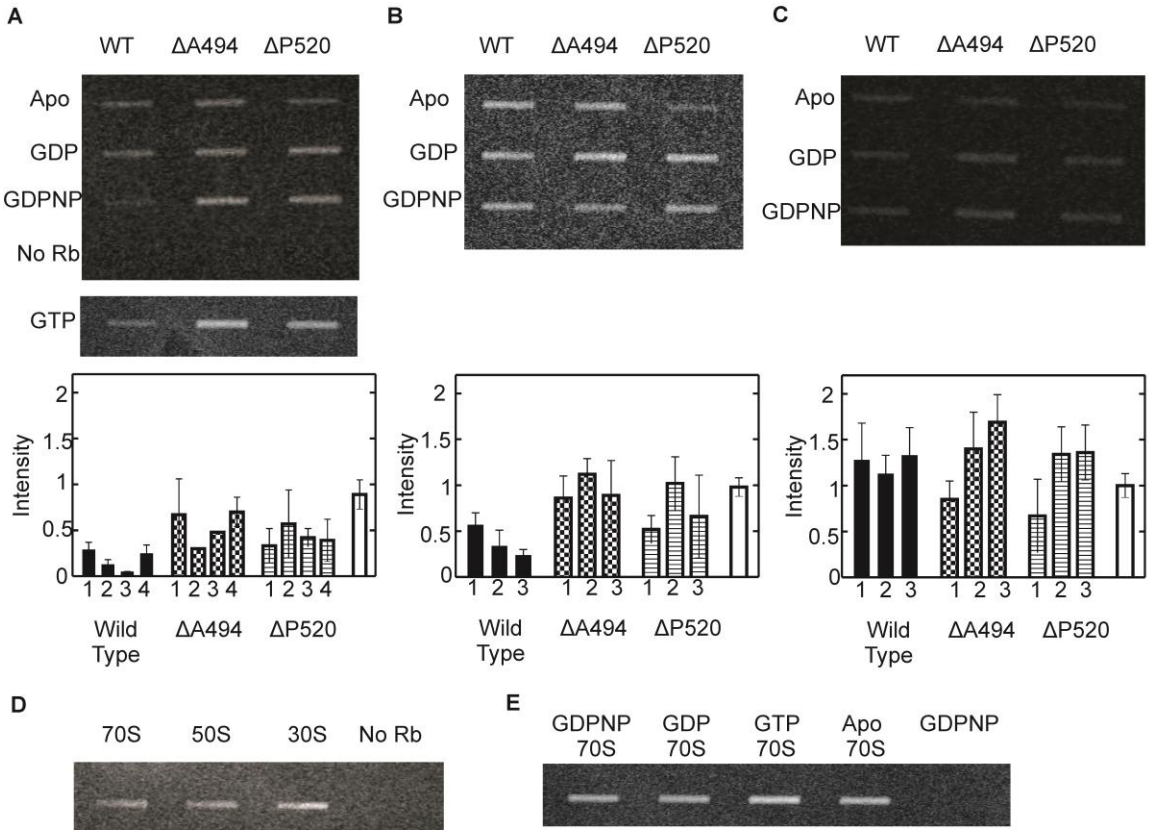

Figure 2.7. Immunodetection of LepA bound to the ribosome following ultracentrifugation. (A) LepA proteins (2 μM) (indicated on top) bound to the 70S (0.1 μM) ribosome in the presence of various guanine nucleotides (GTP, GDPNP, GDP (0.1 mM)) or apo indicated on the left. Pellet following ultracentrifugation of LepA proteins bound to GDPNP in the absence of ribosome is shown (No Rb). Intensity of each band compared to a standard (no fill) is represented as a bar graph below the corresponding immunoblot. LepA wild type (filled), ΔA494 (chequered), ΔP520 (striped) in the presence of (1) 70S, (2) 70S + GDP, (3) 70S + GDPNP and (4) 70S + GTP is represented. (B) LepA proteins (2 μM) bound to the 50S (0.1 μM) subunit in the presence of various guanine nucleotides (GDPNP, GDP (0.1 mM)) or apo. Intensity of each band compared to a standard (no fill) is represented as a bar graph below the corresponding immunoblot. LepA wild type (filled), ΔA494 (chequered), ΔP520 (striped) in the presence of (1) 50S, (2) 50S + GDP and (3) 50S + GDPNP is represented. (C) LepA proteins (2 μM) bound to the 30S (0.1 μM) subunit in the presence of various guanine nucleotides (GDPNP, GDP (0.1 mM)) or apo. Intensity of each band compared to a standard (no fill) is represented as a bar graph below the corresponding immunoblot. LepA wild type (filled), ΔA494 (chequered), ΔP520 (striped) in the presence of (1) 30S, (2) 30S + GDP and (3) 30S + GDPNP is represented. (D) LepA ΔG555 protein (10 μM) bound to the 70S, 50S and 30S (0.1 μM) in the presence of GDPNP (0.1 mM). (E) LepA H81A (2 μM) bound to the 70S (0.1 μM) in the presence of various guanine nucleotides (GDPNP, GDP, GTP (0.1 mM)) or apo indicated on top.

2.3d GTPase Activity of LepA

LepA is classified as a translational GTPase, however its intrinsic GTPase activity has not been characterised so far. Here the characterisation of the intrinsic GTPase activity of LepA and the CTD variants were examined (Figure 2.8). Michaelis-Menten kinetics were used to describe the intrinsic GTPase activity of LepA by determining the Michaelis constant (K_M), v_{max} and the k_{cat} for LepA and the respective variants. Consistent with a putative role of His 81 in the catalysis of GTP hydrolysis, no hydrolysis of GTP was observed over time in the presence of LepA H81A. Therefore, Michaelis-Menten parameters could not be determined for this variant. The K_M obtained for all LepA CTD truncation variants are consistently in the high micro-molar range (wild type LepA = 270 ± 90 µM, LepA ΔA494 = 370 ± 35 µM, LepA ΔP520 = 900 ± 200 µM and LepA ΔG555 = 700 ± 100 µM (Table 2.6)) and are significantly higher than the equilibrium binding constants (K_D) determined here for LepA and GTP. In addition, the K_M values are higher for the LepA CTD truncation variants than for wild type LepA. However, the obtained v_{max} and in turn the determined k_{cat} for LepA (0.003 ± 0.001 s^{-1}) and LepA variants (LepA ΔA494 = 0.005 ± 0.001 s^{-1}, LepA ΔP520 = 0.007 ± 0.001 s^{-1}, LepA ΔG555 = 0.003 ± 0.001 s^{-1}) are similar to each other, indicating that the CTD truncation variants are not impaired in their ability to hydrolyze GTP.

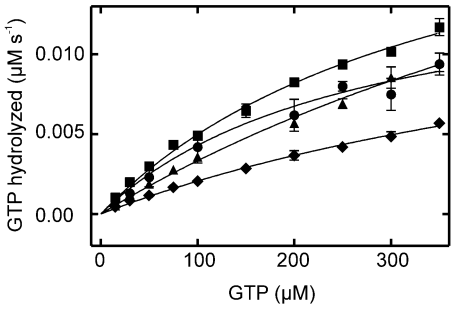

Figure 2.8. Michaelis-Menten titration of the intrinsic GTPase activity of LepA. Initial rates of GTP hydrolysis are plotted as a function of increasing GTP concentration in the presence of (5 μM) wild type (circles), ΔA494 (squares), ΔP520 (triangles), ΔG555 (diamonds).

Table 2.6. Intrinsic GTPase Activity of LepA Variants.

LepA	K_M (μM)	v_{max} (μM s^{-1})	k_{cat} (s^{-1})
Wild Type	270 ± 90	0.016 ± 0.003	0.003 ± 0.001
ΔA494	370 ± 35	0.023 ± 0.001	0.005 ± 0.001
ΔP520	900 ± 200	0.034 ± 0.006	0.007 ± 0.001
ΔG555	700 ± 100	0.017 ± 0.002	0.003 ± 0.001

The GTPase activity of LepA has previously been shown to be stimulated by the 70S ribosome to a similar extent as EF-G (56). However, no detailed kinetic parameters describing this interaction were reported, preventing the mechanistic interpretation of this interaction. The first detailed analysis of the ribosome-stimulated GTPase activity of LepA (Figure 2.9) performing a Michaelis-Menten analysis of wild type LepA and the CTD truncation variants is presented here. K_M and k_{cat} values obtained for full length LepA (0.32 ± 0.08 μM, 2.3 ± 0.3 s^{-1}) are similar to EF-G values (0.4 ± 0.1 μM, 2.7 ± 0.3 s^{-1}) (Table 2.7), which is consistent with the finding from the study by Knud Nierhaus and co-workers (56) and previous studies on EF-G (92). Interestingly, the K_M values obtained here for LepA CTD truncation variants are at least an order of magnitude

larger than values for the full length protein (LepA ΔA494 = 36 ± 26 μM, LepA ΔP520 = 10 ± 5 μM, LepA ΔG555 = 7 ± 3 μM). However, even though all CTD truncations variants exhibit a similar 10 to 100-fold effect on the K_M, the k_{cat} values obtained for the two larger deletions ΔA494 (5.2 ± 3.3 s^{-1}) and ΔP520 (5.3 ± 1.8 s^{-1}) are within error of those obtained for wild type LepA and EF-G. Surprisingly, the k_{cat} value obtained for the shortest deletion LepA ΔG555 (0.6 ± 0.2 s^{-1}) is 10-fold lower, reducing the stimulatory effect of the 70S ribosome from approximately 1000-fold to 100-fold.

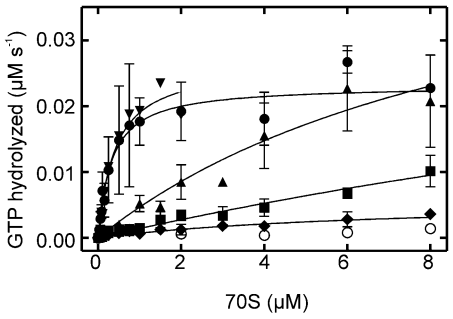

Figure 2.9. Michaelis-Menten titration of the ribosome stimulated GTPase activity of LepA. Initial rates of GTP hydrolysis are plotted as a function of increasing 70S ribosome concentration in the presence of (0.01 μM) LepA wild type (filled circles), EF-G (downward triangles), LepA ΔA494 (squares), LepA ΔP520 (upright triangles), LepA ΔG555 (diamonds), LepA H81A (open circles).

Table 2.7. 70S Stimulated GTPase Activity of LepA Variants.

Protein	**K_M (μM)**	**v_{max} (μM s^{-1})**	**k_{cat} (s^{-1})**
LepA	0.32±0.08	0.023±0.001	2.3±0.3
ΔA494	36±26	0.052±0.033	5.2±3.3
ΔP520	10±5	0.053±0.017	5.3±1.8
ΔG555	7±3	0.006±0.002	0.6±0.2
EF-G	0.40±0.10	0.027±0.002	2.7±0.3

2.3e Catalytic Histidine in LepA

Consistent with the observation that LepA contains a histidine residue (His 81) in a similar position as the catalytic His 84 of EF-Tu (68,70,71), substitution of His 81 in LepA resulted in the decrease of LepAs GTPase activity to background levels which could not be stimulated by the 70S ribosome (Figure 2.9). Therefore, like His 84 in EF-Tu, His 81 of *E. coli* LepA likely plays a key role in the mechanism of GTP hydrolysis by LepA.

2.4 Discussion

Many proteins and complexes that bind to the A site of the bacterial ribosome have very similar structures. For example, the structure of EF-G and the ternary complex of EF-Tu•GTP•aa-tRNA are extremely similar, a fact that has been termed molecular mimicry (93). Although LepA has a similar structure to EF-G (58), it does not contain a domain resembling domain (IV) of EF-G. Instead LepA contains a unique C-terminal domain that assumes a structure resembling a shorter version of EF-Gs domain IV. In this study, the role of LepAs unique CTD was examined with respect to binding guanine nucleotides, GTP hydrolysis and ribosome binding.

2.4a LepA and Guanine Nucleotides

Although LepA has been shown to be a highly conserved translational GTPase (56), its nucleotide binding properties have not been studied so far. Here it is shown that LepA has a micro-molar affinity for guanine nucleotides, which is similar to the structurally related translational GTPase EF-G (91).

Association and dissociation rate constants governing the interaction between LepA and mant-GDP/GTP have been reported here using a pre-steady-state kinetic analysis. The equilibrium binding constants (K_D) obtained from these values provide an estimate for the affinities and reveal that LepA has an approximately 10-fold higher affinity for mant-GDP than for mant-GTP. This is consistent with data obtained for EF-Tu, which also has a 10-fold higher affinity for GDP than for GTP (45). The difference in affinity between LepA and mant-GDP/GTP does not arise from differences in the association rate

constants, as mant-GTP and mant-GDP binding rates are similar to each other. However, a 10-fold faster dissociation of mant-GTP was observed, thus raising the K_D value 10-fold over that between LepA and mant-GDP. It was shown for EF-G that dissociation of mant-GDPNP is extremely fast (91) and approximately 10-fold faster than the dissociation of mant-GTP, which is similar to what is observed here for LepA. However, dissociation of mant-GDP from EF-G was also shown to be extremely fast and, unlike LepA, is faster than the dissociation of mant-GTP. The difference in the rate of mant-GDP dissociation from LepA and EF-G may be due to the presence of the G' domain within EF-G or its absence in LepA. The G' domain of EF-G has been shown to make contacts with its core G-domain (94) similar to contacts made between the GEF EF-Ts and EF-Tu. The two β-hairpins of the G' domain insert into the G-domain of EF-G. Furthermore, there are hydrogen bonds between residues in the G' domain of EF-G and residues involved in interacting with the guanine nucleotide in the G-domain. These contacts indicate that the presence of the G' domain in EF-G may act as a modulator for guanine nucleotide binding in EF-G as a GEF would. Both EF-Tu and LepA lack a G' domain. It has previously been observed for EF-Tu that GTP dissociation is 10-fold faster than GDP dissociation (45), which is similar to what is observed here for LepA. However, dissociation of guanine nucleotides from LepA occurs within seconds and is approximately 1000-fold faster than dissociation of guanine nucleotides from EF-Tu. This gives rise to a 1000-fold lower affinity between LepA and guanine nucleotides compared to EF-Tu and guanine nucleotides. The rapid dissociation of guanine nucleotides observed from LepA, will likely ensure the rapid turnover of the

bound nucleotide. Therefore, similar to EF-G, LepA most likely does not require a GEF to facilitate the rapid exchange of GDP for GTP.

Interestingly, time courses for the association kinetics revealed a two-step binding mechanism, a fast concentration dependent step and a slower step that was independent of guanine nucleotide concentration. This suggests a nucleotide binding mechanism that involves a first rapid binding event, likely followed by a conformational change (Figure 2.10). However, only one phase was observed for any guanine nucleotide dissociation which indicates that the reverse of the second conformational change is likely to rapid to detect (> 300 s^{-1}). Furthermore, the amplitudes for the two phases of association for either mant-GDP or mant-GTP are not equal. The fast phase has greater amplitude (9-fold higher with mant-GTP and 3-fold higher with mant-GDP) than the slower phase. This suggests that the majority of the LepA•guanine nucleotide complex exists in the initial binding complex. However, more of the *LepA*•GDP complex may exist than the *LepA*•GTP complex. This may also explain the discrepancy between the K_D values obtained from the pre-steady state data and the steady state data. Values determined for LepA and mant-GTP interaction are comparable due to the majority of the complex being in the LepA•GTP state. However values obtained for the interaction between LepA and mant-GDP may not correspond due to a mixture of the LepA•GDP and *LepA*•GDP complex.

Figure 2.10. Model of LepA interacting with guanine nucleotides. Based on the available pre-steady state kinetic analysis a two-step binding mechanism is proposed. GTP or GDP binds to LepA rapidly, followed by a conformational change in LepA (represented by the italic font).

2.4b The C-Terminal Domain of LepA is Involved in GTPase Activation on the Ribosome

In order to understand the molecular mechanism of LepA in terms of its function as a translational GTPase, it is important to unravel the specific roles of its individual domains. Given that the CTD of LepA is unique, it is of particular interest to understand the role of this domain within LepA, in particular with its role in binding to the ribosome. The CTD of LepA is not fully resolved in the structure obtained by X-ray crystallography and indicates that it is likely a flexible domain, which may contribute to its function (95). Three variants of *E. coli* LepA were constructed here that were sequentially truncated from the C-terminal end, and analyzed in their ability to interact with guanine nucleotides and the ribosome compared to wild type LepA.

The CTD does not affect the ability of LepA to interact with guanine nucleotides as the LepA CTD truncation variants (ΔA494, ΔP520 and ΔG555) bind to guanine nucleotides with similar affinities as wild type LepA. Furthermore, deletion of the CTD of LepA does not abolish binding to the ribosome as LepA•ribosome complexes are observed for all LepA variants and 70S, 50S and 30S ribosomal particles. This was somewhat surprising given that structural data on LepA shows that the part of the CTD that is resolved contacts the 23S rRNA (60). It was shown that BipA, which is structurally similar to

LepA and also contains a unique CTD, needs this unique CTD for ribosome binding (78). However, removal of domain IV in EF-G does not abolish binding between EF-G and the ribosome (81). This finding indicates that similar to EF-G, LepA utilizes contacts between all other domains and the ribosome to bind. However, the CTD seems to be needed for guanine nucleotide dependant binding of LepA to the ribosome. Furthermore, removal of the CTD seems to increase the amount of LepA bound to the ribosome compared to wild type. Given that the CTD contacts the ribosome, its fold or contacts with the ribosome may influence the fold or contacts between the rest of LepA and the ribosome. Therefore, the presence of the CTD may restrict or direct the overall contacts between LepA and the ribosome. This in turn may facilitate nucleotide dependant binding of LepA to the ribosome.

The CTD is not required for LepA to intrinsically hydrolyze GTP as all the CTD truncation variants of LepA can hydrolyze GTP with similar k_{cat} values as wild type LepA. The K_M values determined here are significantly higher than the K_D values obtained. Given that two phases are observed in guanine nucleotide binding, it is likely that there is at least another step involved, which may be a conformational change following guanine nucleotide binding, which could be required before GTP hydrolysis can occur. In addition, other translational GTPases have been shown to first hydrolyze GTP, release P_i and then release GDP, breaking product release into more than one step (43,96). Control of P_i release has been shown to be important for the downstream function of EF-G (96) and may be important for the function of LepA.

Although truncation of the CTD of LepA does not strongly impede ribosome binding or guanine nucleotide binding, it is required for efficient multiple turnover of GTP

hydrolysis on the ribosome. The LepA CTD truncation variants have a 10-fold higher K_M value than wild type LepA and EF-G. This indicates that the LepA variants can form a complex with the 70S ribosomes, but likely have a lower affinity for the ribosome than wild type. Although the CTD may not be essential for binding to the ribosome like the unique CTD domain in BipA (78), it may be important or contribute to tight interactions made between the ribosome and LepA. Also, given that the K_M values for all the CTD truncation variants are similar indicates that only the last 44 residues of LepA are important for LepA interaction with the ribosome as further truncation of the CTD does not additionally increase the K_M determined here.

Interestingly, the k_{cat} determined for ribosome stimulated GTPase activity of LepA ΔA494 and ΔP520 are similar to that of wild type LepA and EF-G values obtained here and elsewhere (91). However, the k_{cat} determined for ribosome stimulated GTPase activity of LepA ΔG555 was approximately a quarter that of wild type LepA and the other LepA variants. These results were surprising given that LepA ΔG555 has the least amount of the CTD removed. The residues deleted with this variant have not been resolved in the crystal structure (58) and are likely to be highly flexible. These results indicate that the last 44 residues of LepA are required for efficient ribosome-stimulated GTPase activity of LepA. However, when more of the CTD of LepA is removed, the turnover of GTP hydrolyzed in the presence of the ribosome is restored to that of wild type. This indicates that the presence of the last 44 residues within LepA may stabilize the rest of the CTD and promote proper folding of this domain. Removal of this flexible region in LepA may lead to an unstructured CTD or a fold which is different than that of full length and may inhibit the interaction between LepA and the ribosome. Interestingly,

the last 50 amino acids in the C-terminus of *E. coli* LepA are highly conserved (>80% similar) in sequence between the bacterial species aligned here. Therefore, removal of this conserved region may lead to different contacts made between the CTD and the ribosome, which in turn may inhibit ribosome stimulated GTPase activity of LepA. However, when more of the CTD is removed, there is no longer any CTD to inhibit the turnover of GTP. Domain IV of EF-G has been shown to be important, not only for rapid turnover of GTP hydrolysis by EF-G on the ribosome (81), but for the function of EF-G, which is to promote translocation (52). Therefore, the CTD may regulate the GTPase activity of LepA on the ribosome, which in turn may be important for the function of LepA.

These results in combination with the pelleting and immunoblotting results suggest that the CTD of LepA may act to regulate ribosome interaction with LepA and ribosome-stimulated GTPase activity of LepA. Based on the pelleting and immunoblotting results, there seems to be a difference in the amount of wild type LepA bound to the 70S whether GTP/GDPNP or GDP or no nucleotide is bound. Furthermore, there does not seem to be this distinction with the CTD truncation variants. This may indicate that the CTD needs to be present in order for the 70S ribosome to discriminate against the various guanine nucleotide-bound states of LepA. These results were surprising as the CTD is more than 20 Å away from the guanine nucleotide-binding domain. Comparison of the structure of LepA with that of the aa-tRNA•EF-Tu•GTP ternary complex indicates that there may be a role for the CTD of LepA in signalling GTPase activation (70). The signal pathway which leads to stimulation of EF-Tu GTPase activity is not fully understood, however, a communication pathway between the decoding center of the ribosome and the guanosine

triphosphate center of EF-Tu has been suggested (70). The contacts made between the CTD of LepA and the ribosome may be needed to communicate from the decoding center of the ribosome to the G-domain of LepA.

2.4c H81 is the Catalytic Histidine in LepA

It has been shown that histidine 84 within switch II of EF-Tu is important for the translational GTPase EF-Tu (68); however, this has not been confirmed in LepA. LepA contains a histidine (His 81) that is in a similar position as the catalytic histidine in EF-Tu. Furthermore, this histidine is 100% conserved in identity within the 43 bacterial species aligned here (Appendix Figure A.3). Substitution of His 81 to Ala did not significantly affect LepAs ability to bind to the ribosome or guanine nucleotides. Interestingly, this substitution did eliminate the differential binding between wild type LepA and the 70S ribosome in the presence of GTP/GDPNP or GDP/apo. This indicates that this substitution may also cause a conformational change in the G-domain of LepA which is needed for nucleotide dependant binding to the ribosome.

It has been assumed that a histidine located in switch II of translational GTPases is essential for GTPase activity. Data obtained here on the GTPase activity of LepA on and off the ribosome demonstrated that substitution of His 81 severely affects the GTPase activity of LepA, suggesting that His 81 in LepA plays a key role during GTP hydrolysis. Structural studies of EF-Tu bound to the ribosome show that His 84 interacts with A2662 of the 23S rRNA (70,97). This contact may be important, not only in the positioning of the nucleophilic water, but in the overall interaction made with the ribosome.

2.5 Future Directions

Here, effects of LepAs unique CTD and histidine 81 in LepA have been analyzed in terms of their effect on LepAs interaction with guanine nucleotides and the ribosome.

The function of LepA *in vivo* is still not understood. Although LepA is only found in low amounts in bacterial cells and eukaryotic cell organelles (mitochondria and chloroplasts), it is highly conserved (56). It has been shown that the presence of LepA is beneficial under certain stress conditions. However, the functional mechanism of how LepA functions as a GTPase in the cell is unknown. Furthermore, it is unknown whether the ability of LepA to hydrolyze GTP is necessary for the results observed *in vivo* under stress. The functional importance of GTP hydrolysis by LepA can be analyzed by utilizing the LepA H81A variant in knockout *lepA* strains. This will demonstrate whether GTPase activity of LepA is important for its cellular function in the cell during stress conditions.

While it has previously been shown that LepA can catalyze back-translocation (56) as well as forward translocation (67), it is not clear how or when this is carried out in the cell. Given that LepA is a translational GTPase that binds to the A site of the ribosome, it is possible that under stress conditions LepA increases in abundance and targets specific ribosome complexes in an effort to rescue the cell. Given that the only LepA-ribosome contacts that are different than the EF-G-ribosome contacts are between LepA and its unique CTD, it is likely that this domain is utilized in ribosome differentiation between LepA and other proteins which bind to the A site. *In vivo* experiments comparing wild type LepA to these CTD truncation variants and their ability to rescue cells under stress

would give further insight into the functional importance of this unique domain. In addition, the unique CTD in LepA may be used to assist LepA in differentiating between various ribosomal complexes in order to target a specific complex. In an effort to understand if LepA only targets specific ribosomal complexes, it would be interesting to analyze complex formation between various ribosomal complexes, such as Pre and Post-translocated ribosomal complexes, and how the deletion of the CTD of LepA affects this interaction.

Interestingly, 16% of the residues in *E. coli* LepA are cysteine (Appendix Figure A.2). This percentage is significantly higher than for *E. coli* EF-G, which is comprised of only 4% cysteine residues. An alignment of bacterial LepA primary sequences (Appendix Figure A.3 and Table A.2) shows that most bacterial LepA sequences contain 10-20% cysteine residues. It is known that cysteine residues may stabilize the structure of proteins through disulfide bridges (98). Based on the crystal structure of LepA, all cysteine residues are too far apart from each other to form any disulfide bonds. However, some are surface exposed and may form a disulfide bond with another LepA protein, forming a dimer. This may indicate that LepA exists as a dimer until it interacts elsewhere for function or that it may function as a dimer.

Cysteine residues are also involved in enzyme catalysis (99). Four of the 10 cysteine residues in *E. coli* LepA are found to be more than 80% conserved in identity in the alignment of bacterial species performed here (Appendix Table A.2). It is possible that one or all of these cysteines play a role in the functional mechanism of LepA.

Mutagenesis on each cysteine residue in *E. coli* LepA has been performed (Appendix Table A.2). Given that LepA has a high abundance of cysteine residues, it would be interesting to analyze whether these have a role on the ability of LepA to function.

Chapter 3

A Tail of Two Proteins; The C-terminal Module of EF-Ts Alters Nucleotide Exchange in EF-Tu.

3.1 Introduction

3.1a The Function of EF-Tu

Elongation Factors are essential proteins found in all kingdoms of life, and these factors are among the most abundant proteins in any given cell (85). EF-Tu represents up to 5% of the total cellular protein in *E. coli* (85). It is a 43 kDa protein consisting of three domains (Figure 3.1). Domain 1 is the guanine nucleotide binding domain (G-domain) with a consensus Rossmann fold, while domains 2 and 3 each consist of anti-parallel β-barrels (44,69). The G-domain contains five regions of high sequence conservation on the amino acid level that are present in all GTPases (GTPase sequence motifs) (21). These five elements (G1 to G5 sequence motifs) mediate interactions with the guanine nucleotide; G1 is the P-loop which coordinates phosphates of the bound nucleotide, while G2 and G3 form switch I and part of the switch II region, respectively. Switch regions are aptly named as they undergo conformational changes when the protein changes from the GTP to the GDP-bound form. The G4 and G5 motifs coordinate the guanine moiety of the nucleotide.

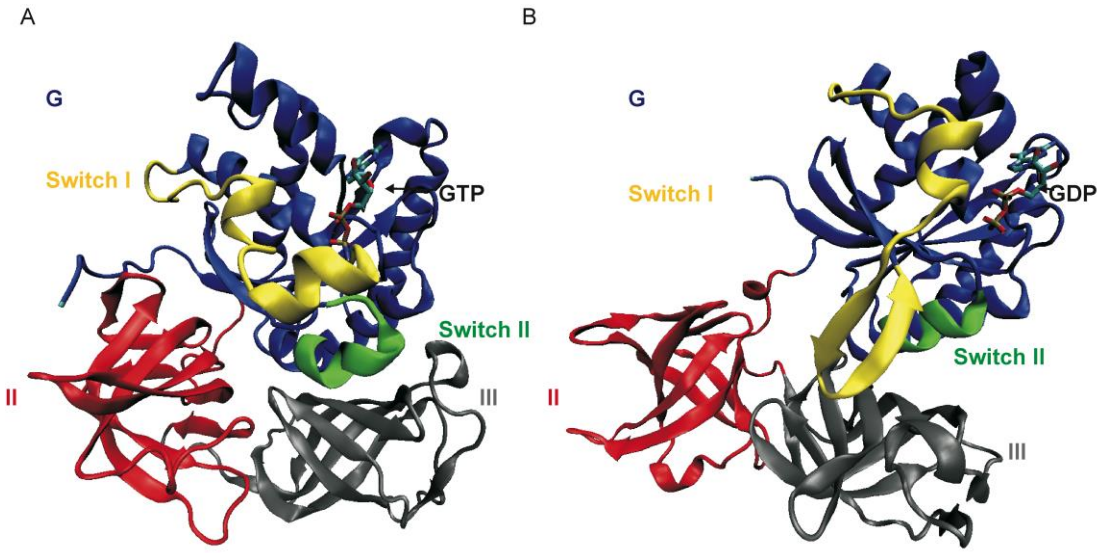

Figure 3.1. Structures of EF-Tu bound to GTP and GDP. Structure of (A) *Thermus aquaticus* EF-Tu with a bound GTP (PDB ID 1EFT (69)) and (B) *E. coli* EF-Tu with a bound GDP (PDB ID 1EFC (44)) determined by X-ray crystallography. The guanine nucleotide is shown in stick representation. EF-Tu is represented in cartoon with domain I coloured in blue, domain II coloured in red and domain III shown in grey. Switch I and switch II regions within domain I are highlighted in yellow and green respectively.

When bound to GTP, EF-Tu has a high affinity for aa-tRNA ($K_D \approx 1 \times 10^{-8}$ M (100)) and forms a ternary complex (TC) (EF-Tu•GTP•aa-tRNA) (Figure 3.2) that can interact with the ribosome (initial binding of the TC to the ribosome has a $K_D \approx 6 \times 10^{-7}$ M (41)). The structure of EF-Tu bound to Phe-tRNA^{Phe} has been determined by X-ray crystallography and shows that all domains of EF-Tu interact with aa-tRNA (101). Domains 1 and 2 interact with the CCA-aa end of the aa-tRNA which protects the aa-ester bond from hydrolysis. The 5'-end of the aa-tRNA binds to the 3-domain-junction of EF-Tu, while the T-stem of the aa-tRNA makes contacts with domain 3 of EF-Tu.

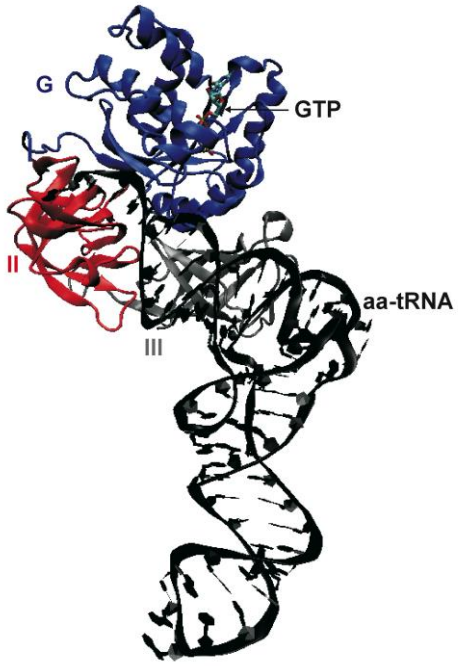

Figure 3.2. Structure of EF-Tu bound to aa-tRNA. Structure of *T. aquaticus* EF-Tu bound to GTP and to yeast Phe-tRNA^{Phe} (PDB ID 1TTT (101)) determined by X-ray crystallography. EF-Tu and GTP are represented as in figure 3.1, while Phe-tRNA^{Phe} is shown in black and by ribbon representation.

Codon dependent delivery of aa-tRNA to the 70S ribosome by EF-Tu is comprised of several steps that have been previously studied (42). X-ray crystallographic structures of the TC bound to the ribosome reveal that EF-Tu binds to the ribosome near the sarcin-ricin loop on the large (50S) ribosomal subunit (70). Initial binding of the TC to the ribosome is followed by codon recognition between the mRNA codon located in the 30S ribosomal A site and the aa-tRNA anticodon. Correct codon-anticodon recognition greatly stabilizes the TC on the ribosome and activates a signal that is transmitted to the G-domain of EF-Tu through a poorly understood mechanism. Structural and biochemical studies of EF-Tu indicate that the phosphate of A2662, which is located in the sarcin-ricin loop of the 23S rRNA, positions histidine 84 of EF-Tu towards the attacking water

(97). In this "active" conformation, the catalytic His 84 can act as a general base in catalyzing a nucleophilic water attack on the gamma-phosphate of the EF-Tu-bound nucleotide (97).

Following GTP hydrolysis and P_i release (42,43), EF-Tu undergoes a large conformational change (44,69) where domain 1 rotates approximately 90° relative to domains 2 and 3, resulting in an open conformation. Rotation of the domains within EF-Tu causes all the aa-tRNA binding sites to move apart (44). The affinity of EF-Tu•GDP for aa-tRNA is thus lowered by two orders of magnitude compared to EF-Tu•GTP ($K_{D(EF\text{-}Tu\bullet GDP)} \approx 1 \times 10^{-6}$M, $K_{D(EF\text{-}Tu\bullet GTP)} \approx 1 \times 10^{-8}$ M (100)). This decrease in affinity leads to the release of aa-tRNA from EF-Tu and the subsequent accommodation of aa-tRNA into the 50S ribosomal A site.

The intrinsic rate of GDP release from EF-Tu is extremely slow (45). In order to accelerate GDP dissociation from EF-Tu, a guanine nucleotide exchange factor (GEF) is needed (46). The GEF for EF-Tu is EF-Ts, facilitating rapid conversion of EF-Tu to its active GTP-bound state required for the rates of protein synthesis (~ 12 amino acids/s (102)) observed *in vivo*.

The three dimensional structure of *E. coli* EF-Tu bound to EF-Ts (47) revealed the contacts between these two proteins (Figure 3.3). Domain 3 of EF-Tu interacts with subdomain C of EF-Ts, while domain 1 (G-domain) of EF-Tu interacts with subdomain N, the N-terminal domain and the C-terminal module of EF-Ts. The interaction with EF-Ts induces movement of EF-Tus helix D away from the nucleotide-binding site so that the ribose and guanine base are no longer stabilized by residues in this helix. EF-Ts

binding to EF-Tu further disrupts the phosphate-binding loop and induces movement of helix B. This disruption breaks the interactions between residues in helix B of EF-Tu and water molecules coordinating the Mg^{2+} ion that is needed to stabilize the bound nucleotide. Structural and biochemical studies have shown that these interactions enhance the rate of GDP dissociation from EF-Tu by a factor of 60 000 (45,103). In this manner EF-Ts enables the rapid turnover of active EF-Tu. The intracellular concentration of GTP is ten times higher than that of GDP (48) and GTP binding to EF-Tu•EF-Ts disrupts this interaction, giving rise to an EF-Tu•GTP complex, allowing another aa-tRNA to bind, forming a new ternary complex able to participate in the elongation cycle.

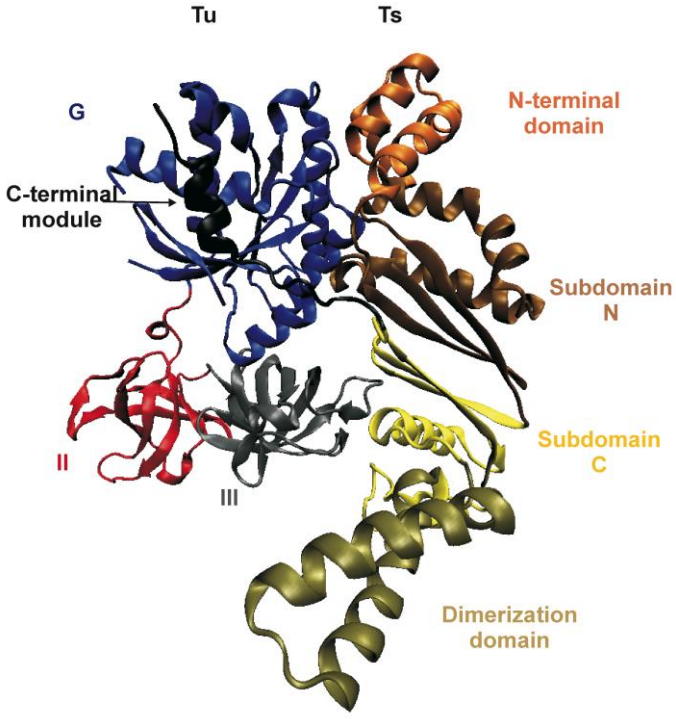

Figure 3.3. Structure of EF-Tu bound to EF-Ts. Structure of *E. coli* EF-Tu bound to EF-Ts (PDB ID 1EFU (47)) determined by X-ray crystallography. EF-Tu is represented as in figure 3.1. EF-Ts is represented in cartoon with the N-terminal domain coloured orange, subdomain N coloured brown, subdomain C coloured yellow, the dimerization domain (coiled-coil) coloured tan and the C-terminal module coloured black.

3.1b Nucleotide Exchange in EF-Tu

The kinetic mechanism of EF-Ts catalyzed nucleotide exchange in EF-Tu has been analyzed in great detail in the model systems of *E. coli* and *S. cerevisiae* (45,104). The homologue of EF-Tu in eukaryotes, eEF1A, has been shown to bind GDP and GTP with an affinity that is 100-fold lower than that of *E. coli* EF-Tu (104). However, even though the rate of GDP dissociation from eEF1A is 100-fold faster than in *E. coli* EF-Tu, it is still not fast enough to maintain the required *in vivo* protein synthesis rates (~ 10 amino acids/s (105)).

The structures of the two nucleotide exchange factor complexes have been determined previously for the eukaryotic (with the C-terminal catalytically active domain of eEF1Bα) and the prokaryotic system (47,106). Although both GEFs disturb the Mg^{2+} to lower the affinity for the guanine nucleotide, these structures reveal two different modes of interaction for the exchange factors in the prokaryotic and eukaryotic system. The C-terminal region of eEF1Bα docks onto domain I of eEF1A and accelerates the rate of GDP dissociation from eEF1A 60-fold (104), which is significantly less than the prokaryotic system, but enough to facilitate *in vivo* rates of protein synthesis. Furthermore, the contacts made between eEF1A and its exchange factor differ between the prokaryotic and eukaryotic factor. eEF1Bα interacts with the opposite side of eEF1A than EF-Ts with EF-Tu (Figure 3.4). As a result, there is no contact made between domain III of eEF1A and eEF1Bα. The N-terminal half of eEF1Bα interacts with domain II of eEF1A, whereas there are no contacts made between EF-Ts and domain II in the prokaryotic EF-Tu. A similar system for nucleotide exchange also exists in mitochondria

where the respective mitochondria specific EF-Ts_{mt} is also required to assist in the rapid dissociation of GDP from mitochondrial EF-Tu_{mt}. The structure of the bovine EF-Tu_{mt}•EF-Ts_{mt} complex (107) determined by X-ray crystallography revealed a three dimensional arrangement very similar to the bacterial complex (Figure 3.4). Even though the amino-terminus of EF-Ts_{mt} makes similar contacts with EF-Tu_{mt} as in the bacterial system, EF-Ts in mitochondria lacks the coiled-coil motif present in bacteria. It was previously shown that deletion of the coiled-coil motif in EF-Ts from *E. coli* reduces the ability of EF-Ts to catalyze the dissociation of guanine nucleotides (108) as well as decrease the stability of the EF-Tu•EF-Ts complex. The lack of a coiled-coil domain in mitochondrial EF-Ts_{mt} indicates that it uses other parts to function, such as its amino-terminus. In addition, EF-Tu_{mt} has a lower affinity for guanine nucleotides (109), which may have abolished the need for the coiled-coil domain in EF-Ts_{mt}.

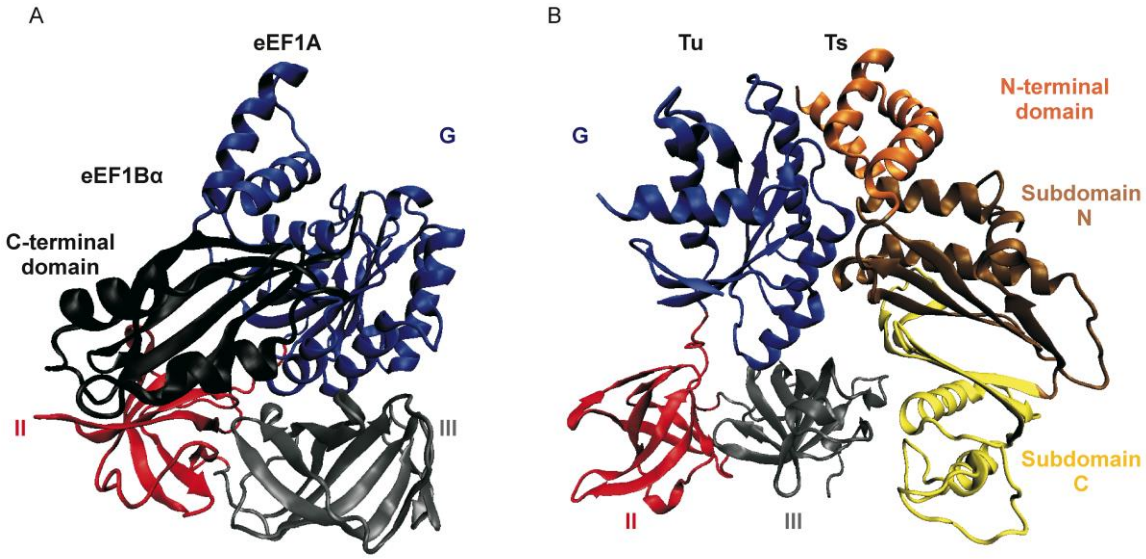

Figure 3.4. Structures of the eEF1A•eEF1Bα and the EF-Tu_{mt}•EF-Ts_{mt} complex. Crystal structure of (A) Yeast eEF1A bound to the C-terminal domain of eEF1Bα represented in cartoon (PDB ID 1F60 (110)). eEF1A is coloured as EF-Tu in figure 3.1 and eEF1Bα is coloured in black. (B) Mitochondrial EF-Tu bound to EF-Ts is represented in cartoon (PDB ID 1XB2 (107)). EF-Tu is coloured as in figure 3.1 and EF-Ts is coloured as in figure 3.3.

3.1c Divergence of EF-Ts

EF-Ts is essential for maintaining protein synthesis rates *in vivo* in *E. coli* (111). In spite of this, EF-Ts is highly divergent in sequence among different species. The question then is if the divergence in the primary sequence of EF-Ts affects the function of EF-Ts to act as a GEF.

Similar to *E. coli, Pseudomonas aeruginosa* is a gram-negative bacteria. *P. aeruginosa* is an opportunistic pathogen and is a current concern for public health. EF-Ts from these two bacterial species share 55% sequence identity, which is high in comparison to other species. A comparative analysis on the ability of EF-Ts to catalyze guanine nucleotide dissociation from EF-Tu was performed here between *E. coli* and *P. aeruginosa*. Both species of EF-Ts can stimulate the rate of guanine nucleotide dissociation from the species-specific EF-Tu to a similar extent, however EF-Ts from *P. aeruginosa* seems to catalyze the exchange of guanine nucleotides in EF-Tu more efficiently than EF-Ts from *E. coli*. Analysis of the differences in the interactions between EF-Tu and EF-Ts show an extension of the C-terminal module of EF-Ts from *P. aeruginosa* compared to EF-Ts from *E. coli*. Examination of the C-terminal module of EF-Ts suggests that it can modulate the rate of guanine nucleotide dissociation from EF-Tu, revealing a novel regulatory element present in EF-Ts.

3.2 Materials and Methods

3.2a Molecular Biology

The ORF for *tufA* from *P. aeruginosa* genomic DNA was PCR amplified in a reaction catalyzed by Phusion polymerase (Finnzymes) using primers 5'-AGA GGA TCC CTG TCG TGG CTA AAG GA-3' and 5'- ATG GCA GGA GCT CCG ATT ACT CGA-3'. The underlined nucleotides denote *Bam*HI and *Sac*I restriction sites engineered into the primers. All restriction enzymes used were purchased from Fermentas. The ORF for *tsf* from *P. aeruginosa* genomic DNA was similarly amplified, using primers 5'- TTC CAT ATG GCA GAA ATT ACT GCA GC-3' and 5'- CAG TCG AAT TCG TCT TTG TTA CTG-3', with engineered *Nde*I and *Eco*RI restriction sites respectively. The resulting PCR products were ligated into *Sma*I digested pUC19 (New England BioLabs) using T4 DNA ligase (Invitrogen). The ligation mixture was transformed into subcloning efficiency *E. coli* DH5α cells (New England BioLabs), which were grown at 37°C on LB-agar plates supplemented with 100 µg/mL ampicillin and 50 µg/mL 5-bromo-4-chloro-3-indolyl-β-D-galactopyranoside (X-gal, Rose Scientific). Blue-white selection and restriction analysis were utilized to isolate cells containing recombinant plasmids (designated pUC*PatufA* and pUC*Patsf*), which were further propagated for plasmid isolation. ORFs were excised using the respective restriction endonucleases and ligated into similarly digested pET28a for *PatufA* and *Patsf*, creating plasmids pET*PatufA* and pET*Patsf*. Plasmids were transformed into *E. coli* DH5α competent cells and grown in LB media, supplemented with 50 µg/mL kanamycin, for plasmid propagation. Sequence

and orientation was confirmed by DNA sequencing (Macrogen DNA Sequencing Services).

pET21a (pKECAHIS) (112) containing the full-length sequence coding for a C-terminal His_6-tagged EF-Tu from *E. coli* was utilized. A construct for EF-Ts from *E. coli* (pHK1Ts) was expressed as a fusion protein with an intein self-splicing element on the C-terminus and chitin binding domain as in (45). The plasmid (pCA24N) containing the *tsf* gene from *E. coli* encoding for EF-Ts with an N-terminal His_6-tag was obtained from the ASKA library of clones (113).

3.2b Mutagenesis

Substitution of Gln 283 to a Met was introduced via site-directed mutagenesis carried out on the pET28a-*Patsf* template using the Quickchange™ method (Stratagene). Primers (forward primer 5'-GCT GCT GAA GTT GCC GCT **ATG** GTA GCC GCC ACC AAG C-3' and reverse primer 5'-GCT TGG TGG CGG CTA CCA **TAG** CGG CAA CTT CAG CAG C-3') were obtained from Integrated DNA Technologies (IDT). The position of mutagenesis is denoted in bold; underlined nucleotides denote the *Acu*1 restriction site (5'-CTGAAG-3') which was inserted via a silent mutation. Reactions were carried out under the following conditions: 25 μL of the reaction mixture contained 1000 ng of template, 0.4 μM of primer pair, 0.4 mM of each dNTP and 3 units of DNA polymerase (TruPfu, Truin Science Ltd.). The reaction was initiated by pre-heating the reaction mixture to 95°C for 5 min followed by 18 cycles of 95°C for 45 s, 55°C for 1 min and 68°C for 15 min followed by a final extension at 68°C for 15 min.

The C-terminal deletion in EF-Ts$_{P.a.}$ was constructed by inserting a stop codon via site-directed mutagenesis as described above. Primers (forward primer 5'-GCC GCT CAA **T<u>AA</u>** <u>GCT T</u>CC ACC AAG C-3' and reverse primer 5'-GCT TGG TGG <u>AAG C</u>**<u>TT</u> A**TT GAG CGG C-3') were obtained from Integrated DNA Technologies (IDT). The position of mutagenesis is denoted in bold; underlined nucleotides denote the *Hind*III restriction site (5'-AAGCTT-3') which was inserted via a silent mutation. Reactions were carried out under the following conditions: 25 μL of the reaction mixture contained 1000 ng of template, 0.4 μM of primer pair, 0.4 mM of each dNTP and 3 units of DNA polymerase (TruPfu, Truin Science Ltd.). The reaction was initiated by pre-heating the reaction mixture to 95°C for 5 min followed by 18 cycles of 95°C for 45 s, 50°C for 1 min and 68°C for 25 min followed by a final extension at 68°C for 25 min.

EF-Ts$_{E.c.P.a.}$ C-terminal chimera was constructed via site-directed mutagenesis carried out on the pHk1Ts via site-directed mutagenesis as above. Primers (forward primer 5'-GTT GCT G<u>CC ATG **G**</u>**TA GCC GCC ACC AAG CAG** TGC TTT GCC AAG G-3' and reverse primer 5'-CCT TGG CAA AGC A**CT GCT TGG TGG CGG CTA <u>C</u>**<u>CA TGG</u> CAG CAA C -3') were obtained from Integrated DNA Technologies (IDT). The position of mutagenesis is denoted in bold; underlined nucleotides denote the *Nco*I restriction site (5'-CCATGG-3') which was inserted via a silent mutation. Reactions were carried out under the following conditions: 25 μL of the reaction mixture contained 1000 ng of template, 0.4 μM of primer pair, 0.4 mM of each dNTP and 3 units of DNA polymerase (TruPfu, Truin Science Ltd.). The reaction was initiated by pre-heating the reaction mixture to 95°C for 5 min followed by 18 cycles of 95°C for 45 s, 55°C for 1 min, 68°C for 20 min followed by a final extension at 68°C for 20 min.

The PCR-amplification products were analyzed on a 1% agarose gel at 80V for 80 min. Products were transformed into *E. coli* DH5α (New England Biolabs) competent cells for propagation and *E. coli* BL21-DE3 (New England Biolabs) for expression. The mutations were confirmed by sequencing (GeneWiz Inc).

3.2c Protein Expression and Purification

EF-Tu and all EF-Ts variants derived from *P. aeruginosa* were expressed in *E. coli* (strain BL21-DE3 (Novagen)) containing the respective plasmid. Cells were grown at 37°C in LB medium supplemented with 50 μg/mL kanamycin to mid-log phase (OD_{600} = 0.6) and induced with 1 mM IPTG (BioBasic). Cells were grown for an additional 3 hrs at 37°C, harvested by centrifugation (5000 × *g* for 10 min at 4°C) and stored at -80°C.

EF-Tu from *E. coli* was expressed in LB supplemented with 100 μg/mL ampicillin and EF-Ts from *E. coli* (obtained from the ASKA collection) expressed in LB supplemented with 30 μg/mL of chloramphenicol. EF-Ts variants derived from *E. coli* (pHK1Ts) were grown at 37°C in LB medium supplemented with 100 μg/mL ampicillin. Cells containing the respective plasmid were grown to mid-log phase (OD_{600} = 0.6) and induced with 1 mM IPTG. Following induction the temperature was reduced to 25°C for 2 hrs, then to 16°C overnight. Cells were harvested by centrifugation as described above.

To analyze protein expression, one OD_{600} samples were taken every 30 min, lysed with 8 M urea in buffer 3.1 (50 mM Tris-Cl pH 7.5 (20°C), 70 mM NH_4Cl, 30 mM KCl and 7 mM $MgCl_2$) and analyzed by 12% SDS-PAGE at 80 V for 30 min, then 200 V for

60 min (BioRad Mini Protean 3 System). Gels were stained with Coomassie Brilliant blue; all other SDS-PAGEs were performed in a similar manner.

Similar purification procedures were followed for EF-Tu from *E. coli* (pKECAHIS) and *P. aeruginosa* (pET*PatufA*) as well as EF-Ts variants from *P. aeruginosa* (pET*Patsf*) and EF-Ts from *E. coli* obtained from ASKA cloning. Cell pellets (approximately 10 g) were resuspended in 7 mL of buffer 3.2 (50 mM Tris-Cl pH 8.0 (4°C), 60 mM NH_4Cl, 7 mM $MgCl_2$, 300 mM KCl, 7 mM BME, 1 mM PMSF, 10 mM imidazole, 15% glycerol and 50 µM GDP) per gram of cells and lysed with 1 mg/mL lysozyme. Cell debris were removed through centrifugation at 3000 x *g* for 30 min followed by 30 000 x *g* for 45 min using a JA-16 rotor (Beckman). The respective protein was purified from the cleared lysate (S30 extract) using affinity chromatography (7 mL Ni^{2+}-Sepharose resin (GE Healthcare) equilibrated with buffer 3.2). The resin was washed 3 times with 50 mL of buffer 3.2 and 4 times with 50 mL of buffer 3.3 (buffer 3.2 with 20 mM imidazole). The protein was then eluted in 10 washes of 7 mL buffer 3.4 (buffer 3.2 with 250 mM imidazole). The obtained His_6-tagged protein was then concentrated via ultrafiltration (Vivaspin 20, 30 000 MWCO for EF-Tu and Vivaspin 20, 10 000 MWCO for EF-Ts (Sartorius)) and further purified by SEC (XK26/100 column; Superdex 75 prep grade (GE Healthcare)) equilibrated in buffer 3.1. Fractions were analyzed by SDS-PAGE, and those containing protein that were >90% pure were pooled and concentrated via ultrafiltration (*vide supra*) and stored at -80°C. The final protein concentration was determined spectrophotometrically at 280 nm using a molar extinction coefficient of 32 900 M^{-1} cm^{-1} for all EF-Tu proteins (calculated using ProtParam (88)) and confirmed using the Bradford Protein Assay (BioRad). Due to the fact that EF-Ts does not contain

any tryptophan residues, protein concentration was determined using the Bradford Protein Assay.

EF-Ts variants from *E. coli* (pHk1Ts) were purified using the following method. Cell pellets (approximately 10 g) were resuspended in 7 mL of buffer 3.5 (25 mM Tris-Cl pH 7.5 (4°C), 50 mM NH_4Cl, 10 mM $MgCl_2$, 0.1% PMSF, and 50 µM GDP) per gram of cells and lysed with 1 mg/mL of lysozyme. Cell debris was removed through centrifugation as above to obtain a cleared lysate (S30 extract). The respective protein was purified from the cleared lysate using affinity chromatography (5 mL chitin beads (New England BioLabs)) equilibrated with buffer 3.5. The resin was washed 3 times with 50 mL of buffer 3.5 and five times with 50 mL of buffer 3.6 (20 mM Tris-Cl pH 8.0 (4°C), 50 mM NH_4Cl, 0.1 mM EDTA and 50 µM GDP). Approximately 20 mL of buffer 3.7 (20 mM Tris-Cl pH 8.0 (4°C), 50 mM NH_4Cl, 0.1 mM EDTA, 60 mM DTT and 400 mM KCl) was added to the column and was incubated for approximately 30 hrs at room temperature. The EF-Ts protein was eluted with 8 washes of 4.5 mL buffer 3.8 (20 mM Tris-Cl pH 8.0 (4°C), 50 mM NH_4Cl, 0.1 mM EDTA, 400 mM KCl and 50 µM GDP). Elutions containing EF-Ts were pooled and concentrated via ultrafiltration (Vivaspin 20, 10 000 MWCO (Sartorius)) and subsequently subjected to SEC (XK26/100 column; Superdex 75 prep grade (GE Healthcare)) equilibrated in buffer 3.1 to further purify the protein. Fractions were analyzed by SDS-PAGE and those containing protein with a purity of >90% were pooled, concentrated via ultrafiltration (*vide supra*) and stored at -80°C for further use. The final EF-Ts protein concentration was determined using the Bradford Protein Assay. The purities of the protein preparations used in this work are summarized on the SDS-PAGE in Appendix Figures A.4 and A.5.

To promote the dissociation of GDP, which is tightly bound to EF-Tu and co-elutes with the factor during purification, EF-Tu•GDP was incubated in buffer 3.9 (25 mM Tris-Cl, pH 7.5 (20°C), 50 mM NH_4Cl, 10 mM EDTA) for 30 min at 37°C. GDP and EF-Tu were separated using SEC (Acorn 10/300 GL column; Superdex 75 (GE healthcare)) equilibrated in buffer 3.10 (25 mM Tris-Cl pH 7.5 (4°C), 50 mM NH_4Cl). To prepare the respective EF-Tu•EF-Ts complexes, EF-Tu•GDP was incubated with equimolar amount of EF-Ts in buffer 3.9 and subsequently purified using SEC as described above for purification of EF-Tu•GDP.

3.2d Preparation of EF-Tu•mant-GDP, EF-Tu•mant-GTP

EF-Tu•GDP was incubated with a 10-fold molar excess of mant-GDP or mant-GTP in buffer 3.1 for 30 min at 37°C. When mant-GTP was used, the incubations were carried out in the presence of 3 mM PEP and 0.1 mg/mL PK (Roche Diagnostic) to convert any nucleotide di-phosphate present into the nucleotide tri-phosphate form (114).

3.2e Rapid Kinetic Measurements

Fluorescence stopped-flow measurements were performed using a KinTek SF-2004 stopped-flow apparatus, as described in (90). Tryptophan fluorescence was excited at 280 nm and measured after passing through LG-305-F cut-off filters (NewPort). Mant-nucleotides were excited via FRET from the single tryptophan (λ_{ex} = 280 nm) present in EF-Tu and measured after passing through LG-400-F cut-off filters (NewPort).

The apparent rate for the bimolecular association of mant-nucleotides to nucleotide free EF-Tu was determined by rapidly mixing 25 μL of nucleotide free *E. coli* EF-Tu$_{E.c.}$ (0.3 μM after mixing) or 25 μL of nucleotide free *P. aeruginosa* EF-Tu$_{P.a.}$ (0.5 μM after mixing) with 25 μL of varying concentrations of mant-nucleotides (ranging from 1 to 10 μM after mixing). Experiments were carried out at 20°C in buffer 3.1. Fluorescence time courses were evaluated by fitting with a single exponential equation (Equation 3.1).

$$F = F_{\infty} + A \times \exp(-k \times t) \qquad \text{(Equation 3.1)}$$

Where F is the fluorescence at time t, F_{∞} is the fluorescence signal at equilibrium. *k* is the apparent rate constant of association (k_{app}) measured independently for each guanine nucleotide concentration. The apparent rate constants were then plotted as a function of nucleotide concentration.

The apparent rate for the bimolecular association of nucleotides to nucleotide free EF-Tu•EF-Ts was determined by rapidly mixing 25 μL of nucleotide free EF-Tu•EF-Ts (0.5 μM after mixing) with 25 μL of varying concentrations of guanine nucleotides (ranging from 2.5 to 1000 μM after mixing) at 20°C in buffer 3.1. Fluorescence time courses of tryptophan emission were fit with equation 3.1 and k_{app} values obtained were plotted as a function of increasing guanine nucleotide concentration. Previous analysis of *E. coli* EF-Tu has demonstrated that at low concentrations of GTP the slope of the line is given by equation 3.2 (45). At low concentrations of GDP the slope of the line is given by equation 3.3.

$$\text{Slope} = k_7 / (1 + k_{-7}/k_{-6}) \qquad \text{(Equation 3.2)}$$

$$\text{Slope} = k_4 / (1 + k_{-4}/k_{-3}) \qquad \text{(Equation 3.3)}$$

Dissociation rate constants were determined by rapidly mixing 25 μL EF-Tu•mant-GTP/mant-GDP (0.3 μM after mixing) with 25 μL GTP/GDP (30 μM after mixing) at 20°C in buffer 3.1. Under these conditions only the dissociation of mant-labelled nucleotide contributed to the observed fluorescence change as the presence of excess unlabelled nucleotide prevents the rebinding of mant-nucleotide. The observed fluorescence time courses were fit with Eq. 3.1, yielding *k* as the respective dissociation rate constant (k_{-1}, k_{-5} for GDP and GTP, respectively). Using similar conditions, the dissociation of mant-GTP/mant-GDP from 25 μL EF-Tu•mant-GTP/GDP (0.3 μM after mixing) was stimulated with 25 μL of varying concentrations of EF-Ts (1 to 20 μM after mixing) at 20°C in buffer 3.1. The observed fluorescence time courses were fit with Eq. 3.1, thus providing the apparent rates for nucleotide dissociation in the presence of different concentrations of EF-Ts. The apparent rates for nucleotide dissociation in the presence of the different EF-Ts concentrations were plotted as a function of increasing EF-Ts concentration. At low concentrations of EF-Ts, the initial slope of k_{app} for mant-GTP dissociation is given by equation 3.4 and mant-GDP dissociation is given by equation 3.5.

$$\text{Slope} = k_6 / (1 + k_{-6}/k_{-7}) \qquad \text{(Equation 3.4)}$$

$$\text{Slope} = k_3 / (1 + k_{-3}/k_{-4}) \quad \text{(Equation 3.5)}$$

To determine the association rate constants (k_2) for the EF-Tu-EF-Ts interaction, increasing concentrations of EF-Ts (1 to 5 µM final) were mixed with EF-Tu (1µM final) and the resulting decrease in tryptophan fluorescence was observed as a function of time. The resulting linearly concentration dependence of the observed association rates gave the respective k_2 from the slope. Subsequently k_{-2} can be calculated based on the law of mass action from either the GTP or the GDP branch of the scheme in figure 3.5 using equations 3.6 and 3.7.

$$k_{-2} = k_{-5}k_2k_{-6}k_7 / (k_5k_6k_{-7}) \quad \text{(Equation 3.6)}$$

$$k_{-2} = k_{-1}k_2k_{-3}k_4 / (k_1k_3k_{-4}) \quad \text{(Equation 3.7)}$$

Calculations were performed using TableCurve (Jandel Scientific) and Prism (GraphPad Software).

3.2f Sequence alignment

Protein primary sequences for EF-Ts and EF-Tu were obtained from the Swiss-Prot database (115). More than 40 bacterial sequences were aligned using ClustalW (116) to assess the conservation of EF-Tu and EF-Ts. Alignments were analyzed using GeneDoc (117). Percent identity for every amino acid was calculated based on the number of

identical residues present in the alignment and percent similarity was calculated based on conserved substitutions of residues observed in the alignment.

3.3 Results

The interaction of EF-Tu with guanine nucleotides has been studied extensively in the model systems of *E. coli* (45) and yeast (104). However, no kinetic data is available for pathogenically relevant organisms such as *P. aeruginosa*. As *E. coli* and yeast are typical model systems, it is implied that findings in these model systems also translate to other organisms. In order to investigate if this holds true within bacteria, the kinetic mechanism of nucleotide exchange in *P. aeruginosa* has been determined here and compared to the rate constants in the *E. coli* system. These results will allow a better understanding of the similarities and differences between the *P. aeruginosa* and the *E. coli* nucleotide exchange mechanism. The kinetic mechanism of EF-Ts stimulated guanine nucleotide exchange in EF-Tu is depicted in Figure 3.5. In this mechanism, EF-Tu can bind to GDP (k_1), GTP (k_5) or EF-Ts (k_2) and can subsequently dissociate. EF-Ts can interact with the EF-Tu•guanine nucleotide complex and stimulate the dissociation of guanine nucleotide from EF-Tu.

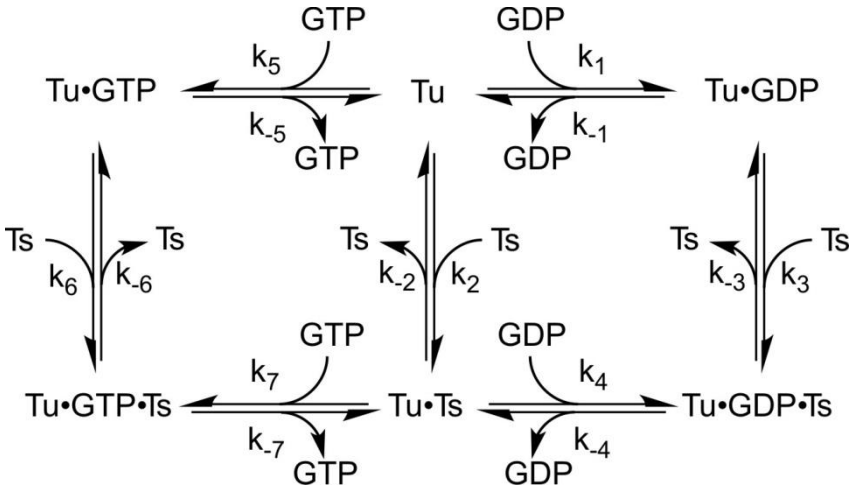

Figure 3.5. Kinetic mechanism of nucleotide exchange in EF-Tu catalyzed by EF-Ts.

3.3a Interaction of GDP/GTP with EF-Tu (k_1, k_{-1}, k_5, k_{-5})

The rate constants for guanine nucleotide association and dissociation in the absence of EF-Ts were determined using a stopped-flow apparatus by measuring FRET between a single tryptophan in EF-Tu$_{P.a.}$ (Trp 40) or EF-Tu$_{E.c.}$ (Trp 184) and the mant-group on mant-GTP/mant-GDP. Nucleotide dissociation rate constants for the EF-Tu•mant-GDP (k_{-1}) and the EF-Tu•mant-GTP (k_{-5}) complexes were determined by mixing with excess GDP or GTP. Mant-GTP or mant-GDP dissociation from EF-Tu occurs with an exponential fluorescence decrease (Figure 3.6). The dissociation rate constants k_{-1} and k_{-5} for GDP and GTP were directly obtained by fitting the observed time courses with a single-exponential function (Eq. 3.1) and are summarized in Table 3.1. The values obtained for both GTP and GDP dissociation rate constants for EF-Tu$_{P.a.}$ ($k_{-1} = 0.0007 \pm 0.0001$ s^{-1}, $k_{-5} = 0.007 \pm 0.001$ s^{-1}) are slightly lower than for EF-Tu$_{E.c.}$ (k_{-1} 0.0018 ± 0.0001 s^{-1}, $k_{-5} = 0.013 \pm 0.001$ s^{-1}). The rates of dissociation from EF-Tu$_{E.c.}$ is consistent with previous reports (45).

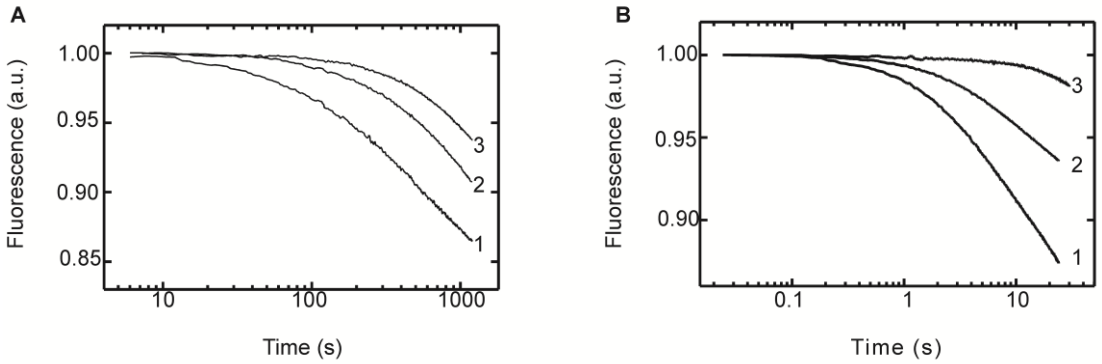

Figure 3.6. Dissociation of mant-GTP and mant-GDP from EF-Tu. (A) Time course of (1) EF-Tu$_{E.c.}$•mant-GDP complex (0.3 μM) dissociation in the presence of excess unlabelled GDP (30 μM) (2) EF-Tu$_{P.a.}$•mant-GDP complex (0.3 μM) dissociation in the presence of excess unlabelled GDP (30 μM). (3) Mant-GDP (3 μM) alone. (B) Time course of (1) EF-Tu$_{E.c.}$•mant-GTP complex (0.3 μM) dissociation in the presence of excess unlabelled GTP (30 μM) (2) EF-Tu$_{P.a.}$•mant-GTP complex (0.3 μM) dissociation in the presence of excess unlabelled GTP (30 μM). (3) Mant-GTP (3 μM). The fluorescence of the mant group was monitored following excitation through the intrinsic tryptophan residue in EF-Tu.

Table 3.1. Kinetic Parameters Governing the Nucleotide Interaction with EF-Tu.

Constant	EF-Tu$_{P.a.}$	EF-Tu$_{E.c.}$
k_{-1} (s^{-1})	0.0007 ± 0.0001	0.0018 ± 0.0001
k_1 ($M^{-1}s^{-1}$)	(1.5 ± 0.1) x 10^6	(1.3 ± 0.1) x 10^6
k_{-5} (s^{-1})	0.007 ± 0.001	0.013 ± 0.001
k_5 ($M^{-1}s^{-1}$)	(1.2 ± 0.1) x 10^6	(0.4 ± 0.1) x 10^6
K_1 (nM)	0.5 ± 0.1	1.4 ± 0.1
K_5 (nM)	6 ± 1	30 ± 10

The rates of nucleotide association were measured at varying concentrations of mant-GTP or mant-GDP using a constant concentration of nucleotide-free EF-Tu (Figure 3.7). The respective apparent rate constants (k_{app}) at different nucleotide concentrations were determined from the fluorescence time courses by fitting with a single-exponential function (Eq. 3.1). The linear dependence of k_{app} on the concentration of mant-GTP/mant-GDP (Figure 3.7) was used to determine the respective association rate constants (k_1 and k_5 for GDP and GTP, respectively). Values were determined for EF-Tu$_{E.c.}$ (k_1 = (1.3 ± 0.1) x 10^6 $M^{-1}s^{-}1$, k_5 = (0.4 ± 0.1) x 10^6 $M^{-1}s^{-1}$) and EF-Tu$_{P.a.}$ (k_1 = (1.5 ± 0.1) x 10^6 $M^{-1}s^{-}1$, k_5 = (1.2 ± 0.1) x 10^6 $M^{-1}s^{-1}$) (summarized in Table 3.1).

These results indicate a 2-fold increase in the rate of mant-GTP association observed for EF-Tu$_{P.a.}$, but no difference was observed between the mant-GDP association rate constants for EF-Tu$_{P.a.}$ and EF-Tu$_{E.c.}$.

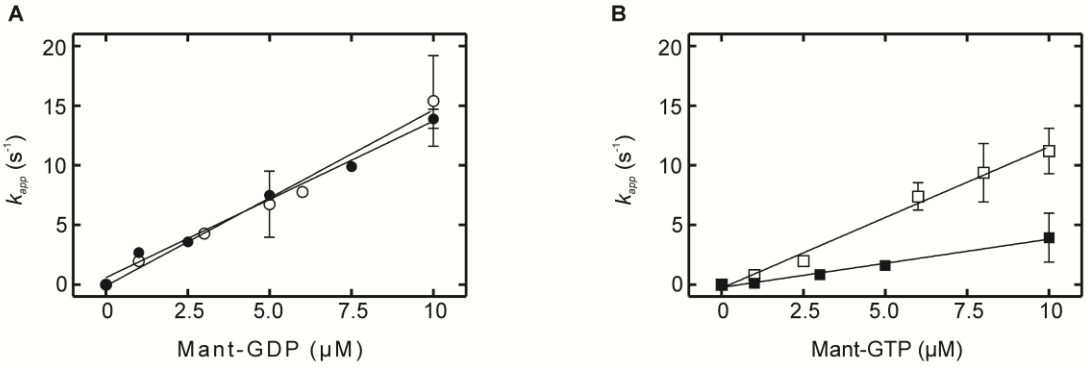

Figure 3.7. Association of mant-GDP and mant-GTP to EF-Tu. The concentration dependence of the respective apparent rate constants are plotted against increasing concentrations of (A) mant-GDP or (B) mant-GTP. (A) mant-GDP association to EF-Tu$_{E.c.}$ (0.3 μM) is shown as filled circles or to EF-Tu$_{P.a.}$ (0.5 μM) is shown as open circles. (B) mant-GTP association to EF-Tu$_{E.c.}$ (0.3 μM) is shown as filled squares or to EF-Tu$_{P.a.}$ (0.5 μM) shown as open squares.

Based on the above rate constants, the equilibrium dissociation constants (K_D) can be calculated from k_{-1}/k_1 and k_{-5}/k_5 (summarized in Table 3.1) revealing a 5-fold (GTP) and a 3-fold (GDP) higher affinity of EF-Tu$_{P.a.}$ ($K_{D(GTP•TuP.a.)}$ = 6 ± 1 nM, $K_{D(GDP•TuP.a.)}$ = 0.5 ± 0.1 nM) for the respective nucleotides when compared to EF-Tu$_{E.c.}$ ($K_{D(GTP•TuE.c.)}$ = 30 ± 10 nM, $K_{D(GDP•TuE.c.)}$ = 1.4 ± 0.1 nM).

3.3b Interaction of EF-Tu with EF-Ts in the presence of GTP

E. coli EF-Tu has a 10-fold higher affinity for GDP than for GTP (45). Although the concentration of GTP in the cell is 10-fold higher than that of GDP (48), GDP dissociation from EF-Tu is too slow (within minutes) to maintain the rates of protein

synthesis observed *in vivo.* EF-Ts stimulates the low intrinsic rate of guanine nucleotide dissociation from the EF-Tu•nucleotide complex by at least 5000-fold (45). The interaction of EF-Tu•GDP or EF-Tu•GTP with EF-Ts can be described by two consecutive steps (k_3,k_{-3},k_4,k_{-4} or k_6,k_{-6},k_7,k_{-7} in Figure 3.5). These two coupled equilibria represent the formation of the EF-Tu•nucleotide•EF-Ts ternary complex, followed by the release of the bound nucleotide (GDP or GTP).

To study the EF-Ts-catalyzed dissociation of GTP from EF-Tu•GTP, experiments were carried out with mant-GTP (Materials and Methods). Upon mixing pre-formed EF-Tu•mant-GTP complex with EF-Ts, mant-GTP dissociates with an observed single-exponential behavior. At low concentrations of EF-Ts, k_{app} increased linearly, indicating the formation of the ternary complex (EF-Tu•mant-GTP•EF-Ts). At high concentrations of EF-Ts, the rate of the reaction reaches saturation and equals the rate constant for GTP dissociation from the ternary complex, k_{-7} (Figure 3.8a). In order to assess the interchangeability of GEF EF-Ts from *E. coli* and *P. aeruginosa*, the experiment was performed with EF-$Tu_{E.c.}$•mant-GTP in the presence of EF-$Ts_{E.c.}$ or EF-$Ts_{P.a.}$ as well as with EF-$Tu_{P.a.}$•mant-GTP in the presence of EF-$Ts_{E.c.}$ or EF-$Ts_{P.a.}$ Analysis of the data gives values for $k_{-7(TuE.c.•mantGTP•TsE.c.)} = 125 \pm 20\ s^{-1}$; $k_{-7(TuE.c.•mantGTP•TsP.a.)} = 280 \pm 90\ s^{-1}$; $k_{-7(TuP.a.•mantGTP•TsE.c.)} = 5 \pm 1\ s^{-1}$; $k_{-7(TuP.a.•mantGTP•TsP.a.)} = 40 \pm 2s^{-1}$ (summarized in Table 3.2). It should be noted that at high concentrations of EF-$Ts_{P.a.}$ (>4 μM), dissociation of mant-GTP from EF-$Tu_{E.c.}$ was two-exponential. Not surprisingly, mant-GTP dissociation from EF-$Tu_{P.a.}$ was efficiently catalyzed 5000-fold by EF-$Ts_{P.a.}$, similar to the *E. coli* system. Dissociation of mant-GTP from EF-$Tu_{P.a.}$ is only catalyzed 500-fold by EF-$Ts_{E.c.}$. Interestingly, mant-GTP dissociation from EF-$Tu_{E.c.}$ is increased by 5000-fold with

EF-Ts$_{E.c.}$ and 10 000-fold with EF-Ts$_{P.a.}$. This indicates that EF-Ts$_{P.a.}$ is able to stimulate GTP dissociation to a greater extent than EF-Ts$_{E.c.}$ with either EF-Tu present.

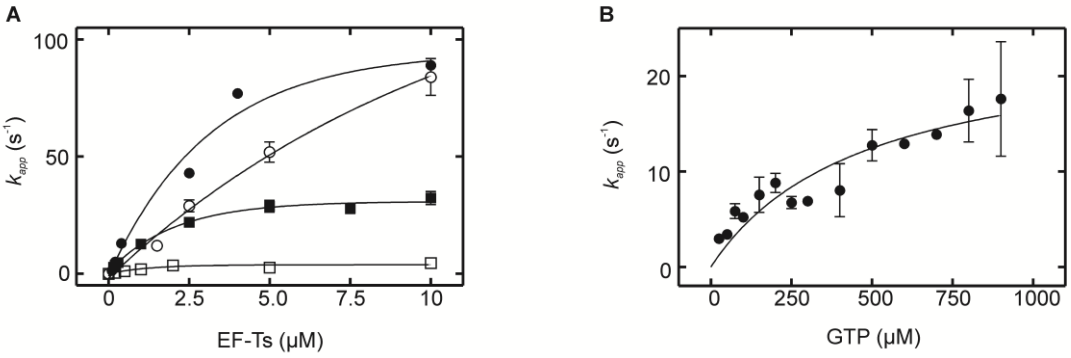

Figure 3.8. Interaction of EF-Tu with GTP and EF-Ts. (A) Concentration dependence of the rate of nucleotide dissociation (k_{app}) as a function of increasing EF-Ts concentrations. EF-Tu$_{E.c.}$•mant-GTP dissociated by EF-Ts$_{E.c.}$, shown as filled circles. EF-Tu$_{E.c.}$•mant-GTP dissociated by increasing EF-Ts$_{P.a.}$ is shown as open circles. EF-Tu$_{P.a.}$•mant-GTP dissociated by EF-Ts$_{P.a.}$ shown as filled squares. EF-Tu$_{P.a.}$•mant-GTP dissociated by increasing EF-Ts$_{E.c.}$ is shown as open squares. (B) Concentration dependence of the rate of EF-Tu$_{E.c.}$•Ts$_{P.a.}$ (0.5 μM) dissociation (k_{app}) calculated by single-exponential fitting from time courses of EF-Tu$_{E.c.}$•Ts$_{P.a.}$ (0.5 μM) against increasing GTP concentrations (0 – 1000 μM).

When stimulating EF-Tu•GTP dissociation at low concentrations of EF-Ts, the initial slope of the titration curve is equal to $k_6/(1 + k_{-6}/k_{-7})$ (Eq. 3.4) allowing for the calculation of k_6 when k_{-6} is known. In order to determine k_{-6}, GTP was titrated against a fixed concentration of the purified EF-Tu•EF-Ts complex. The change in the intrinsic tryptophan fluorescence of EF-Tu reflects the dissociation of EF-Ts from the transiently formed EF-Tu•GTP•EF-Ts complex. The rates of EF-Ts dissociation were determined from the time courses using single-exponential fits and plotted as a function of increasing GTP concentration (Figure 3.8b). At saturating concentrations of GTP, where rebinding of EF-Ts is negligible and EF-Ts dissociation is not limited by GTP binding, the value of k_{-6} is estimated to be 24 ± 5 s^{-1} for the EF-Tu$_{E.c.}$•EF-Ts$_{P.a.}$ complex (Table 3.3). This is slower than the previously reported rate for the EF-Tu$_{E.c.}$•EF-Ts$_{E.c.}$ complex (60 s^{-1} (45)).

The initial slope of the curve is equal to $k_7/(1 + k_{-7}/k_{-6})$ (Eq. 3.2), giving a value for GTP association to the EF-Tu•EF-Ts complex, k_7 equal to approximately 5 x 10^5 $M^{-1}s^{-1}$ for the EF-$Tu_{E.c.}$•EF-$Ts_{P.a.}$ complex which is 10-fold less than the EF-$Tu_{E.c.}$•EF-$Ts_{E.c.}$ complex (6 x 10^6 $M^{-1}s^{-1}$ (45)) (Table 3.3). The association rate constant for EF-Ts binding to EF-Tu•GTP (k_6) is determined to be approximately 1.2 x 10^7 $M^{-1}s^{-1}$ for the EF-$Tu_{E.c.}$•EF-$Ts_{P.a.}$ complex, which is 3-fold less than the EF-$Tu_{E.c.}$•EF-$Ts_{E.c.}$ complex (3 x 10^7 $M^{-1}s^{-1}$ (45)) (Table 3.3). Therefore, the determined constant for EF-Ts interacting with the EF-Tu•GTP complex (K_6) are comparable whether EF-$Ts_{E.c.}$ or EF-$Ts_{P.a.}$ is present. However, the constant describing the interaction of GTP with the EF-Tu•EF-Ts complex (K_7) is significantly higher (more than 10-fold) in the presence of EF-$Ts_{P.a.}$.

Due to the location of the tryptophan residue within EF-$Tu_{P.a.}$, no change in the tryptophan signal in EF-$Tu_{P.a.}$ was observed for EF-Tu•EF-Ts induced dissociation upon GTP binding. Therefore, k_{-6}, k_6 and k_7 could not be determined for the EF-$Tu_{P.a.}$•EF-$Ts_{P.a.}$ or the EF-$Tu_{P.a.}$•EF-$Ts_{E.c.}$ complex.

3.3c Interaction of EF-Tu with EF-Ts in the presence of GDP

The interactions of EF-Tu, EF-Ts, and GDP were studied in the same way as described above for GTP (Section 3.3b). Dissociation of GDP from EF-Tu in the presence of EF-Ts was monitored by the fluorescence of mant-GDP. Titrations were performed at constant concentrations of EF-Tu•mant-GDP and increasing concentrations of EF-Ts in the presence of excess unlabelled nucleotide (Figure 3.9a). k_{-4} was determined at saturating conditions of EF-Ts. Rates are summarized in Table 3.2;

($k_{-4(TuE.c.•mant\text{-}GDP•TsE.c.)}$ = 220 ± 20 s^{-1}; $k_{-4(TuE.c.•mant\text{-}GDP•TsP.a.)}$ = 450 ± 60 s^{-1}; $k_{-4(TuP.a.•mant\text{-}GDP•TsE.c.)}$ = 10 ± 1 s^{-1}; $k_{-4(TuP.a.•mant\text{-}GDP•TsP.a.)}$ = 40 ± 10 s^{-1}. It should be noted that at high concentrations of EF-Tu (>4 μM), dissociation of mant-GDP was two-exponential. This indicates that similar to the GTP case, EF-$Ts_{P.a.}$ stimulates the rate of GDP dissociation from EF-$Tu_{E.c.}$ 2-fold faster than EF-$Ts_{E.c.}$. EF-$Ts_{P.a.}$ enhances the rate of GDP dissociation from EF-$Tu_{P.a.}$ by more than 50 000-fold. However, EF-$Ts_{E.c.}$ is not able to stimulate the rate of GDP dissociation from EF-$Tu_{P.a.}$ to a similar extent (approximately 15 000-fold). Therefore, EF-$Ts_{P.a.}$ stimulates GDP dissociation from either EF-Tu more efficiently than EF-$Ts_{E.c.}$.

Similar to the GTP case, when stimulating dissociation of the EF-Tu•GDP complex by low concentrations of EF-Ts, the initial slope of the titration curve is equal to $k_3/(1 + k_{-3}/k_{-4})$ (Eq. 3.5). In order to determine the EF-Ts association rate constant to the EF-Tu•GDP complex (k_3) the stimulated GDP dissociation from EF-Tu by EF-Ts (k_{-4}) and the dissociation of EF-Ts from the ternary complex, k_{-3} were determined. To determine k_{-3}, GDP was titrated against a fixed concentration of the purified EF-Tu•EF-Ts complex and the change in the intrinsic tryptophan fluorescence of EF-Tu reporting the dissociation of EF-Ts was monitored. The rates of EF-Ts dissociation were determined from the resulting time courses by fitting with a single-exponential equation and subsequent analysis of the GDP concentration dependence of the respective apparent rates (Figure 3.9b). As determined at saturating concentrations of GDP, the value of k_{-3} is approximately 150 s^{-1} for the EF-$Tu_{E.c.}$•EF-$Ts_{P.a.}$ complex (Table 3.3). This value is lower than the previously reported rate for the EF-$Tu_{E.c.}$•EF-$Ts_{E.c.}$ complex (350 s^{-1} (45)). The initial slope of the curve is equal to $k_4/(1 + k_{-4}/k_{-3})$ (Eq. 3.3), giving a value of k_4 equal to

approximately 5 x 10^6 $M^{-1}s^{-1}$ for the EF-$Tu_{E.c.}$•EF-$Ts_{P.a.}$ complex which is one half that of the EF-$Tu_{E.c.}$•EF-$Ts_{E.c.}$ complex (1.4 x 10^7 $M^{-1}s^{-1}$ (45)) (Table 3.3). For the EF-$Tu_{E.c.}$•EF-$Ts_{P.a.}$ complex, k_3 is approximately 2 x 10^7 $M^{-1}s^{-1}$ which is 3-fold less than for the EF-$Tu_{E.c.}$•EF-$Ts_{E.c.}$ complex (6 x 10^7 $M^{-1}s^{-1}$ (45)) (Table 3.3). These results give K_3 values which are similar whether EF-$Ts_{E.c.}$ or EF-$Ts_{P.a.}$ is present. However, K_4 in the presence of EF-$Ts_{P.a.}$ is higher than that with EF-$Ts_{E.c.}$.

Again, the location of the tryptophan residue within EF-$Tu_{P.a.}$ did not allow for a detectable change in the tryptophan signal for EF-$Tu_{P.a.}$ upon GDP induced dissociation of the EF-Tu•EF-Ts complex. Therefore, k_{-3}, k_3 and k_4 could not be determined for the EF-$Tu_{P.a.}$•EF-$Ts_{P.a.}$ or the EF-$Tu_{E.c.}$•EF-$Ts_{E.c.}$ complex.

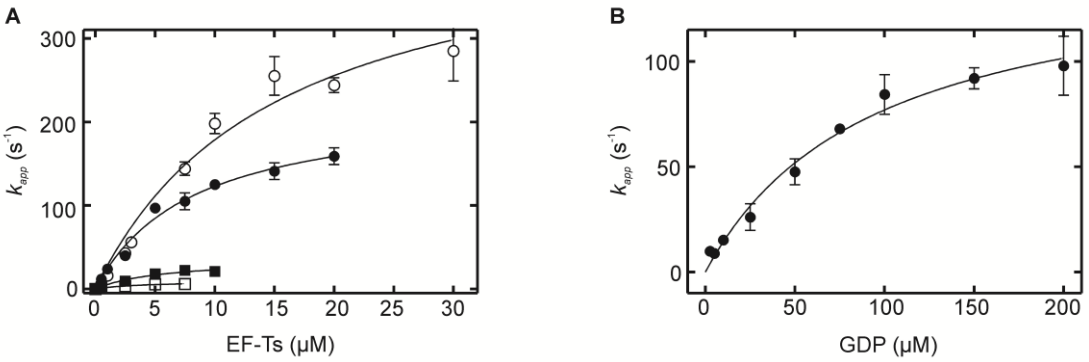

Figure 3.9. Interaction of EF-Tu with GDP and EF-Ts. (A) Concentration dependence of the rate of nucleotide dissociation (k_{app}) as a function of increasing EF-Ts concentrations. EF-$Tu_{E.c.}$•mant-GDP dissociated by increasing EF-$Ts_{E.c.}$ is shown as filled circles, while EF-$Ts_{P.a.}$ is shown as open circles. EF-$Tu_{P.a.}$•mant-GDP dissociated by increasing EF-$Ts_{P.a.}$ is shown as filled squares, while EF-$Ts_{E.c.}$ is shown as open squares. (B) Concentration dependence of the rate of EF-$Tu_{E.c.}$•$Ts_{P.a.}$ dissociation (k_{app}) as a function of increasing GDP concentrations (0 – 200 μM).

3.3d Interaction of EF-Tu with EF-Ts (k_2, k_{-2})

The formation of the EF-Tu•EF-Ts complex was monitored through the change of the intrinsic tryptophan fluorescence of EF-$Tu_{E.c.}$ upon EF-Ts binding, where a fluorescence

decrease is indicative of EF-Ts binding. Increasing concentrations of EF-Ts were used to determine the association constant (k_2) from the linear dependence of k_{app} on the respective EF-Ts concentration (Figure 3.10). The value for k_2 determined here between EF-Tu$_{E.c.}$ and EF-Ts$_{E.c.}$ is approximately 1.9 x 10^7 $M^{-1}s^{-1}$, which is in agreement with previously published data (45). The value for k_2 between EF-Tu$_{E.c.}$ and EF-Ts$_{P.a.}$ is approximately (0.5 ± 0.1) x 10^7 $M^{-1}s^{-1}$, which is about a quarter of EF-Ts$_{E.c.}$ (1.9 ± 0.5) x 10^7 $M^{-1}s^{-1}$.

The dissociation of the EF-Tu•EF-Ts complex is extremely slow and gives a poor signal such that this cannot be measured directly, however, it can be calculated from the other rate constants (Eq. 3.6 and 3.7). k_{-2} for EF-Tu$_{E.c.}$•EF-Ts$_{E.c.}$ and EF-Tu$_{E.c.}$•EF-Ts$_{P.a.}$ is equal to approximately 0.05 s^{-1} and 0.0006 s^{-1} respectively (Table 3.3). This results in K_2 for EF-Tu$_{E.c.}$•EF-Ts$_{P.a.}$ (0.1 nM) which is 30-fold lower than that of EF-Tu$_{E.c.}$•EF-Ts$_{E.c.}$ (3 nM).

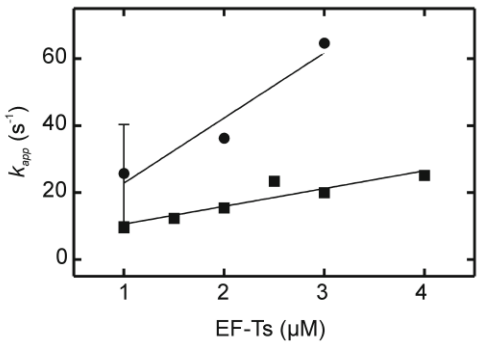

Figure 3.10. Interaction of EF-Tu with EF-Ts (k_2). Dependence of k_{app} on increasing concentrations of EF-Ts. The values of k_{app} were calculated by single-exponential fitting of the respective time courses. EF-Tu$_{E.c.}$ in the presence of increasing EF-Ts$_{E.c.}$ is shown as filled circles, while EF-Tu$_{E.c.}$ in the presence of increasing EF-Ts$_{P.a.}$ is shown as filled squares.

Table 3.2. EF-Ts Induced Dissociation of GDP and GTP from EF-Tu.

	GDP	GTP
	k_{-4} (s^{-1})	k_{-7} (s^{-1})
EF-$Tu_{P.a.}$ vs. EF-$Ts_{P.a.}$	40 ± 10	40 ± 2
EF-$Tu_{E.c.}$ vs. EF-$Ts_{E.c.}$	220 ± 20	125 ± 20
EF-$Tu_{P.a.}$ vs. EF-$Ts_{E.c.}$	10 ± 1	5 ± 1
EF-$Tu_{E.c.}$ vs. EF-$Ts_{P.a.}$	450 ± 60	280 ± 90

Table 3.3. Determined Rate Constants for the Kinetic Mechanism of Nucleotide Exchange in EF-$Tu_{E.c.}$.

Constant		EF-$Tu_{E.c.}$ vs. EF-$Ts_{E.c.}$	EF-$Tu_{E.c.}$ vs. EF-$Ts_{P.a.}$
k_{-2} (s^{-1})	Dissociation of Ts from Tu•Ts	0.05	0.0006
k_2($M^{-1}s^{-1}$)	Association of Ts to Tu	1.9 ± 0.5 x 10^7	5 ± 1 x 10^6
k_{-3} (s^{-1})	Dissociation of Ts from Tu•GDP•Ts	350 *	150 ± 14
k_3($M^{-1}s^{-1}$)	Association of Ts to Tu•GDP	6 x 10^{7*}	2 ± 1 x 10^7
k_{-4} (s^{-1})	Dissociation of GDP from Tu•GDP•Ts	220 ± 20	450 ± 60
k_4($M^{-1}s^{-1}$)	Association of GDP to Tu•Ts	1.4 x 10^{7*}	5 ± 3 x 10^6
k_{-6} (s^{-1})	Dissociation of Ts from Tu•GTP•Ts	60*	24 ± 5
k_6($M^{-1}s^{-1}$)	Association of Ts to Tu•GTP	3 ± 1 x 10^{7*}	1.2 ± 0.1 x 10^7
k_{-7} (s^{-1})	Dissociation of GTP from Tu•GTP•Ts	125 ± 20	280 ± 90
k_7($M^{-1}s^{-1}$)	Association of GTP to Tu•Ts	6 ± 1 x 10^{6*}	5 ± 2 x 10^5
K_2 (μM)		3 x 10^{-3}	1 x 10^{-4}
K_3 (μM)		6	8
K_4 (μM)		30	170
K_6 (μM)		2	2
K_7 (μM)		20	550

*Data previously published (45)

3.3e Interaction of EF-Tu with EF-Ts Variants

It was surprising that EF-Ts$_{P.a.}$ is able to catalyze the dissociation of guanine nucleotides from EF-Tu$_{E.c.}$ more efficiently than EF-Ts$_{E.c.}$. The primary sequence of EF-Ts from *E. coli* and *P. aeruginosa* share 55% identity and 69% similarity. The residues involved in the interaction surface between EF-Tu and EF-Ts are highly conserved between the species and the only variation in the interaction surface between EF-Tu and EF-Ts is in the C-terminal module (helix 13) of EF-Ts, pointing at a putative role of this helix in modulating nucleotide dissociation from the EF-Tu•nucleotide•EF-Ts complex.

The difference in sequence is subtle and includes a two amino acid extension of helix 13 (Appendix Figure A.6). The increased helix length and the variation in the sequence of the helix might enable additional interactions between domain I of EF-Tu and helix 13 of EF-Ts$_{P.a.}$ that are not possible with the shorter EF-Ts$_{E.c.}$. These interactions could either stabilize the EF-Tu•EF-Ts interaction or stimulate guanine nucleotide dissociation from EF-Tu to a larger extent. In order to further dissect the role of helix 13 for the nucleotide exchange mechanism in EF-Tu, a C-terminal truncation variant of EF-Ts$_{P.a.}$ as well as a C-terminal chimera replacing the last 6 amino acids in EF-Ts$_{E.c.}$ with the C-terminal end of EF-Ts$_{P.a.}$ (Figure 3.11) was constructed.

Met 278 of EF-Ts$_{E.c.}$ is located in helix 13 and makes hydrophobic contacts with residues in the guanine nucleotide binding pocket, Ala 29 and Thr 25 in EF-Tu$_{E.c.}$ (47). Met 278 in *E. coli* EF-Ts is substituted with a glutamine in EF-Ts$_{P.a.}$ (Q283), a residue of similar length but different chemical properties. To analyze whether this position influences the interaction made between the C-terminal module and domain I of EF-Tu, a substitution in

EF-Ts$_{P.a.}$ replacing the Gln sidechain at position 283 with Met (Figure 3.11) was constructed.

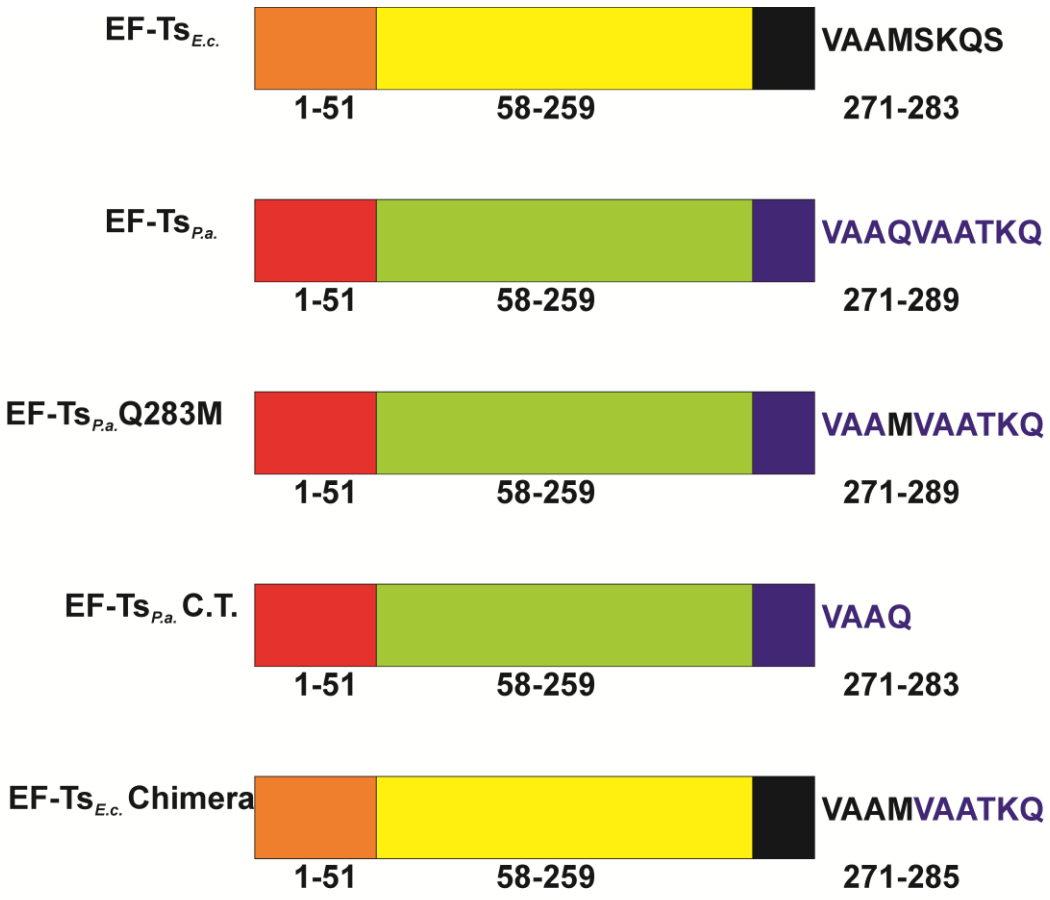

Figure 3.11. EF-Ts variants constructed. Domain alignment of EF-Ts$_{E.c.}$, (N-terminal domain shown in orange, core domain in yellow and the C-terminal domain shown in black) with EF-Ts$_{P.a.}$ (N-terminal domain shown in red, core domain in green and the C-terminal domain in blue). Residue numbers for each domain are shown below the respective domains. The end of the C-terminal module sequence is shown on the right and the name of each EF-Ts represented is shown on the left. The substitution of Q283M is shown in the sequence (EF-Ts$_{P.a.Q283M}$), highlighted in black. Residues corresponding to EF-Ts$_{P.a.}$ are denoted in blue, and residues corresponding to EF-Ts$_{E.c.}$ are denoted in black.

The kinetic parameters describing interactions of EF-Tu, EF-Ts, and GDP as well as GTP were studied in a similar manner as described above. Dissociation of mant-GDP and mant-GTP from EF-Tu was observed at increasing concentrations of EF-Ts (Figure 3.12). At saturating concentrations of EF-Ts, k_{-4} and k_{-7} were determined. k_{-4} and k_{-7} for the

EF-Tu$_{E.c.}$ and the EF-Ts$_{P.a.}$ C-terminal truncation variant (EF-Ts$_{P.a.\text{C.T.}}$) is approximately 10-fold slower ($k_{-4(TuE.c.\bullet mant\text{-}GDP\bullet TsP.a.C.T.)}$ = 30 ± 3 s^{-1} and $k_{-7(TuE.c.\bullet mant\text{-}GTP\bullet TsP.a.C.T).}$ = 6 ± 1 s^{-1}) than for wild type EF-Ts$_{P.a.}$ (Table 3.4). Similarly, stimulated dissociation of mant-GDP (k_{-4}) and mant-GTP (k_{-7}) from EF-Tu$_{P.a.}$ in the presence of EF-Ts$_{P.a.\text{C.T.}}$ is approximately 10-fold slower ($k_{-4(TuP.a.\bullet mant\text{-}GDP\bullet TsP.a.C.T.)}$ = 3 ± 1 s^{-1} and $k_{-7(TuP.a.\bullet mant\text{-}GTP\bullet TsP.a.C.T.)}$ = 0.9 ± 0.1 s^{-1}) than for wild type EF-Ts$_{P.a.}$. This indicates that the truncation of helix 13 in EF-Ts$_{P.a.}$ affects nucleotide dissociation from either EF-Tu$_{E.c.}$ and EF-Tu$_{P.a.}$ to a similar extent, whether mant-GDP or mant-GTP is present.

Substitution of Gln 283 with Met in EF-Ts$_{P.a.}$ (EF-Ts$_{P.a.\text{Q283M}}$) yielded k_{-4} and k_{-7} values for EF-Tu$_{P.a.}$ ($k_{-4(TuP.a.\bullet mant\text{-}GDP\bullet TsP.a.Q283M)}$ >50 s^{-1} and $k_{-7(TuP.a.\bullet mant\text{-}GTP\bullet TsP.a.Q283M)}$ = 190 ± 50 s^{-1}) and EF-Tu$_{E.c.}$ ($k_{-4(TuE.c.\bullet mant\text{-}GDP\bullet TsP.a.Q283M)}$ = 1000 ± 500 s^{-1} and $k_{-7(TuE.c.\bullet mant\text{-}GTP\bullet TsP.a.Q283M)}$ = 400 ± 100 s^{-1}) (Table 3.4). The values obtained with EF-Tu$_{E.c.}$ are similar to results with EF-Ts$_{P.a.}$ ($k_{-4(TuE.c.\bullet mant\text{-}GDP\bullet TsP.a.)}$ = 450 ± 60 s^{-1} and $k_{-7(TuE.c.\bullet mant\text{-}GTP\bullet TsP.a.)}$ = 280 ± 90 s^{-1}), indicating that substitution of Gln 283 does not significantly affect the ability of EF-Ts$_{P.a.}$ to catalyze mant-GDP or mant-GTP dissociation from EF-Tu$_{E.c.}$. However, results obtained show an increased rate of mant-GDP and mant-GTP dissociation from EF-Tu$_{P.a.}$ compared with wild type EF-Ts$_{P.a.}$ ($k_{-4(TuP.a.\bullet mant\text{-}GDP\bullet TsP.a.)}$ = 40 ± 10 s^{-1} and $k_{-7(TuP.a.\bullet mant\text{-}GTP\bullet TsP.a.)}$ = 40 ± 2 s^{-1}).

The value obtained here for dissociation of GTP from EF-Tu$_{E.c.}$ (k_{-7}) catalyzed by the EF-Ts$_{E.c.}$ chimera is equal to 120 ± 20 s^{-1} (Table 3.4) which is similar to EF-Ts$_{E.c.}$. The value for k_{-4} obtained for EF-Tu$_{E.c.}$ with this chimera is 380 ± 80 s^{-1} (Table 3.4), which is

similar to EF-Ts$_{P.a.}$. The EF-Ts$_{E.c.}$ chimera also seems to saturate at a lower concentration of EF-Ts and follows the trend of EF-Ts$_{P.a.}$ despite the fact that 98% of this protein is identical to EF-Ts$_{E.c.}$ (Figure 3.12). The EF-Ts$_{E.c.}$ chimera is able to catalyze the rate of mant-GTP dissociation and mant-GDP dissociation from EF-Tu$_{P.a.}$ (k_{-7} and k_{-4}) more like EF-Ts$_{P.a.}$ than EF-Ts$_{E.c.}$ (Figure 3.12), giving values for k_{-7} of 25 ± 2 s^{-1} and k_{-4} of >40 s^{-1} (Table 3.4).

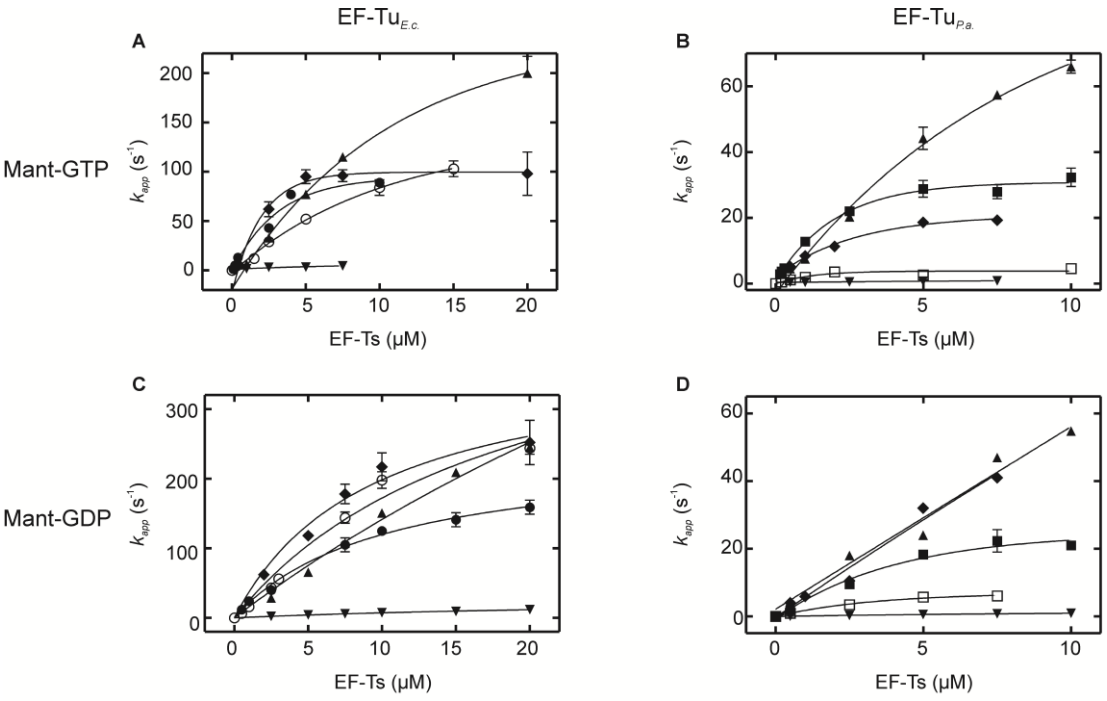

Figure 3.12. Catalyzed dissociation of guanine nucleotides from EF-Tu with EF-Ts variants. (A) Concentration dependence of k_{app} of EF-Tu$_{E.c.}$•mant-GTP dissociated by increasing concentrations of EF-Ts$_{E.c.}$ (filled circles), EF-Ts$_{P.a.}$ (open circles), EF-Ts$_{P.a.C.T.}$ (downward triangles), EF-Ts$_{P.a.Q283M}$ (upwards triangles) and EF-Ts$_{E.c.}$ chimera (diamonds). (B) Concentration dependence of k_{app} of EF-Tu$_{P.a.}$•mant-GTP dissociated by increasing concentrations of EF-Ts$_{E.c.}$ (open squares), EF-Ts$_{P.a.}$ (filled squares), EF-Ts$_{P.a.C.T.}$ (downward triangles), EF-Ts$_{P.a.Q283M}$ (upwards triangles) and EF-Ts$_{E.c.}$ chimera (diamonds). (C) Concentration dependence of k_{app} of EF-Tu$_{E.c.}$•mant-GDP dissociated by increasing concentrations of EF-Ts, as in A. (D) Concentration dependence of k_{app} of EF-Tu$_{P.a.}$•mant-GDP dissociated by increasing concentrations of EF-Ts, as in B.

Table 3.4 Determined Rate Constants for the Interaction between EF-Tu, EF-Ts Variants and Guanine Nucleotides

	GDP	GTP
	k_{-4} (s^{-1})	k_{-7} (s^{-1})
EF-$Tu_{P.a.}$vs. EF-$Ts_{P.a.}$ C.T..	3 ± 1	0.9 ± 0.1
EF-$Tu_{E.c}$ vs.EF-$Ts_{P.a.}$ C.T..	30 ± 3	6 ± 1
EF-$Tu_{P.a.}$ vs. EF-$Ts_{P.a.}$Q283M	>50	190 ± 50
EF-$Tu_{E.c.}$ vs. EF-$Ts_{P.a.}$ Q283M	1000 ± 500	400 ± 100
EF-$Tu_{P.a.}$ vs. EF-$Ts_{E.c.}$ Chimera	>40	25 ± 2
EF-$Tu_{E.c.}$ vs. EF-$Ts_{E.c.}$ Chimera	380 ± 80	120 ± 20
EF-$Tu_{P.a.}$ vs. EF-$Ts_{P.a.}$	40 ± 10	40 ± 2
EF-$Tu_{E.c.}$ vs. EF-$Ts_{E.c.}$	220 ± 20	125 ± 20
EF-$Tu_{P.a.}$ vs. EF-$Ts_{E.c.}$	10 ± 1	5 ± 1
EF-$Tu_{E.c.}$ vs. EF-$Ts_{P.a.}$	450 ± 60	280 ± 90

3.4 Discussion

3.4a Guanine Nucleotide Exchange in E. coli and P. aeruginosa EF-Tu.

The complete kinetic mechanism for the nucleotide exchange reaction in the human opportunistic pathogen *P. aeruginosa* has been determined and compared to the nucleotide exchange mechanism of *E. coli* to gain a better understanding of the evolutionary conservation of the kinetic parameters governing this central process during protein synthesis. The kinetic scheme describing the interaction of EF-Tu, EF-Ts and guanine nucleotides is shown in Figure 3.5. When comparing the obtained GTP and GDP dissociation rate constants it is observed that these are very similar between the two species of EF-Tu. However, a slight decrease in the rate of GTP dissociation from EF-Tu$_{P.a.}$ and a 2-fold increase in the rate of GTP association for EF-Tu$_{P.a.}$ when compared to EF-Tu$_{E.c.}$ gives rise to a 10-fold increase in the affinity of EF-Tu$_{P.a.}$ for GTP. This was surprising, given that the GDP binding properties are comparable between the two species and there is a high level of sequence conservation of both factors (84% identity and 90% similarity (Appendix Figure A.7)). The amino acid residues that are directly involved in binding to GTP are 100% conserved in identity between *E. coli* and *P. aeruginosa* EF-Tu. This then suggests that there is an altered contribution from other non-conserved residues towards the overall dynamics in the GTP-bound form of EF-Tu between organisms.

Stimulation of guanine nucleotide dissociation from EF-Tu$_{P.a.}$ is most efficient in the presence of EF-Ts$_{P.a.}$ than EF-Ts$_{E.c.}$. Given that EF-Tu$_{P.a.}$ has a slightly slower intrinsic guanine nucleotide dissociation rate than EF-Tu$_{E.c.}$, EF-Ts$_{P.a.}$ may have evolved additional structural features that increase its ability to stimulate the rate of guanine

nucleotide dissociation from EF-Tu$_{P.a.}$ more than EF-Ts$_{E.c.}$, thus overcoming the tighter binding of the respective nucleotide. It has been shown that mutations made in the nucleotide binding pocket of EF-Tu can accelerate the rate of GDP dissociation and can eliminate the need for EF-Ts (118). This is consistent with the kinetic constants determined here. The equilibrium binding constants for the interaction of EF-Ts with the respective nucleotide-bound complex of EF-Tu$_{E.c.}$ (K_3 and K_6) are virtually identical whether *P. aeruginosa* or *E. coli* EF-Ts is present (Table 3.3). However, the interaction of guanine nucleotides with the EF-Tu•EF-Ts complex (K_4 and K_7) differ significantly depending on the identity of EF-Ts present. A closer investigation of the rate constants for these steps reveal that EF-Ts$_{P.a.}$ can stimulate GTP and GDP dissociation from EF-Tu$_{E.c.}$ 2-fold more efficiently than EF-Ts$_{E.c.}$ regardless of the guanine nucleotide present. Interestingly, there was a second-phase observed in the dissociation of GDP/GTP from EF-Tu$_{E.c.}$ in the presence of high EF-Ts$_{P.a.}$ concentrations. Although this phase was not observed for lower concentrations of EF-Ts$_{P.a.}$, the rate of the second phase did not dependent on the concentration of EF-Ts$_{P.a.}$. This is indicative of a further conformational change within EF-Tu$_{E.c.}$ upon interaction with EF-Ts$_{P.a.}$ in the presence of guanine nucleotides. Given that EF-Ts$_{P.a.}$ has a C-terminal extension, it is likely that this extension interacts with or close to Trp 184 on helix F of EF-Tu$_{E.c.}$ which excites mant-GDP/GTP through FRET (Figure 3.13).

The values for GDP or GTP association to the Tu•Ts complex (k_4 and k_7) determined for EF-Tu$_{E.c.}$ in complex with EF-Ts$_{P.a.}$ are significantly lower than with EF-Ts$_{E.c.}$, suggesting that EF-Ts$_{P.a.}$ has evolved the ability to further destabilize nucleotide binding in the ternary (EF-Tu•nucleotide•EF-Ts) complex. A sequence analysis between *E. coli* and

P. aeruginosa EF-Ts showed that they exhibit only 55% identity in sequence compared to 84% identity between the respective EF-Tu proteins. Even though there are a large number of residues with low conservation in EF-Ts (Appendix Figure A.6), there are only a few differences in the amino acid residues participating in interactions with EF-Tu. Given the higher sequence variability observed in EF-Tss primary sequence compared to EF-Tu, the observed differences in the kinetic mechanism of nucleotide exchange between the two species likely arises mostly from structural differences in EF-Ts and not EF-Tu.

3.4b Variation in the C-terminal module of EF-Ts

The most prominent sequence variability in the contacts made between the EF-Tu•EF-Ts interaction is between domain I (G-domain) of EF-Tu and the C-terminal module (helix 13) in EF-Ts. Helix 13 of EF-Ts is highly variable among bacteria in terms of length and sequence conservation (Appendix Figure A.6). EF-Ts$_{P.a.}$ has a two amino acid extension compared to EF-Ts$_{E.c.}$ and shows no sequence conservation in the last 7 amino acids. Previous work has revealed that deletion of helix 13 in *E. coli* EF-Ts decreases the EF-Tu•EF-Ts binding affinity by 2-fold (119). However, the kinetic effect of this deletion in terms of the ability of EF-Ts to act as a GEF was not analyzed. Given that EF-Ts in *E. coli* and *P. aeruginosa* both contain a C-terminal module but exhibit different rates of nucleotide dissociation, the length is likely important for the function of EF-Ts for catalysis. The C-terminal domain in EF-Ts$_{P.a.}$ was truncated by only 6 amino acids to see if the length of this variable extension in the C-terminal module is important for EF-Ts$_{P.a.}$ to catalyze the rate of facilitated guanine nucleotide dissociation. Interestingly,

independent of the nucleotide (mant-GTP or mant-GDP) bound to EF-Tu, the ability of EF-Ts$_{P.a.\text{C.T.}}$ to catalyze dissociation of guanine nucleotides is reduced by an order of magnitude but is still 100-fold higher than the uncatalyzed dissociation of nucleotide. This effect of the EF-Ts$_{P.a.\text{C.T.}}$ variant is observed in both EF-Tu from *E. coli* and *P. aeruginosa*. Therefore, even though the C-terminal module may not be essential for the function of EF-Ts, it is still important for fine-tuning the maximal rate of EF-Ts catalyzed dissociation of guanine nucleotides from EF-Tu.

EF-Ts$_{E.c.}$ has a shorter C-terminal module than EF-Ts$_{P.a.}$ and it is therefore unknown how the additional C-terminal residues if EF-Ts$_{P.a.}$ fold (47). However, it can be hypothesized that helix 13 in EF-Ts$_{P.a.}$ protrudes further into domain I of EF-Tu than helix 13 from EF-Ts$_{E.c.}$ forming additional interactions that are responsible for facilitating the acceleration of guanine nucleotide dissociation. This hypothesis is strongly supported by the results obtained with the EF-Ts$_{E.c.}$ chimera, which is able to stimulate the dissociation of guanine nucleotides from EF-Tu$_{P.a.}$ to a similar extent as wild type EF-Ts$_{P.a.}$, even though 98% of this protein is identical to EF-Ts$_{E.c.}$. Based on the *E. coli* EF-Tu•EF-Ts X-ray crystal structure (47), the C-terminal module of EF-Ts$_{P.a.}$ could contact helix A of EF-Tu, just before the switch I region, and/or make contacts with helix F in EF-Tu (Figure 3.12). These regions have low sequence conservation between EF-Tu$_{E.c.}$ and EF-Tu$_{P.a.}$ and may contribute to the interaction between the C-terminal extension of EF-Ts$_{P.a.}$ and EF-Tu. Although these regions within EF-Tu have not been shown to be involved in coordinating the guanine nucleotide in the binding pocket, their flexibility is likely important for the structure of the G-domain as a whole and its ability to interact with guanine nucleotides.

Interestingly, this EF-Ts$_{E.c.}$ chimera is able to stimulate the rate of GTP dissociation from EF-Tu$_{E.c.}$ like wild type EF-Ts$_{E.c.}$, however, GDP dissociation from EF-Tu$_{E.c.}$ is more similar to wild type EF-Ts$_{P.a.}$. This indicates that the core of EF-Ts can work synergistically with the C-terminal module in catalyzing the dissociation of guanine nucleotides from EF-Tu. Furthermore, the interaction made between the C-terminal module and helices F and/or A in EF-Tu may influence the ability of EF-Ts to catalyze GTP or GDP dissociation from EF-Tu. Even though the majority of the residues that contact EF-Tu are conserved in EF-Ts, the primary sequence of EF-Ts is poorly conserved. The variability in the rest of EF-Ts could result in differences in the overall dynamics of EF-Ts. The highly conserved Phe 81 in subdomain N of EF-Ts$_{E.c.}$ has been shown to intrude into helix B and C of EF-Tu (47), which leads to the disruption of the magnesium binding site in domain 1 of EF-Tu. The region following this conserved motif is highly variable in sequence (Figure 3.12) and may be one of the variable regions within EF-Ts that influences the dynamic movement of essential regions within EF-Ts that contact EF-Tu.

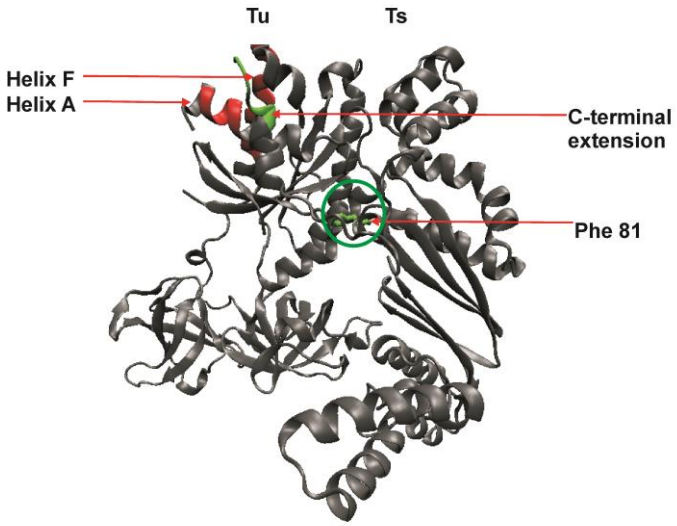

Figure 3.13. Variance in EF-Tu•EF-Ts contacts. EF-Tu (left) bound to EF-Ts (right) from *E. coli* (PDB ID 1EFU (47)) is represented in cartoon and coloured in black. Variable residues between *E. coli* and *P. aeruginosa* in helix A and F in EF-Tu are highlighted in red. Variable residues between *E. coli* and *P. aeruginosa* in the C-terminal extension in EF-Ts are highlighted in green. Phe 81 in EF-Ts is represented in licorice (coloured green) and residues following this that are variable between *E. coli* and *P. aeruginosa* are highlighted with a green circle.

Given that EF-Tu has other interaction partners besides EF-Ts, mainly aa-tRNA and the ribosome, it is not feasible for this protein to substitute amino acids as this may interfere with essential contacts needed for the function of EF-Tu. Since EF-Ts does not have as many interaction partners as EF-Tu, it is likely that EF-Ts has evolved within each organism to fine-tune the rates of nucleotide exchange. The general strategy of GEFs is to destabilize the positive charges within the G-domain of the protein with that of the nucleotide phosphates. EF-Ts$_{E.C.}$ contacts domain I of EF-Tu with its N-terminal domain, subdomain N and the C-terminal module (47). It has been previously shown that the N-terminal domain of EF-Ts is important for complex formation and catalysis of GDP dissociation from EF-Tu (103,119). Furthermore, EF-Ts in mitochondria as well as eEF1Bα do not contain a C-terminal module (107,110). However, the affinity between guanine nucleotides and mitochondrial EF-Tu and yeast eEF1A is an order of magnitude

less than bacterial EF-Tu (104). Furthermore, the spontaneous rate of GDP dissociation from eEF1A is 100-fold faster than from bacterial EF-Tu. These findings indicate that when EF-Tu has evolved to have a strong interaction with guanine nucleotides, an exchange factor develops strategies to overcome this tight binding and for EF-Ts may be in the evolution or divergence of the C-terminal module.

Met 278 of EF-Ts$_{E.c.}$ has previously been shown to make hydrophobic interactions with Ala 29 and Thr 25 in domain I of EF-Tu (47). Thr 25 has been shown to assist in coordinating Mg^{2+} within the G-domain of EF-Tu (44). The interaction between Met 278 of EF-Ts$_{E.c.}$ with Thr 25 of EF-Tu$_{E.c.}$ may help disrupt the magnesium binding site in domain I of EF-Tu. Interestingly, only 12% of the 34 bacterial species aligned here that contain a C-terminal module, have a methionine in this position and 50% contain a glutamine (Appendix Figure A.6). Analysis of the substitution variant Gln 283 to Met in EF-Ts$_{P.a.}$ gave similar rates of catalyzed guanine nucleotide dissociation from EF-Tu$_{E.c.}$ as that of wild type EF-Ts$_{P.a.}$. However, this variant is able to catalyze the rate of guanine nucleotide dissociation from EF-Tu$_{P.a.}$ more efficiently than wild type EF-Ts$_{P.a.}$. This suggests that position 283 is not critical for nucleotide exchange in EF-Tu$_{E.c.}$ but has an impact in EF-Tu$_{P.a.}$, supporting the idea that the core of EF-Ts works synergistically with the C-terminal module. In the *E. coli* system, EF-Ts has evolved in such a way that the core of EF-Ts mainly contributes to its ability to act as a GEF and the length of the C-terminal module is more important than the sequence. However, in the *P. aeruginosa* system the C-terminal module has evolved to have a stronger influence on the ability of EF-Ts to act as a GEF. This may be due to the variability in helices A and F of EF-Tu, which may have allowed for evolutionary changes within the C-terminal module of

EF-Ts. This reveals a molecular mechanism that can be used by some species to further maximize nucleotide dissociation rates and that the stimulation of guanine nucleotide dissociation from EF-Tu can be altered by the C-terminal module.

3.5 Future Directions

P. aeruginosa is a gram-negative bacteria that can be found in water all over the world. It is not often found to infect healthy humans (120), however, it is a major cause of nosocomial infection in hospitals and in particular in patients with cystic fibrosis (121) and is becoming a major threat to public health. Infection can spread by patient-to-patient contacts or from a contaminated environment. Even though measures have been taken over the past few years to limit the spread of this pathogen in hospitals, such as separating infected patients from non-infected and decontaminate environments surrounding patients, the number of cystic fibrosis patients infected with this pathogen has not decreased (120).

Most drugs that are currently in use either target the synthesis of the cell wall, protein synthesis or DNA replication and repair (122). However, prevalence of *P. aeruginosa* multidrug resistance has increased significantly over the past 20 years (123).

Antibiotic resistance can arise from antibiotic modification, efflux of the antibiotics out of the cells or by altering the antibiotic binding site (122). One approach to overcome antibiotic resistance is to obtain knowledge on the mechanism of resistance such that a new compound that is active against the mechanism of resistance can be developed. Furthermore, the use of virtual screening is being used as a cost-effective method for rational drug design (124). However, the development of novel drugs/antibiotics, which would not harm the host, is hampered by the high level of conservation of the protein translation machinery among species.

Here it is observed that EF-Ts is highly variable in sequence and can have altered function through modulation of the C-terminal domain. Virtual screening can be utilized

to identify antibiotics that may target the C-terminal module of EF-Ts to inhibit its function. In addition, the dissociation of nucleotides from EF-Tu can be targeted at various steps so that dissociation of guanine nucleotides from EF-Tu can be fine-tuned. In this way, EF-Ts might be a promising target for novel species-specific antibiotics, which would not harm the host.

Chapter 4

Construction of a Fully Active Cys-less Elongation Factor Tu: Functional Role of Conserved Cysteine 81.

*(Previously published in Biochimica et biophysica acta. 2011 May; 1814 (5): 684-692)

4.1 Introduction

EF-Tu and its eukaryotic counterpart eEF1 are essential proteins involved in gene expression. In rapidly growing bacterial cells, EF-Tu accounts for approximately 5% of the cellular proteins (85). As a GTP-dependent translation factor, EF-Tu participates in the cyclic process of mRNA-directed polypeptide synthesis through the delivery of aminoacyl-tRNA (aa-tRNA) to the A site of actively translating ribosomes. In its GTP-bound active state, EF-Tu binds to aa-tRNA with high affinity ($K_D \approx 10^{-8}$ M) (100), forming an EF-Tu•GTP•aa-tRNA ternary complex (101). During aa-tRNA delivery this ternary complex first interacts with the ribosome in a codon independent initial binding step (42). Following codon recognition, a signal is transmitted, originating from the decoding site on the 30S ribosomal subunit, to domain I of EF-Tu, leading to GTPase activation and subsequent nucleotide hydrolysis (97). GTP hydrolysis is then followed by the release of inorganic phosphate (P_i) (43), causing a major conformational change in EF-Tu (44) and lowering the affinity of EF-Tu for aa-tRNA (100) significantly and allowing for the release of aa-tRNA into the ribosomal A site. The active GTP-bound state of EF-Tu (EF-Tu•GTP) is regenerated from the inactive GDP-bound state (EF-Tu•GDP) by the guanine nucleotide exchange factor EF-Ts (46) which enhances the rate of GDP dissociation from EF-Tu approximately 60 000-fold (45), enabling the rapid turnover of EF-Tu consistent with elongation rates found *in vivo* (102).

Crystal structures of EF-Tu have allowed the identification of amino acid residues in EF-Tu critical for the interactions between the ribosome (70), EF-Ts (47), aa-tRNA (101), and guanine nucleotides (44,69). However, little is known about the dynamic processes that lead up to and follow GTP hydrolysis and P_i release. Detailed knowledge of these processes is of great interest for understanding the design principles underlying the function of this cellular machine, in turn enabling the identification and characterization of, for example, novel antibiotics.

Generally, little is known about the functional roles of residues that do not directly participate in the molecular interactions identified in crystal structures of the respective macromolecule. Nevertheless, these residues can be members of a critical 3-dimensional communication network regulating and fine-tuning the functional properties of a protein. Understanding the functional role of these often highly conserved secondary shell residues is pivotal for the rational design of novel biomolecular machines and tools. One important class of molecular tools consists of proteins covalently linked to non-fluorescent (e.g. crosslinking groups) or fluorescent reporter groups. These modified proteins are frequently used to study molecular dynamics by measuring distance changes using FRET between two dyes attached to the components of a molecular system such as the ribosome (125). Development of such molecular probes often requires the precise positioning of reporter groups on the molecular surface of the respective macromolecule(s). This problem is routinely addressed by introducing cysteine residues at positions of interest and subsequent labelling with a reporter group of choice. The power of this approach has been demonstrated in a number of studies (126,127). However, in order to allow for specific cysteine-directed labelling, naturally occurring

cysteine residues in the protein have to be removed first. The activity of the protein may be affected when functionally important cysteine residues are replaced. Functional importance is typically indicated by strict evolutionary conservation. EF-Tu from *E. coli* contains three cysteine residues (Figure 4.1) from which only one, cysteine 81 (Cys 81), exhibits significant evolutionary conservation (79% conserved, Appendix Figure A.7). This highly conserved cysteine is buried near the nucleotide binding pocket in domain I of EF-Tu. Although Cys 81 does not interact directly with the bound guanine nucleotide, it is involved in the formation of several hydrogen bonds with water molecules that participate in coordinating the bound magnesium ion and one of the nucleotide's β-phosphate oxygen atoms (44). Previous studies revealed that Cys 81 can be modified with *N*-tosyl-L-phenylalanylchloromethane (TPCK) and that this modification essentially abolishes aa-tRNA binding (128). Further analysis on the functional role of Cys 81 used a glycine substitution, which significantly impaired GDP and aa-tRNA binding (129). These reports may have discouraged the development of a cysteine-free (Cys-less) version of EF-Tu, pivotal for further studies relying on the site-specific introduction of fluorescent and non-fluorescent labels. Availability of such a Cys-less version of EF-Tu will be of great value for the study of EF-Tus function on and off the ribosome. These processes are currently not accessible by techniques such as single molecule (sm) FRET, which have provided valuable information on a number of steps preceding and subsequent to accommodation (42,130).

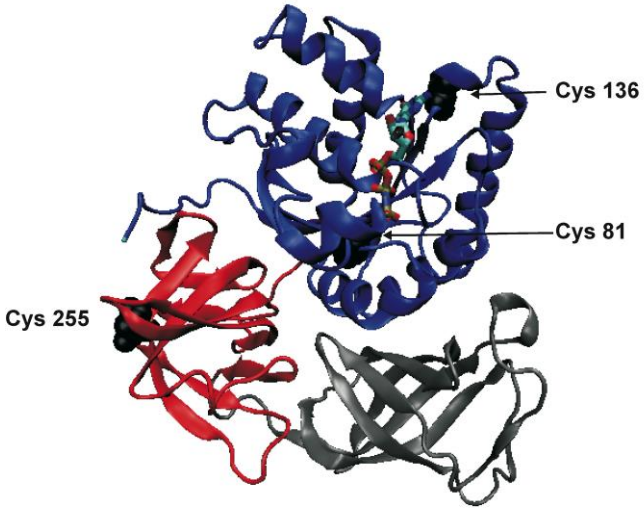

Figure 4.1. Overview of cysteine residues present in the EF-Tu•GTP complex. The positions of the three cysteine residues present in EF-Tu from *E. coli* are indicated in black and represented in space fill. EF-Tu is represented in cartoon and coloured as in figure 3.1. (Figure was generated using coordinates from PDB ID 1EFT (44))

Previous attempts to construct a Cys-less version of EF-Tu were based on the structurally conservative substitution of cysteine with the isosteric serine (131). This approach resulted in a version of EF-Tu that was significantly impaired in aa-tRNA binding, significantly limiting its use for further kinetic studies. In this work, this problem is revisited and addressed from an evolutionary perspective based on the assumption that conservation of a particular amino acid reflects the constraints imposed by functional requirements in this position. Therefore naturally occurring substitutions in this position are likely to conserve the function of the protein. Based on the analysis of EF-Tu sequences available in the SwissProt Database (115), three Cys-less versions of EF-Tu were constructed containing serine, alanine or methione in position 81. The properties of these Cys-less variants were characterized with respect to the interaction with guanine nucleotides, EF-Ts, aa-tRNA and the ribosome. Here it is demonstrated that the Cys-less

variant of EF-Tu, based on an alanine substitution in position 81, does indeed exhibit wild-type activity as opposed to the respective methionine and serine variants. Therefore the introduction of cysteine residues into the Cys-less EF-Tu background for subsequent labelling should be based on the alanine rather than the serine or methionine variant.

4.2 Materials and Methods

4.2a Cloning and Site-Directed Mutagenesis

Amino acid substitutions were introduced into a derivative of pET21a (pKECAHIS (112)) containing the full-length sequence coding for an N-terminal His_6-tagged EF-Tu and valine (GTC) substituting cysteine in positions 137 and 255 (introducing restriction sites for *SgrA*I and *Sal*I, respectively) using the Quikchange™ method. Primers were obtained from Invitrogen. Reactions were carried out in a $T_{Gradient}$ (Biometra) thermocycler: 25 μL of the reaction mixture contained 1000 ng of template plasmid DNA, 0.4 μM primer pair, 400 μM of each dNTP, and 3 units of DNA polymerase (*Pfu*, Fermentas).

The reaction was carried out by heating the reaction mixture to 95°C for 3 min followed by 18 cycles of 95°C for 1 min, 64°C for 1 min, 70°C for 16 min and subsequent final elongation at 70°C for 15 min. To remove the template DNA the reactions were treated with restriction enzyme *Dpn*I (Fermentas) for 16 hrs at 37°C. 1.5 μL aliquots of the resulting product were transformed into 15 μL *E. coli* DH5α competent cells (New England Biolabs), which were grown on LB media supplemented with 100 μg/mL ampicillin. Plasmids were isolated from selected colonies using a mini-prep purification kit (EZ-10 Spin Column Plasmid DNA Kit, BioBasic). Positive mutants were identified by restriction digestion with *Sma*I (New England BioLabs Inc.). All mutants were confirmed by sequencing (Macrogen DNA Sequencing Services).

For all primers, the position of mutagenesis is denoted in bold; and the *Sma*I restriction site (CCCGGG) was removed through a silent mutation (underlined) to enable restriction screening.

C81A-f 5'- CGCACACGTAGAC**GCA**CCGGGGCACGCC-3'

C81A-r 5'- GGCGTGCCCCGG**TGC**GTCTACGTGTGCG-3'

C81S-f 5'- CACTACGCACACGTAGAC**AGT**CCGGGGCACG-3'

C81S-r 5'- AGTCGGCGTGCCCCGG**ACT**GTCTACGTGTG-3'

C81M-f 5' –CGCACACGTAGAC**ATG**CCGGGGCACGCC – 3'

C81M-r 5' – GGCGTGCCCCGG**CAT**GTCTACGTGTGCG – 3'

4.2b Protein Expression and Purification

Wild-type and variant EF-Tu proteins were expressed in *E. coli* strain BL21-DE3 (Novagen). Cells were grown at 37°C in LB medium supplemented with 100 μg/mL ampicillin to mid-log phase (OD_{600}=0.6) and induced with 1 mM IPTG (Bio Basic) as in section 3.2c.

Similar purification procedures were followed for wild-type EF-Tu and variant proteins from *E. coli*. This was performed as section 3.2c. The final protein concentration was determined spectrophotometrically at 280 nm using a molar extinction coefficient of 32 900 M^{-1} cm^{-1} (calculated using ProtParam (88)) and confirmed using the Bradford Protein Assay (BioRad).

4.2c Preparation of Nucleotide-Free EF-Tu

To promote the dissociation of GDP, which is tightly bound to EF-Tu and co-elutes with the factor during purification, nucleotide-free EF-Tu was prepared as in section 3.2d.

4.2d Preparation of EF-Tu•mant-GDP, EF-Tu•mant-GTP

EF-Tu•GDP was incubated with a 10-fold molar excess of mant-GDP or mant-GTP in buffer 4.1 (50 mM Tris-Cl pH 7.5 (20°C), 70 mM NH_4Cl, 30 mM KCl and 7 mM $MgCl_2$) for 30 min at 37°C. These reactions were carried out in the presence of 3 mM PEP and 0.1 mg/mL PK (Roche Diagnostic) to convert any nucleotide diphosphate present into their respective nucleotide triphosphate forms.

4.2e Rapid Kinetic Measurements

Fluorescence stopped-flow measurements were performed using a KinTek SF-2004 stopped-flow apparatus similar to that previously described in reference (90) and in section 3.2e. Mant-nucleotides were excited via FRET from the single tryptophan (λ_{ex} = 280 nm) present in EF-Tu and fluorescent emission was measured after passing through LG-400-F cut off filters (NewPort). The apparent rate for the bimolecular association of mant-nucleotides to nucleotide free EF-Tu was determined by rapidly mixing 25 µL of nucleotide free EF-Tu (0.3 µM after mixing) with 25 µL varying concentrations of mant-nucleotides (ranging from 0.3 to 10 µM after mixing) at 20°C in buffer 4.1. Fluorescence time courses were evaluated by fitting with a single exponential

equation, based on the one-step binding behavior (Equation 1) as only single exponential time courses were observed.

$$F = F_{\infty} + A \times \exp(-k \times t) \qquad \text{(Equation 4.1)}$$

Where F is the fluorescence at time t, F_{∞} is the fluorescence at equilibrium, A is the amplitude and k is the apparent rate constant of association (k_{app}). The apparent rate constants were plot as a function of nucleotide concentration; the slope of this function yields the association rate constant (k_{on}).

Dissociation rate constants were determined by rapidly mixing 25 μL EF-Tu•mant-GTP/GDP (0.3 μM after mixing) with 25 μL GTP/GDP (30 μM after mixing) at 20°C in buffer 4.1. Due to the excess of unlabelled nucleotide present, only the dissociation of the mant-labelled nucleotide contributed to the observed fluorescence change and rebinding of the mant-nucleotide is negligible. Using similar conditions the dissociation of mant-GTP/GDP from 25 μL EF-Tu•mant-GTP/GDP (0.3 μM after mixing) was stimulated with 25 μL EF-Ts (1 μM after mixing) at 20°C in buffer 4.1. Fitting the observed fluorescence time courses with equation 4.1 yielded the rate of nucleotide dissociation in the presence of 1 μM EF-Ts. Calculations were performed using TableCurve (Jandel Scientific) and Prism (GraphPad Software).

4.2f Components of the Translation Machinery

Ribosomes from *E. coli* were prepared as in section 2.2d and [^{14}C]Phe-tRNA^{Phe} was prepared as described in Milon *et. al.*, 2007 (89). [^{14}C]Phe-tRNA^{Phe} was prepared through the aminoacylation of 10 µM *E. coli* tRNA^{Phe} (Sigma) with 40 µM [^{14}C]Phe (MP Biomedical), 5% crude synthetase, 3 mM ATP (Sigma) in buffer 4.2 (25 mM Tris-acetate (OAc) pH 7.5 (20°C), 8 mM $Mg(OAc)_2$, 3 mM ATP, 100 mM NH_4OAc, 30 mM KOAc, 1 mM DTT) to a final volume of 500 µL. [^{14}C]Phe-tRNA^{Phe} was separated from tRNA^{Phe} with a Jupiter 5 µm C18 300A reverse phase chromatography column (Phenomenex) on an HPLC (BioCad Sprint Perfusion Chromatography system) using a linear ethanol gradient from buffer 4.3 (20 mM NH_4OAc pH 5, 10 mM $Mg(OAc)_2$, 400 mM NaCl) to buffer 4.4 (buffer 4.3 with 30% ethanol).

4.2g Hydrolysis Protection Assay

To form the EF-Tu•GTP complex, 2.25 µM EF-Tu, 1.5 mM GTP, 3 mM PEP, 0.1 mg/mL PK and 0.9 µM EF-Ts was incubated (total volume of 40 µL) in buffer 4.5 (50 mM Tris-Cl pH 7.5 (4°C), 70 mM NH_4Cl, 30 mM KCl, 10 mM $MgCl_2$) for 20 min at 37°C. Subsequently, 2 µM [^{14}C]Phe-tRNA^{Phe} in 20 µL buffer 4.5 was added to the EF-Tu mixture to form the EF-Tu•GTP•[^{14}C]Phe-tRNA^{Phe} ternary complex. The ternary complex was then incubated at 37°C and aliquots of 10 µL (~7 pmol ternary complex) of the reaction mixture were removed at various time points (from 0 to 100 min) and spotted onto pre-soaked 5% Trichloroacetic acid (TCA) Whatman paper (2.5 cm^2 3MM CHR). Free [^{14}C]Phe liberated by spontaneous hydrolysis was removed with three washes of 5%

TCA, excess TCA was subsequently removed by washing with 30% ethanol. Filter papers were dried at 80°C for 30 min and then added to 5 mL scintillation cocktail (EcoLite, MP Biomedical) in 20 mL liquid scintillation vials (Wheaton). Radioactivity was measured using a Tri-Carb 2800TR Perkin Elmer Liquid Scintillation Analyzer. Data was plotted as the natural logarithm of the ratio of the concentration of remaining [^{14}C]Phe-tRNA^{Phe} at time t (c_t) relative to the concentration at time 0 (c_0).

4.2h Dipeptide formation

Ribosomes (0.5 μM) were programmed with poly(U) (1 mg/mL) by incubation at 37°C for 15 min in a total of 10 μL buffer 4.6 (buffer 4.5 with 1 mM DTT) followed by the addition of an equal volume (10 μL) of EF-Tu•GTP (1 μM EF-Tu, 1mM GTP, 3 mM PEP and 0.1 mg/mL PK in buffer 4.6). Dipeptide formation was initiated by adding 5 μL of 1 μM [^{14}C]Phe-tRNA^{Phe} to the above mixture and further incubated at 37°C for 30 s. The reaction was quenched with one volume (30 μL) of 2 M KOH and incubated at 37°C for 15 min. An equal volume (60 μL) of glacial acetic acid was added and the solution was centrifuged at 15 000 x *g* for 10 min using a Hermle Z180M (Labnet International, Inc.) centrifuge. 60 μL of the supernatant was removed and added to 125 μL of buffer 4.7 (0.1% Trifluoroacetic acid (TFA) in H_2O). The dipeptide content was subsequently analyzed on an EC 250/4 NUCLEOSIL 100-5 C18 column (Macherey-Nagel) using a linear acetonitrile gradient from buffer 4.7 to buffer 4.8 (0.1% TFA, 65% Acetonitrile in H_2O) on a Breeze HPLC system (Waters).

4.3 Results

4.3a Evolution-Based Construction of a Cysteine-Free Variant of EF-Tu

Based on the assumption that evolutionary conservation can provide important clues on the functional conservation of specific positions within a protein, a multiple sequence alignment was performed on bacterial EF-Tu sequences (Appendix Figure A.7) available in the SwissProt Database (115) using ClustalW (116). Analysis of the conservation levels, as well as specific substitutions found in a particular position can provide critical information regarding the identity of residues tolerated in the respective position. The conservation levels and substitutions of the three cysteine residues present in EF-Tu (Cys 81, Cys 136, and Cys 255) from *E. coli* were analyzed using GeneDoc software version 2.7 (117). This analysis revealed that the cysteine residue in position 81 is present in 79% of the aligned bacterial sequences whereas alanine was found in 19% and methionine in one (2%) of the sequences (Appendix Figure A.7). The sequence alignment also showed Cys 136 and Cys 255 to be 31% and 25% conserved, respectively (Appendix Figure A.7). Based on this observation, three different variants were constructed for a cysteine-free EF-Tu, alanine (EF-Tu_{AVV}), methionine (EF-Tu_{MVV}), as well as the structurally conservative serine (isosteric to cysteine) variant (EF-Tu_{SVV}), in which the non-conserved cysteine residues (position 136 and 255) were replaced with the most frequent substitution, valine (25%, 35% respectively), found in the multiple sequence alignment. Subsequently, the activity of the three cysteine-free variants of EF-Tu were assessed through a comparative analysis with respect to the four key catalytic activities of EF-Tu: GDP/GTP binding, EF-Ts interaction, aa-tRNA binding, and aa-tRNA delivery to the translating ribosome (peptide-bond formation).

4.3b Interaction with Guanine Nucleotides (GDP/GTP)

The kinetic parameters governing the interaction of EF-Tu with the respective guanine nucleotides have previously been successfully determined using a FRET-based rapid-kinetics approach (45). Based on this approach, rate constants of nucleotide binding and dissociation for the three constructed EF-Tu variants have been determined, as well as for the wild type enzyme using the stopped-flow technique, measuring FRET between the single tryptophan (Trp 184) in EF-Tu to mant-GDP and mant-GTP.

The apparent rate of nucleotide association was measured at varying concentrations of mant-GDP/mant-GTP using a constant concentration of nucleotide-free EF-Tu (Figure 4.2a, 4.2b). Only a single binding step was observed and the respective apparent rate constants (k_{app}) were determined from the collected fluorescence time courses by fitting with an exponential function at each titration point (Eq. 4.1). The linear dependence of k_{app} on the concentration of mant-GDP/GTP (Figure 4.2c, 4.2d) was used to determine the GTP and GDP association rate constants. Values were determined for all variant and wild type proteins (summarized in Table 4.1): EF-Tu wt ($k_{on(TuwtGTP)} = (3.7 \pm 0.2) \times 10^5\ M^{-1}s^{-1}$, $k_{on(TuwtGDP)} = (1.6 \pm 0.2) \times 10^6\ M^{-1}s^{-1}$); EF-$Tu_{AVV}$ ($k_{on(TuAVVGTP)} = (1.7 \pm 0.1) \times 10^5\ M^{-1}s^{-1}$, $k_{on(TuAVVGDP)} = (1.6 \pm 0.2) \times 10^6\ M^{-1}s^{-1}$); EF-$Tu_{MVV}$ ($k_{on(TuMVVGTP)} = (3.9 \pm 0.1) \times 10^5\ M^{-1}s^{-}1$, $k_{on(TuMVVGDP)} = (4.3 \pm 0.2) \times 10^6\ M^{-1}s^{-1}$); EF-$Tu_{SVV}$ ($k_{on(TuSVVGTP)} = (2.2 \pm 0.1) \times 10^5\ M^{-1}s^{-1}$, $k_{on(TuSVVGDP)} = (1.2 \pm 0.1) \times 10^6\ M^{-1}s^{-1}$). These results indicate that EF-Tu_{AVV}, EF-Tu_{MVV}, and EF-Tu_{SVV} have similar association rate constants for both guanine nucleotides when compared to wild-type EF-Tu.

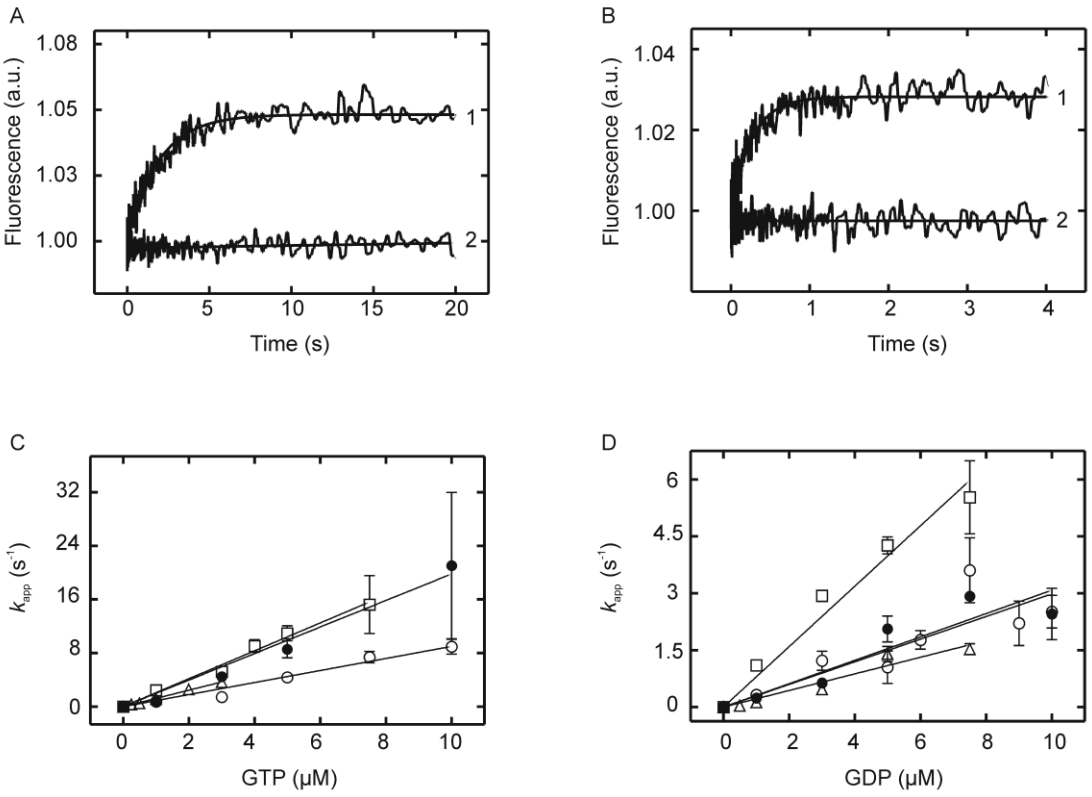

Figure 4.2. Determination of nucleotide association rate constants. (A) Time course of 3 μM mant-GTP association to (1) EF-Tu wt (0.3 μM) measured via FRET excitation of mant fluorescence; (2) control without EF-Tu. (B) Time course of 3 μM mant-GDP association to (1) EF-Tu wt (0.3 μM), (2) control without EF-Tu. (C, D) Concentration dependence of k_{app} determined by fitting time courses similar to (A, B) at various nucleotide concentrations with a single-exponential function. Filled circles, EF-Tu wt; open circles, EF-Tu_{AVV}; open squares, EF-Tu_{MVV}; open triangles, EF-Tu_{SVV}.

Table 4.1. Kinetic Constants Governing the Interactions Between EF-Tu and Guanine Nucleotides.

Constant	EF-Tu wt	EF-Tu_{AVV}	EF-Tu_{MVV}	EF-Tu_{SVV}
k_{onGTP} $M^{-1}s^{-1}$	$3.7 \pm 0.2 \times 10^5$	$1.7 \pm 0.1 \times 10^5$	$3.9 \pm 0.1 \times 10^5$	$2.2 \pm 0.1 \times 10^5$
k_{onGDP} $M^{-1}s^{-1}$	$1.6 \pm 0.2 \times 10^6$	$1.6 \pm 0.2 \times 10^6$	$4.3 \pm 0.2 \times 10^6$	$1.2 \pm 0.1 \times 10^6$
k_{offGTP} s^{-1}	0.04 ± 0.01	0.06 ± 0.01	0.04 ± 0.01	0.06 ± 0.01
k_{offGDP} s^{-1}	0.002 ± 0.001	0.004 ± 0.001	0.002 ± 0.001	0.003 ± 0.001
K_D (GTP) nM	110 ± 30	350 ± 80	100 ± 30	270 ± 60
K_D (GDP) nM	1.3 ± 0.8	3 ± 1	0.5 ± 0.3	3 ± 1

Nucleotide dissociation rate constants for the EF-Tu•mant-GTP and EF-Tu•mant-GDP complexes were determined by mixing with excess GDP/GTP using FRET between the

single tryptophan present in EF-Tu and the bound mant-GDP/GTP (Figure 4.3a, 4.3b). The presence of excess unlabelled nucleotide inhibits the rebinding of free mant-GDP/mant-GTP, resulting in fluorescence time courses reflecting a single dissociation step. Consequently, the dissociation rate constants were obtained by fitting the observed time courses in Figures 4.3a and 4.3b with a single-exponential function (Eq. 4.1). Values obtained for the respective k_{off} are summarized in Table 4.1: EF-Tu wt ($k_{off(TuwtGTP)} = 0.04 \pm 0.01 s^{-1}$, $k_{off(TuwtGDP)} = 0.002 \pm 0.001 s^{-1}$); EF-$Tu_{AVV}$ ($k_{off(TuAVVGTP)} = 0.06 \pm 0.01\ s^{-1}$, $k_{off(TuAVVGDP)} = 0.004 \pm 0.001\ s^{-1}$); EF-$Tu_{MVV}$ ($k_{off(TuMVVGTP)} = 0.04 \pm 0.01\ s^{-1}$, $k_{off(TuMVVGDP)} = 0.002 \pm 0.001\ s^{-1}$); EF-$Tu_{SVV}$ ($k_{off(TuSVVGTP)} = 0.06 \pm 0.01\ s^{-1}$, $k_{off(TuSVVGDP)} = 0.003 \pm 0.001\ s^{-1}$). The values obtained for both GDP and GTP dissociation rate constants are similar for all three variants of EF-Tu as well as wild type EF-Tu and are consistent with those reported previously (45). Based on these results, equilibrium binding constants (K_D) for the variants and the wild type protein can be calculated from $K_D = k_{off}/k_{on}$ (summarized in Table 4.1) revealing only slight effects (3-fold) of the substitutions on the respective binding constants.

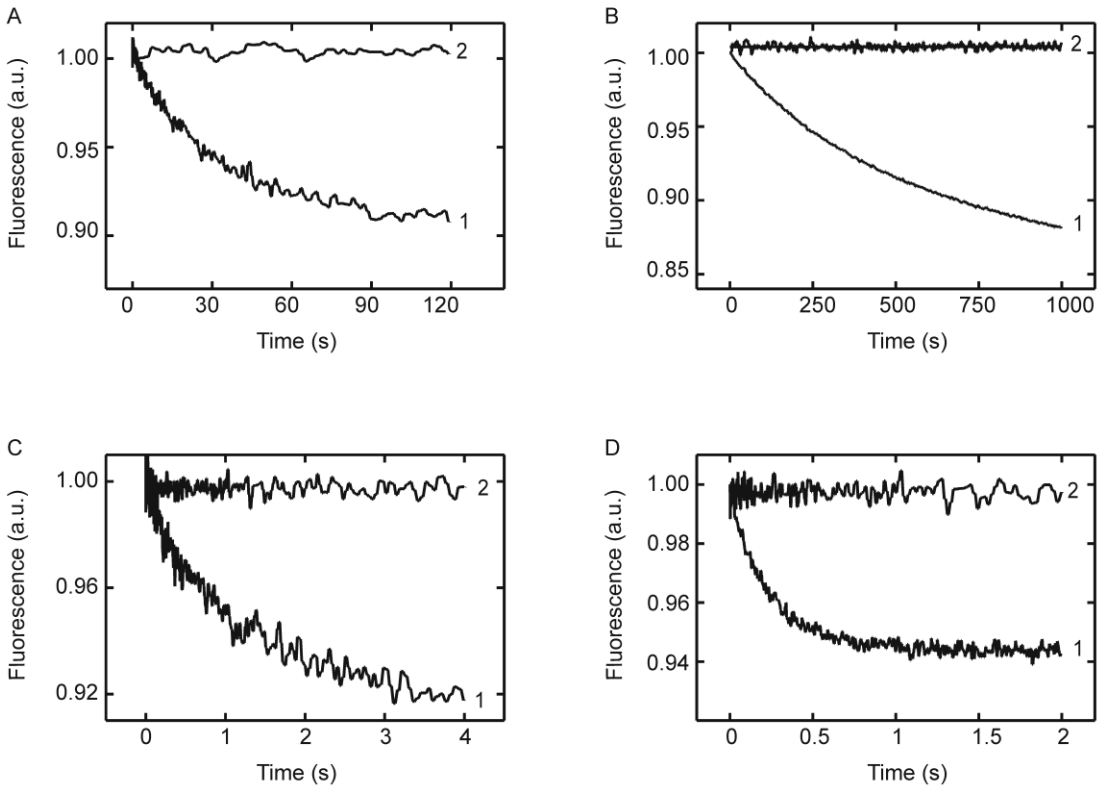

Figure 4.3. Determination of nucleotide dissociation rate constants. (A) Time course of mant-GTP dissociation from (1) EF-Tu wt (0.3 μM) measured via FRET excitation of mant fluorescence; (2) control without EF-Tu. (B) Time course of mant-GDP dissociation from (1) EF-Tu wt (0.3 μM); (2) control without EF-Tu. (C) Time course of mant-GTP dissociation from EF-Tu wt (0.3 μM) stimulated by EF-Ts (1 μM). (D) Time course of mant-GDP dissociation from EF-Tu wt (0.3 μM) stimulated by EF-Ts (1 μM).

4.3c EF-Ts Stimulated Guanine Nucleotide Dissociation

In order to assess the effect of replacing cysteine residues present in EF-Tu on interactions with its nucleotide exchange factor EF-Ts, stopped-flow measurements of the nucleotide dissociation rates in the presence of a fixed concentration of EF-Ts were performed. Under these conditions, effects on the affinity of the variant EF-Tus to EF-Ts and on the mechanism of nucleotide dissociation was assayed. EF-Tu•mant-GDP/EF-Tu•mant-GTP was rapidly mixed with EF-Ts in the presence of excess unlabelled nucleotide, and a decrease in the fluorescence of the mant reporter

group due to the dissociation of the nucleotide was recorded (Figure 4.3c, 4.3d). As for the intrinsic dissociation reaction, the observed time courses were fit with a single-exponential function (Eq. 4.1). The obtained values (summarized in Table 4.2) indicate that nucleotide dissociation from variant EF-Tu is stimulated by EF-Ts similar to rates obtained with wild type EF-Tu under these conditions. This suggests that the introduced substitutions do not affect the EF-Ts stimulated nucleotide exchange reaction, nor the interaction between the two proteins.

Table 4.2. EF-Ts Induced Dissociation of mant-Nucleotides from EF-Tu.

EF-Tu	k_{app} s^{-1} (GTP + Ts)	k_{app} s^{-1} (GDP + Ts)
EF-Tu wt	6.9 ± 0.1	2.6 ± 0.1
$EF\text{-}Tu_{AVV}$	6.3 ± 0.2	4.4 ± 0.1
$EF\text{-}Tu_{MVV}$	7.1 ± 0.1	2.5 ± 0.1
$EF\text{-}Tu_{SVV}$	4.9 ± 0.2	1.7 ± 0.1

4.3d Interaction of aa-tRNA with EF-Tu

Results here confirm that nucleotide binding properties are not significantly affected by the introduced amino acid residue substitutions. The effect of these substitutions on the interaction with another main cellular interaction partner of EF-Tu, aa-tRNA, was also analyzed. To this end, the ability of wild-type EF-Tu and the three variants to protect the aminoacyl-ester bond between [^{14}C]-labelled phenylalanine and the $tRNA^{Phe}$ body against spontaneous hydrolysis was examined. A fixed amount of [^{14}C]Phe-$tRNA^{Phe}$ was incubated in the presence of EF-Tu•GTP and the amount of [^{14}C]Phe-$tRNA^{Phe}$ remaining intact was measured as function of time (Figure 4.4). The half-life ($t_{1/2}$) of [^{14}C]Phe-$tRNA^{Phe}$ in the presence of each variant was calculated and compared to wild

type EF-Tu (Table 4.3). The calculated $t_{1/2}$ in the presence of EF-Tu wt and EF-Tu_{AVV} were comparable (90 ± 5 min and 80 ± 20 min, respectively), whereas the $t_{1/2}$ in the presence of EF-Tu_{MVV} and EF-Tu_{SVV} was significantly affected (40 ± 4 min and 30 ± 8 min, respectively) indicating an altered mode of interaction with aa-tRNA for the latter two variants. However, both variants are still capable of protecting the aminoacyl-ester bond against spontaneous hydrolysis to some extent, when compared to the hydrolysis in the absence of EF-Tu (Figure 4.4, Table 4.3) which has a half-life of 10 ± 7 min. This suggests that a ternary complex also forms in the presence of the EF-Tu_{MVV} and EF-Tu_{SVV} variants, but the interaction might be weaker and thus more dynamic with the aa-tRNA dissociating more frequently from EF-Tu. Furthermore, the observation showing EF-Tu_{AVV} exhibiting wild type-like behavior in this assay suggests that the substitutions at position 255 and 136 do not effect aa-tRNA interaction.

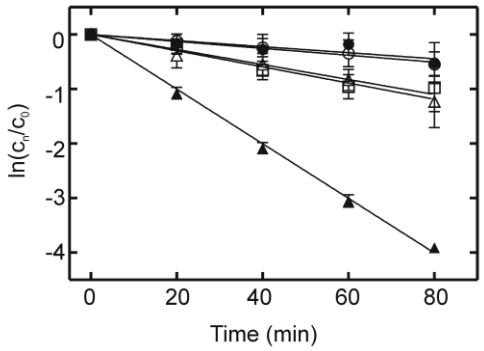

Figure 4.4. EF-Tu•GTP•aa-tRNA ternary complex stability. Time dependence of 0.5 μM [^{14}C]Phe-$tRNA^{Phe}$ hydrolysis, incubated in the presence of EF-Tu wt (filled circles) EF-Tu_{AVV} (open circles) EF-Tu_{MVV} (open squares) EF-Tu_{SVV} (open triangles) and absence of factor (filled triangles). $\ln(c_n/c_0)$ is plotted over time, where the slope indicates the rate of aminoacyl-ester bond cleavage. c_n is the concentration of [^{14}C]Phe-$tRNA^{Phe}$ at a given time point and c_0 is the concentration of [^{14}C]Phe-$tRNA^{Phe}$ at time 0.

Table 4.3. EF-Tu Mediated Protection of Phe-tRNA^{Phe} against Spontaneous Hydrolysis.

EF-Tu	$t_{1/2}$ Phe-tRNA^{Phe} (min)
EF-Tu wt	90 ± 5
EF-Tu$_{AVV}$	80 ± 20
EF-Tu$_{MVV}$	40 ± 4
EF-Tu$_{SVV}$	30 ± 8
No EF-Tu	10 ± 7

4.3e EF-Tu Dependent Dipeptide Formation

During the elongation phase of protein synthesis, EF-Tu interacts with the ribosome as a ternary complex EF-Tu•GTP•aa-tRNA in a codon-dependent manner. Productive interaction results in peptide-bond formation between the ribosome-bound growing peptide chain and the amino acid of the incoming aa-tRNA. To assess the ability of the three variants to sustain ribosome-dependent protein synthesis, the ability to promote dipeptide formation was measured using a poly(U)-dependent *in vitro* translation assay (Figure 4.5). The amount of dipeptide formed was analyzed using HPLC and quantified using scintillation counting (Material and Methods). When compared to the dipeptide formation promoted by wild-type EF-Tu (100 ± 20%), all three variants (EF-Tu$_{AVV}$, EF-Tu$_{MVV}$ and EF-Tu$_{SVV}$) showed a similar dipeptide formation activity (84 ± 8 %, 72 ± 11 %, and 85 ± 12%, respectively) under these conditions. This is significantly higher than in the absence of EF-Tu (8 ± 3%). These findings indicated that all three variants of EF-Tu are not significantly affected in their interactions with the translating ribosomes comprising all the different steps of A site binding up to dipeptide formation.

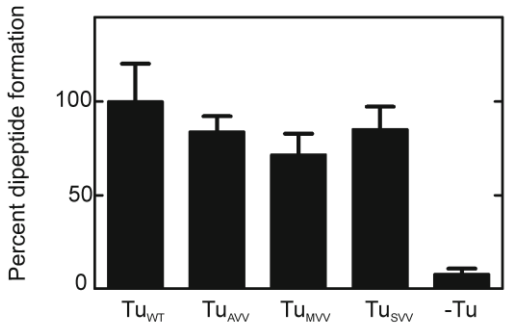

Figure 4.5. Peptide-bond formation. Percent dipeptide formation of [^{14}C]Phe-[^{14}C]Phe dipeptide within 30 s at 10 mM Mg^{2+} in the presence of EF-Tu wt, EF-Tu$_{AVV}$ EF-Tu$_{MVV}$, EF-Tu$_{SVV}$ or no EF-Tu as indicated on the x-axis. Purified 70S ribosomes were programmed with poly(U) and dipeptide formation was initiated by the addition of [^{14}C]Phe-tRNA^{Phe} in the presence of the respective EF-Tu•GTP. Dipeptides formed were separated using HPLC and subsequently quantified using scintillation counting.

4.4 Discussion

Over recent years, fluorescence-based rapid kinetic approaches have provided valuable information regarding the structural dynamics and functional mechanism of translation in bacteria (41,132). A detailed understanding of the underlying principles of this last step in gene expression is of great importance for a large number of applications, ranging from the rational design of biomolecular machines to the development of novel antibiotics. With the advent of sophisticated single-molecule fluorescence techniques, further detail about structural dynamics of involved macromolecules has been added to the existing knowledge (125). However, the picture generated by these combined techniques still has several blind spots, including a detailed description of the structural dynamics of EF-Tu during aa-tRNA release into the ribosomal A site following GTP hydrolysis and P_i release. This is mainly due to a lack of appropriate molecular tools to address this step, such as an EF-Tu allowing for the specific incorporation of fluorescent dyes optimal for both ensemble and single molecule measurements. Therefore, the focus of this study was to develop a cysteine-free variant of EF-Tu, which retains wild type properties and can serve as a starting point for the development of novel fluorescence-based assays to study the structural dynamics of EF-Tu during protein synthesis.

4.4a Evolution-Based Design and Previous Studies

The need to maintain the structural and functional integrity of an evolving protein severely restricts the repertoire of acceptable amino acid substitutions. The selective constraint imposed on evolving proteins can be very strong, therefore amino acid

conservation provides critical information on the functional importance of particular amino acids. Based on the evolutionary analysis performed here, it was confirmed that only one (Cys 81) of the three cysteine residues present in EF-Tu from *E. coli* (Cys 81, Cys 136, and Cys 255) is highly conserved. Furthermore, the cysteine residues in position 136 and 255 can be substituted with valine, the most abundant amino acid substitution occurring in these positions. The high degree of evolutionary conservation of Cys 81, as well as evidence from previous studies (129), suggests that a cysteine side chain in this position is important for the function of EF-Tu. The fact that Cys 81 displays reactivity against TPCK and that this modification strongly affects EF-Tu dependent poly(Phe) synthesis (128), demonstrates the necessity to replace the cysteine side chain in this position with a side chain that will not be reactive in subsequent labelling reactions. One of these potential substitutions replacing cysteine with glycine has previously been reported (129). Although this variant was originally constructed to study the role of Cys 81 during aa-tRNA binding, it also demonstrated that the reduction of the side chain to a hydrogen atom in this position cannot be tolerated by EF-Tu. This substitution resulted in an overall slower rate of poly(Phe) synthesis, decreased protection of the aminoacyl-ester bond against spontaneous hydrolysis (40%), as well as altered nucleotide binding properties (i.e. a 13-fold higher K_D for GDP) (129). This phenotype is consistent with the multiple sequence alignment performed here in which no glycine residue was found at this position.

Interestingly, although highly conserved, it was found that the cysteine is replaced in a small number of bacterial sequences with only two other amino acids, alanine and methionine, suggesting that these mutations may be tolerated. Variants of EF-Tu were

therefore constructed based on this evolutionary clue. As expected, these variants did not have the strong phenotype associated with the glycine substitution as they exhibited wild type-like behavior with respect to a number of key functions of EF-Tu, including nucleotide binding and poly(Phe) synthesis. However, the respective methionine and serine, but not the alanine, substitutions were significantly impaired in protecting the labile aa-ester bond against spontaneous hydrolysis. This might be the reason why this substitution was only found in one of the bacterial sequences. The fact that the protein containing methionine at position 81 is from *Streptomyces coelicolor* can be explained by the presence of several copies of genes coding for EF-Tu in its genome. In addition to the gene giving rise to the nonessential methionine variant, it also contains a version of EF-Tu containing cysteine in this position, enabling *S. coelicolor* to overcome any negative effect that might be associated with the methionine substitution *in vivo*. Furthermore, *S. coelicolor* produces several antibiotics, such as actinorhodin, methylenomycin, undecylprodigiosin, and perimycin (133). It is believed that the alternate versions of EF-Tu in this organism are necessary for cellular resistance strategies against the produced antibiotics.

In order to further test these hypothesis that maintaining the function of EF-Tu is the reason for the observed limited sequence variability (Ala and Met) at this position, a Cys-less variant of EF-Tu containing serine at position 81 was also constructed. Although the serine variant was not as strongly affected as the previously reported glycine variant, it also displayed decreased protection activity against the spontaneous hydrolysis of the aa-ester bond between the phenylalanine and the $tRNA^{Phe}$.

4.4b Functional Role of Cysteine 81

No direct interactions of the cysteine side chain with either the aa-tRNA or the nucleotide have been identified in the available crystal structures and it is not clear what the mechanistic/structural reason for the observed limited sequence variability in position 81 is. Findings reported here suggest that the main functional constraint is imposed by the ability of EF-Tu to form a stable ternary complex with aa-tRNA rather than the general effects observed in the previously reported glycine variant (129). Substitution with glycine affects aa-tRNA binding, nucleotide binding properties of EF-Tu as well as its thermal stability, which is most likely due to the increased backbone flexibility and decreased side chain packing around this position. This is further supported by the observation that replacing cysteine with either serine or methionine restores nucleotide binding properties, as well as the interaction with EF-Ts to promote nucleotide dissociation, but not the protection of the aa-ester bond. This is surprising since the cysteine, and therefore also the methionine and serine side chain, are more than 15 Å away from the aa-ester bond in the ternary complex (101) and should not have any direct influence on the stability of this bond. Mutational studies to identify the thermodynamically relevant interactions between EF-Tu and aa-tRNA revealed a cluster of amino acids (Tyr 87, Lys 89, Asn 90) in helix B of EF-Tu (six amino acids downstream of Cys 81) that are involved in aa-tRNA binding by forming a molecular clamp recognizing the phosphate backbone of the bound aa-tRNA acceptor arm (134).

Selective mutations of these invariant amino acids lead to the disruption of the specific interactions and a 10-fold decrease in the affinity for aa-tRNA (134), which is within the same order of magnitude as the reduction of protection found in these experiments. Helix

B is of particular interest since it participates in the drastic conformational change occurring during the transition from the active GTP-bound state to the inactive GDP-bound form of EF-Tu. In the GTP-bound form, residues 54-59 in the switch I region of the G-domain fold into helix A, whereas the same residues are part of β-strand b' in the GDP conformation (44). All this occurs in close proximity to helix B, which in the GTP-bound form of EF-Tu is shifted by 42° compared to the GDP-bound form. In the GTP conformation, side chain packing around Cys 81 is high and its side chain is in close proximity (4.1 Å) to the invariant Gly 94 on the other side (downstream) of helix B, aiding in its positioning. In the GDP-bound state of EF-Tu, helix B reorients and this distance increases to 10.2 Å, moving Tyr 87 into the spatial position previously occupied by Cys 81. Based on the participation of helix B in binding of the aa-tRNA, slight differences in the positioning of the molecular clamp formed by helix B (residues Tyr 87, Lys 89, Asn 90) are likely to have consequences on the aa-tRNA binding affinity. The consideration of the complex structural arrangements leading to the formation of the EF-Tu•GTP•aa-tRNA ternary complex, as well as the high density of side chain packing around Cys 81 would suggest that only alanine can be tolerated in this position, as indicated by its evolutionary conservation. Based on this it is possible to speculate on the effects of methionine at this position. Due to its larger size it can interfere with this packing and ultimately alter the positioning of helix B, in turn affecting the binding mode of the aa-tRNA. Whereas the interpretation of the methionine effect is straightforward, the reason why serine cannot be tolerated in this position is more complicated. As serine and cysteine are isosteric, the steric properties of the side chain are most likely not responsible for the observed effect on aa-tRNA binding. It is more likely that the

physicochemical properties of the OH-versus the SH-group, and therefore the altered protonation and hydrogen bonding properties give rise to the observed effects. This would point towards altered dynamics based on, for example, different hydrogen bonding interactions available during the transition between the GTP and GDP-bound forms of EF-Tu or a different positioning of helix B and the respective amino acids. However, in either case (methionine or serine), altered interactions around position 81 are likely to affect the dynamics observed during conformational change from the GTP to the GDP-bound state and vice versa, as well as during aa-tRNA binding and dissociation, making these two substitutions a poor choice for the construction of a Cys-less version of EF-Tu for subsequent studies on the dynamics of this protein during protein synthesis.

4.5 Future Directions

Based on the results reported here, it is demonstrated that a Cys-less variant of EF-Tu retaining wild type dynamic and biochemical properties can be constructed by replacing the highly conserved cysteine in position 81 with alanine, but not with methionine or serine. This Cys-less EF-Tu will be the background of choice for future studies on the function of EF-Tu using site-specific introduction of fluorescent and non-fluorescent reporter groups. These modified proteins will provide powerful tools for the identification and characterization of novel antibiotics targeting the translational machinery, as well as provide important insights into the highly dynamic process of aa-tRNA delivery.

The Cys-less EF-Tu_{AVV} has been used as a background for the construction of a series of EF-Tu variants with either a single or two cysteines introduced at positions on the protein surface that are non-conserved and ideal for chemical modification with thiol specific, fluorescent reporter groups.

Singly fluorescently labelled EF-Tu will allow for studies on the interaction between EF-Tu and the ribosome. This can shed light on whether EF-Tu dissociates from the ribosome before or after tRNA accommodation in the A site. Intramolecular hetero-labelled EF-Tu will allow monitoring of the dynamics of the conformational change within EF-Tu. This data will be a beneficial screening tool for potential inhibitors of EF-Tu function. Labelling strategy and efficiency is provided in the appendix section A.3.

Chapter 5 Conclusion

Protein synthesis is one of the most fundamental processes in all living cells. As such it is an effective current target for antibiotics (57) as inhibiting this process stops cellular growth. However, antibiotic resistance continues to increase and is a major public health concern.

The cyclic process of peptide elongation during protein synthesis is a highly conserved process and is the target of many currently utilized antibiotics (135). Not only do antibiotics interfere with protein synthesis by binding to the ribosome, but some target translation elongation factors. EF-Tu and EF-G are the targets for some antibiotics currently in use. Pulvomycin and GE2270A inhibit EF-Tu function by preventing aa-tRNA from binding to EF-Tu, and kirromycin and enacyloxin IIa prevent the release of EF-Tu from the ribosome (136). Fusidic acid targets EF-G and prevents the release of EF-G from the ribosome (136). Inhibiting the function of these translation factors efficiently inhibits protein synthesis.

Beyond the canonical translation factors, LepA has been identified to function as a translational GTPase, and its functional mechanism is only poorly understood. Here it is demonstrated that, similar to EF-Tu, LepA contains a catalytic histidine that is needed for efficient GTPase activity of LepA on and off the ribosome. Furthermore, the unique CTD of LepA is required for tight binding of LepA to the ribosome and efficient ribosome-stimulated GTPase activity, making the CTD of LepA a possible unique future target for antibiotics.

The comparison of the kinetics of EF-Ts mediated nucleotide exchange between *E. coli* and *P. aeruginosa* revealed that the catalytic ability of EF-Ts to stimulate guanine

nucleotide dissociation from the highly conserved EF-Tu can be modulated though the C-terminal module of EF-Ts. In most organisms, EF-Ts is necessary to sustain *in vivo* rates of protein synthesis, however, it is currently not a target for antibiotics. Given the importance of EF-Ts for maintaining protein synthesis rates in bacteria, it is surprising that it is currently not an antibiotic target. Findings here demonstrate that the length of the C-terminal module is important for the function of EF-Ts. Furthermore, the sequence of the C-terminal extension can influence the ability of EF-Ts to act as a GEF, depending on what system is being analyzed. The variability in the sequence and length of the C-terminal module can be utilized in virtual screening methods to specifically target an organism without affecting another.

Little is known about the dynamics of the conformational change EF-Tu undergoes. A Cys-less EF-Tu that is functional has been developed here and can be utilized in future dynamic analysis. Identification of new potential intermediates may serve as a new target for antibiotics. As EF-Tu is a current effective target for antibiotics, identification of new functional states will allow for the development of new effective drugs which can target this essential protein.

REFERENCES

1. Jacob, F. and Monod, J. (1961) Genetic Regulatory Mechanisms in Synthesis of Proteins. *J. Mol. Biol.*, **3**, 318-356.
2. Voet, D. and Voet, J.G. (2010) *Biochemistry*. 3rd Edition ed. Wiley and Sons, New Jersey.
3. Tissieres, A. and Watson, J.D. (1958) Ribonucleoprotein Particles from *Escherichia coli*. *Nature*, **182**, 778-780.
4. Voorhees, R.M., Weixlbaumer, A., Loakes, D., Kelley, A.C. and Ramakrishnan, V. (2009) Insights into substrate stabilization from snapshots of the peptidyl transferase center of the intact 70S ribosome. *Nat. Struct. Mol. Biol.*, **16**, 528-533.
5. Mora, G., Donner, D., Thammana, P., Lutter, L., Kurland, C.G. and Craven, G.R. (1971) Purification and characterization of 50S ribosomal proteins of *Escherichia coli*. *Molec. Gen. Genet.*, **112**, 229-242.
6. Hardy, S.J.S., Kurland, C.G., Voynow, P. and Mora, G. (1969) Ribosomal proteins of *Escherichia coli*. I. Purification of the 30 S ribosomal proteins. *Biochemistry*, **8**, 2897-2905.
7. Rheinberger, H.J., Sternbach, H. and Nierhaus, K.H. (1981) Three tRNA binding sites on *Escherichia coli* ribosomes. *Proc. Natl. Acad. Sci. U. S. A.*, **78**, 5310-5314.
8. Gegenheimer, P. and Apirion, D. (1980) Precursors to 16S and 23S ribosomal RNA from a ribonuclease III strain of Escherichia coli contain intact RNaseIII processing sites *Nucleic Acids Res.*, **8**, 1873-1891.
9. Li, Z.W., Pandit, S. and Deutscher, M.P. (1999) RNase G (CafA protein) and RNase E are both required for the 5 ' maturation of 16S ribosomal RNA. *Embo J.*, **18**, 2878-2885.
10. Li, Z.W., Pandit, S. and Deutscher, M.P. (1999) Maturation of 23S ribosomal RNA requires the exoribonuclease RNase T. *RNA-Publ. RNA Soc.*, **5**, 139-146.
11. Spierer, P., Wang, C.C., Marsh, T.L. and Zimmermann, R.A. (1979) Cooperative interactions among protein and RNA components of the 50S ribosomal-subunit of *Escherichia coli Nucleic Acids Res.*, **6**, 1669-1682.
12. Mizushim.S and Nomura, M. (1970) Assembly mapping of 30S ribosomal proteins from *E. coli Nature*, **226**, 1214.
13. Schluenzen, F., Tocilj, A., Zarivach, R., Harms, J., Gluehmann, M., Janell, D., Bashan, A., Bartels, H., Agmon, I., Franceschi, F. *et al.* (2000) Structure of functionally activated small ribosomal subunit at 3.3 angstrom resolution. *Cell*, **102**, 615-623.
14. Ogle, J.M., Carter, A.P. and Ramakrishnan, V. (2003) Insights into the decoding mechanism from recent ribosome structures. *Trends Biochem.Sci.*, **28**, 259-266.
15. Simonovic, M. and Steitz, T.A. (2009) A structural view on the mechanism of the ribosome-catalyzed peptide bond formation. *Biochim. Biophys. Acta-Gene Regul. Mech.*, **1789**, 612-623.
16. Diaconu, M., Kothe, U., Schlunzen, F., Fischer, N., Harms, J.M., Tonevitsky, A.G., Stark, H., Rodnina, M.V. and Wahl, M.C. (2005) Structural basis for the function of the ribosomal L7/12 stalk in factor binding and GTPase activation. *Cell*, **121**, 991-1004.
17. Wahl, M.C. and Moller, W. (2002) Structure and function of the acidic ribosomal stalk proteins *Curr. Protein Pept. Sci.*, **3**, 93-106.
18. Li, G. and Zhang, X.C. (2004) GTP Hydrolysis Mechanism of Ras-like GTPases. *J. Mol. Biol.*, **340**, 921-932.
19. Lee, H.W., Kyung, T., Yoo, J., Kim, T., Chung, C., Ryu, J.Y., Lee, H., Park, K., Lee, S., Jones, W.D. *et al.* (2013) Real-time single-molecule co-immunoprecipitation analyses reveal cancer-specific Ras signalling dynamics. *Nat Commun*, **4**, 1505.
20. Mohr, D., Wintermeyer, W. and Rodnina, M.V. (2002) GTPase Activation of Elongation Factors Tu and G on the Ribosome. *Biochemistry*, **41**, 12520-12528.

21. Caldon, C.E. and March, P.E. (2003) Function of the universally conserved bacterial GTPases. *Current Opinion in Microbiology*, **6**, 135-139.
22. Laursen, B.S., Sorensen, H.P., Mortensen, K.K. and Sperling-Petersen, H.U. (2005) Initiation of protein synthesis in bacteria. *Microbiol. Mol. Biol. Rev.*, **69**, 101-123.
23. Alekhina, O.M. and Vassilenko, K.S. (2012) Translation initiation in eukaryotes: Versatility of the scanning model. *Biochem.-Moscow*, **77**, 1465-1477.
24. Shine, J. and Dalgarno, L. (1975) Determinant of Cistron Specificity in Bacterial Ribosomes *Nature*, **254**, 34-38.
25. Milon, P., Maracci, C., Filonava, L., Gualerzi, C.O. and Rodnina, M.V. (2012) Real-time assembly landscape of bacterial 30S translation initiation complex. *Nat. Struct. Mol. Biol.*, **19**, 609-615.
26. Rodnina, M.V. and Wintermeyer, W. (2009) Recent mechanistic insights into eukaryotic ribosomes. *Curr. Opin. Cell Biol.*, **21**, 435-443.
27. Brunelle, J.L., Shaw, J.J., Youngman, E.M. and Green, R. (2008) Peptide release on the ribosome depends critically on the 2 ' OH of the peptidyl-tRNA substrate. *RNA-Publ. RNA Soc.*, **14**, 1526-1531.
28. Laurberg, M., Asahara, H., Korostelev, A., Zhu, J.Y., Trakhanov, S. and Noller, H.F. (2008) Structural basis for translation termination on the 70S ribosome. *Nature*, **454**, 852-857.
29. Grentzmann, G., Brechemierbaey, D., Heurgue, V., Mora, L. and Buckingham, R.H. (1994) Localization and Characterization of the Gene Encoding Release Factor RF3 in *Escherichia-coli Proc. Natl. Acad. Sci. U. S. A.*, **91**, 5848-5852.
30. Pisareva, V.P., Pisarev, A.V., Hellen, C.U.T., Rodnina, M.V. and Pestova, T.V. (2006) Kinetic analysis of interaction of eukaryotic release factor 3 with guanine nucleotides. *J. Biol. Chem.*, **281**, 40224-40235.
31. Fan-Minogue, H., Du, M., Pisarev, A.V., Kallmeyer, A.K., Salas-Marco, J., Keeling, K.M., Thompson, S.R., Pestova, T.V. and Bedwell, D.M. (2008) Distinct eRF3 requirements suggest alternate eRF1 conformations mediate peptide release during eukaryotic translation termination. *Mol. Cell.*, **30**, 599-609.
32. Savelsbergh, A., Rodnina, M.V. and Wintermeyer, W. (2009) Distinct functions of elongation factor G in ribosome recycling and translocation. *RNA-Publ. RNA Soc.*, **15**, 772-780.
33. Pisarev, A.V., Skabkin, M.A., Pisareva, V.P., Skabkina, O.V., Rakotondrafara, A.M., Hentze, M.W., Hellen, C.U.T. and Pestova, T.V. (2010) The Role of ABCE1 in Eukaryotic Posttermination Ribosomal Recycling. *Mol. Cell.*, **37**, 196-210.
34. Crick, F.H.C. (1966) Codon-Anticodon Pairing - Wobble Hypothesis. *J. Mol. Biol.*, **19**, 548-555.
35. Holmquis.R, Jukes, T.H. and Pangburn, S. (1973) Evolution of transferRNA *J. Mol. Biol.*, **78**, 91-116.
36. Sussman, J.L., Holbrook, S.R., Warrant, R.W., Church, G.M. and Kim, S.H. (1978) Crystal-structure of yeast phenylalanine transfer-RNA .1. Crystallographic refinement. *J. Mol. Biol.*, **123**, 607-630.
37. Hou, Y.M. (1997) Discriminating among the discriminator bases of tRNAs. *Chem. Biol.*, **4**, 93-96.
38. Lengyel, P. and Soll, D. (1969) Mechanism of protein biosynthesis. *Bacteriological Reviews*, **33**, 264-301.
39. Miller, D.L. and Weissbac.H. (1970) Studies on Purification and Properties of Factor Tu from *E. coli Arch. Biochem. Biophys.*, **141**, 26-37.
40. Miller, D.L. and Weissbach, H. (1977) Factors Involved in the Transfer of Aminoacyl Transfer RNA to the Ribosome *Weissbach, Herbert and Sidney Pestka*, 323-373.

41. Rodnina, M.V., Gromadski, K.B., Kothe, U. and Wieden, H.J. (2005) Recognition and selection of tRNA in translation. *FEBS Lett.*, **579**, 938-942.
42. Pape, T., Wintermeyer, W. and Rodnina, M.V. (1998) Complete kinetic mechanism of elongation factor Tu-dependent binding of aminoacyl-tRNA to the A site of the *E. coli* ribosome. *EMBO J*, **17**, 7490-7497.
43. Kothe, U. and Rodnina, M.V. (2006) Delayed release of inorganic phosphate from elongation factor Tu following GTP hydrolysis on the ribosome. *Biochemistry*, **45**, 12767-12774.
44. Song, H., Parsons, M.R., Rowsell, S., Leonard, G. and Phillips, S.E. (1999) Crystal structure of intact elongation factor EF-Tu from *Escherichia coli* in GDP conformation at 2.05 angstrom resolution. *J. Mol. Biol.*, **285**, 1245-1256.
45. Gromadski, K.B., Wieden, H.J. and Rodnina, M.V. (2002) Kinetic mechanism of elongation factor Ts-catalyzed nucleotide exchange in elongation factor Tu. *Biochemistry*, **41**, 162-169.
46. Chau, V., Romero, G. and Biltonen, R.L. (1981) Kinetic studies on the interactions of *Escherichia coli* K12 elongation factor Tu with GDP and elongation factor Ts. *J Biol Chem*, **256**, 5591-5596.
47. Kawashima, T., Berthet-Colominas, C., Wulff, M., Cusack, S. and Leberman, R. (1996) The structure of the *Escherichia coli* EF-Tu.EF-Ts complex at 2.5 angstrom resolution. *Nature*, **379**, 511-518.
48. Bochner, B.R. and Ames, B.N. (1982) Complete Analysis of Cellular Nucleotides by Two-Dimensional Thin-Layer Chromatography. *J. Biol. Chem.*, **257**, 9759-9769.
49. Wohlgemuth, I., Beringer, M. and Rodnina, M.V. (2006) Rapid peptide bond formation on isolated 50S ribosomal subunits. *EMBO Rep.*, **7**, 699-703.
50. Wohlgemuth, I., Brenne, S., Beringer, M. and Rodnina, M.V. (2008) Modulation of the Rate of Peptidyl Transfer on the Ribosome by the Nature of Substrates. *J. Biol. Chem.*, **283**, 32229-32235.
51. Rodnina, M.V. and Wintermeyer, W. (2011) The ribosome as a molecular machine: the mechanism of tRNA-mRNA movement in translocation. *Biochem Soc Trans*, **39**, 658-662.
52. Gao, Y.G., Selmer, M., Dunham, C.M., Weixlbaumer, A., Kelley, A.C. and Ramakrishnan, V. (2009) The structure of the ribosome with elongation factor G trapped in the posttranslocational state. *Science*, **326**, 694-699.
53. Lill, R., Robertson, J.M. and Wintermeyer, W. (1986) Affinities of Transfer-RNA Binding-Sites of Ribosomes from *Escherichia coli Biochemistry*, **25**, 3245-3255.
54. Cukras, A.R., Southworth, D.R., Brunelle, J.L., Culver, G.M. and Green, R. (2003) Ribosomal proteins S12 and S13 function as control elements for translocation of the mRNA : tRNA complex. *Mol. Cell.*, **12**, 321-328.
55. Konevega, A.L., Fischer, N., Semenkov, Y.P., Stark, H., Wintermeyer, W. and Rodnina, M.V. (2007) Spontaneous reverse movement of mRNA-bound tRNA through the ribosome. *Nat. Struct. Mol. Biol.*, **14**, 318-324.
56. Qin, Y., Polacek, N., Vesper, O., Staub, E., Einfeldt, E., Wilson, D.N. and Nierhaus, K.H. (2006) The highly conserved LepA is a ribosomal elongation factor that back-translocates the ribosome. *Cell*, **127**, 721-733.
57. Yonath, A. (2005), *Annual Review of Biochemistry*. Annual Reviews, Palo Alto, Vol. 74, pp. 649-679.
58. Evans, R.N., Blaha, G., Bailey, S. and Steitz, T.A. (2008) The structure of LepA, the ribosomal back translocase. *Proc. Natl. Acad. Sci. U. S. A.*, **105**, 4673-4678.
59. Dibb, N.J. and Wolfe, P.B. (1986) lep operon proximal gene is not required for growth or secretion by *Escherichia coli*. *J Bacteriol*, **166**, 83-87.

60. Connell, S.R., Topf, M., Qin, Y., Wilson, D.N., Mielke, T., Fucini, P., Nierhaus, K.H. and Spahn, C.M.T. (2008) A new tRNA intermediate revealed on the ribosome during EF4-mediated back-translocation. *Nat. Struct. Mol. Biol.*, **15**, 910-915.
61. Date, T. and Wickner, W. (1981) Isolation of the *Escherichia coli* leader peptidase gene and effects of leader peptidase overproduction in vivo. *Proc Natl Acad Sci U S A*, **78**, 6106-6110.
62. March, P.E. and Inouye, M. (1985) Characterization of the lep operon of *Escherichia coli*. Identification of the promoter and the gene upstream of the signal peptidase I gene. *J Biol Chem*, **260**, 7206-7213.
63. Bauerschmitt, H., Funes, S. and Herrmann, J.M. (2008) The membrane-bound GTPase Guf1 promotes mitochondrial protein synthesis under suboptimal conditions. *J. Biol. Chem.*, **283**, 17139-17146.
64. March, P.E. and Inouye, M. (1985) GTP-binding membrane protein of *Escherichia coli* with sequence homology to initiation factor 2 and elongation factors Tu and G. *Proc Natl Acad Sci U S A*, **82**, 7500-7504.
65. Bijlsma, J.J., Lie, A.L.M., Nootenboom, I.C., Vandenbroucke-Grauls, C.M. and Kusters, J.G. (2000) Identification of loci essential for the growth of *Helicobacter pylori* under acidic conditions. *J Infect Dis*, **182**, 1566-1569.
66. Ji, D.L., Lin, H., Chi, W. and Zhang, L.X. (2012) CpLEPA Is Critical for Chloroplast Protein Synthesis Under Suboptimal Conditions in *Arabidopsis thaliana*. *PLoS One*, **7**, e49746.
67. Pech, M., Karim, Z., Yamamoto, H., Kitakawa, M., Qin, Y. and Nierhaus, K.H. (2011) Elongation factor 4 (EF4/LepA) accelerates protein synthesis at increased Mg2+ concentrations. *Proc Natl Acad Sci U S A*, **108**, 3199-3203.
68. Daviter, T., Wieden, H.J. and Rodnina, M.V. (2003) Essential role of histidine 84 in elongation factor Tu for the chemical step of GTP hydrolysis on the ribosome. *J. Mol. Biol.*, **332**, 689-699.
69. Kjeldgaard, M. and Nyborg, J. (1992) Refined structure of elongation factor EF-Tu from *Escherichia coli*. *J. Mol. Biol.*, **223**, 721-742.
70. Schmeing, T.M., Voorhees, R.M., Kelley, A.C., Gao, Y.G., Murphy, F.V.t., Weir, J.R. and Ramakrishnan, V. (2009) The crystal structure of the ribosome bound to EF-Tu and aminoacyl-tRNA. *Science*, **326**, 688-694.
71. Villa, E., Sengupta, J., Trabuco, L.G., LeBarron, J., Baxter, W.T., Shaikh, T.R., Grassucci, R.A., Nissen, P., Ehrenberg, M., Schulten, K. *et al.* (2009) Ribosome-induced changes in elongation factor Tu conformation control GTP hydrolysis. *Proc. Natl. Acad. Sci. U. S. A.*, **106**, 1063-1068.
72. Laurberg, M., Kristensen, O., Martemyanov, K., Gudkov, A.T., Nagaev, I., Hughes, D. and Liljas, A. (2000) Structure of a mutant EF-G reveals domain III and possibly the fusidic acid binding site. *J. Mol. Biol.*, **303**, 593-603.
73. Farris, M., Grant, A., Richardson, T.B. and O'Connor, C.D. (1998) BipA: a tyrosine-phosphorylated GTPase that mediates interactions between enteropathogenic *Escherichia coli* (EPEC) and epithelial cells. *Molecular microbiology*, **28**, 265-279.
74. Burdett, V. (1991) Purification and characterization of Tet(M), a protein that renders ribosomes resistant to tetracycline. *J Biol Chem*, **266**, 2872-2877.
75. Manavathu, E.K., Fernandez, C.L., Cooperman, B.S. and Taylor, D.E. (1990) Molecular studies on the mechanism of tetracycline resistance mediated by Tet(O). *Antimicrob Agents Chemother*, **34**, 71-77.
76. Kiss, E., Huguet, T., Poinsot, V. and Batut, J. (2004) The *typA* gene is required for stress adaptation as well as for symbiosis of Sinorhizobium meliloti 1021 with certain Medicago truncatula lines. *Mol Plant Microbe Interact*, **17**, 235-244.

77. Nocek, B., Mulligan, R., Duggan, E., Clancy, S. and Joachimiak, A. (2008) The c-terminal part of bipa protein from vibrio parahaemolyticus.
78. deLivron, M.A., Makanji, H.S., Lane, M.C. and Robinson, V.L. (2009) A novel domain in translational GTPase BipA mediates interaction with the 70S ribosome and influences GTP hydrolysis. *Biochemistry*, **48**, 10533-10541.
79. Li, W., Atkinson, G.C., Thakor, N.S., Allas, ú., Lu, C.-c., Chan, K.-Y., Tenson, T., Schulten, K., Wilson, K.S., Hauryliuk, V. *et al.* (2013) Mechanism of tetracycline resistance by ribosomal protection protein Tet(O). *Nat Commun*, **4**, 1477.
80. Jenner, L., Starosta, A.L., Terry, D.S., Mikolajka, A., Filonava, L., Yusupov, M., Blanchard, S.C., Wilson, D.N. and Yusupova, G. (2013) Structural basis for potent inhibitory activity of the antibiotic tigecycline during protein synthesis. *Proc. Natl. Acad. Sci. U. S. A.*, **110**, 3812-3816.
81. Savelsbergh, A., Matassova, N.B., Rodnina, M.V. and Wintermeyer, W. (2000) Role of domains 4 and 5 in elongation factor G functions on the ribosome. *J. Mol. Biol.*, **300**, 951-961.
82. Rodnina, M.V., Savelsbergh, A., Katunin, V.I. and Wintermeyer, W. (1997) Hydrolysis of GTP by elongation factor G drives tRNA movement on the ribosome. *Nature*, **385**, 37-41.
83. Spahn, C.M., Blaha, G., Agrawal, R.K., Penczek, P., Grassucci, R.A., Trieber, C.A., Connell, S.R., Taylor, D.E., Nierhaus, K.H. and Frank, J. (2001) Localization of the ribosomal protection protein Tet(O) on the ribosome and the mechanism of tetracycline resistance. *Mol Cell*, **7**, 1037-1045.
84. Walter, J.D., Hunter, M., Cobb, M., Traeger, G. and Spiegel, C.P. (2011) Thiostrepton inhibits stable 70S ribosome binding and ribosome-dependent GTPase activation of elongation factor G and elongation factor 4. *Nucleic Acids Research*, **40**, 360-370.
85. Arike, L., Valgepea, K., Peil, L., Nahku, R., Adamberg, K. and Vilu, R. (2012) Comparison and applications of label-free absolute proteome quantification methods on *Escherichia coli*. *J Proteomics*, **75**, 5437-5448.
86. Liu, H., Chen, C., Zhang, H., Kaur, J., Goldman, Y.E. and Cooperman, B.S. (2011) The conserved protein EF4 (LepA) modulates the elongation cycle of protein synthesis. *Proc Natl Acad Sci U S A*, **108**, 16223-16228.
87. Cole, C., Barber, J.D. and Barton, G.J. (2008) The Jpred 3 secondary structure prediction server. *Nucleic Acids Res.*, **36**, W197-W201.
88. Wilkins, M., Gasteiger, E., Bairoch, A., Sanchez, J.-C., Williams, K., Appel, R. and Hochstrasser, D. (1999) Protein Identification and Analysis Tools in the ExPASy Server. *2-D Proteome Analysis Protocols*, **112**, 531-552.
89. Milon, P., Konevega, A.L., Peske, F., Fabbretti, A., Gualerzi, C.O. and Rodnina, M.V. (2007) Transient kinetics, fluorescence, and fret in studies of initiation of translation in bacteria. *Translation Initiation: Reconstituted Systems and Biophysical Methods*, **430**, 1-30.
90. Shields, M.J., Fischer, J.J. and Wieden, H.J. (2009) Toward Understanding the Function of the Universally Conserved GTPase HflX from *Escherichia coli*: A Kinetic Approach. *Biochemistry*, **48**, 10793-10802.
91. Wilden, B., Savelsbergh, A., Rodnina, M.V. and Wintermeyer, W. (2006) Role and timing of GTP binding and hydrolysis during EF-G-dependent tRNA translocation on the ribosome. *Proc. Natl. Acad. Sci. U. S. A.*, **103**, 13670-13675.
92. Peske, F., Matassova, N.B., Savelsbergh, A., Rodnina, M.V. and Wintermeyer, W. (2000) Conformationally restricted elongation factor G retains GTPase activity but is inactive in translocation on the ribosome. *Mol. Cell.*, **6**, 501-505.
93. Nissen, P., Kjeldgaard, M. and Nyborg, J. (2000) Macromolecular mimicry. *Embo J.*, **19**, 489-495.

94. Aevarsson, A., Brazhnikov, E., Garber, M., Zheltonosova, J., Chirgadze, Y., Al-Karadaghi, S., Svensson, L.A. and Liljas, A. (1994) 3-dimensional structure of the ribosomal translocase - Elongation-Factor-G from *Thermus-thermophilus*. *Embo J.*, **13**, 3669-3677.
95. Anurag, M. and Dash, D. (2009) Unraveling the potential of intrinsically disordered proteins as drug targets: application to *Mycobacterium tuberculosis*. *Mol. Biosyst.*, **5**, 1752-1757.
96. Savelsbergh, A., Mohr, D., Kothe, U., Wintermeyer, W. and Rodnina, M.V. (2005) Control of phosphate release from elongation factor G by ribosomal protein L7/12. *Embo J.*, **24**, 4316-4323.
97. Voorhees, R.M., Schmeing, T.M., Kelley, A.C. and Ramakrishnan, V. (2010) The mechanism for activation of GTP hydrolysis on the ribosome. *Science*, **330**, 835-838.
98. Wedemeyer, W.J., Welker, E., Narayan, M. and Scheraga, H.A. (2000) Disulfide bonds and protein folding. *Biochemistry*, **39**, 4207-4216.
99. Gutteridge, A. and Thornton, J.M. (2005) Understanding nature's catalytic toolkit. *Trends Biochem.Sci.*, **30**, 622-629.
100. Pingoud, A., Gast, F.U., Block, W. and Peters, F. (1983) The Elongation Factor-Tu from *Escherichia-coli*, aminoacyl-transfer RNA, and guanosine tetraphosphate form a ternary complex which is bound by programmed ribosomes. *J. Biol. Chem.*, **258**, 4200-4205.
101. Nissen, P., Kjeldgaard, M., Thirup, S., Polekhina, G., Reshetnikova, L., Clark, B.F. and Nyborg, J. (1995) Crystal structure of the ternary complex of Phe-tRNAPhe, EF-Tu, and a GTP analog. *Science*, **270**, 1464-1472.
102. Young, R. and Bremer, H. (1976) Polypeptide-Chain-Elongation Rate in *Escherichia-coli* B/r as a Function of Growth-Rate *Biochem. J.*, **160**, 185-194.
103. Wieden, H.J., Gromadski, K., Rodnin, D. and Rodnina, M.V. (2002) Mechanism of elongation factor (EF)-Ts-catalyzed nucleotide exchange in EF-Tu - Contribution of contacts at the guanine base. *J. Biol. Chem.*, **277**, 6032-6036.
104. Gromadski, K.B., Schummer, T., Stromgaard, A., Knudsen, C.R., Kinzy, T.G. and Rodnina, M.V. (2007) Kinetics of the interactions between yeast elongation factors 1A and 1Balpha, guanine nucleotides, and aminoacyl-tRNA. *J Biol Chem*, **282**, 35629-35637.
105. Boehlke, K.W. and Friesen, J.D. (1975) Cellular Content of Ribonucleic-acid and Protein in *Saccharomyces cerevisiae* as a Function of Exponential-Growth Rate - Calculation of Apparent Peptide Chain Elongation Rate. *J. Bacteriol.*, **121**, 429-433.
106. Andersen, G.R., Pedersen, L., Valente, L., Chatterjee, I., Kinzy, T.G., Kjeldgaard, M. and Nyborg, J. (2000) Structural basis for nucleotide exchange and competition with tRNA in the yeast elongation factor complex eEF1A : eEF1B alpha. *Mol. Cell.*, **6**, 1261-1266.
107. Jeppesen, M.G., Navratil, T., Spremulli, L.L. and Nyborg, J. (2005) Crystal structure of the bovine mitochondrial elongation factor Tu(.)Ts complex. *J. Biol. Chem.*, **280**, 5071-5081.
108. Karring, H., Bjornsson, A., Thirup, S., Clark, B.F.C. and Knudsen, C.R. (2003) Functional effects of deleting the coiled-coil motif in *Escherichia coli* elongation factor Ts. *Eur. J. Biochem.*, **270**, 4294-4305.
109. Cai, Y.C., Bullard, J.M., Thompson, N.L. and Spremulli, L.L. (2000) Interaction of mitochondrial elongation factor Tu with aminoacyl-tRNA and elongation factor Ts. *J. Biol. Chem.*, **275**, 20308-20314.
110. Pittman, Y.R., Valente, L., Jeppesen, M.G., Andersen, G.R., Patel, S. and Kinzy, T.G. (2006) Mg2+ and a key lysine modulate exchange activity of eukaryotic translation elongation factor 1B alpha. *J. Biol. Chem.*, **281**, 19457-19468.
111. Gerdes, S.Y., Scholle, M.D., Campbell, J.W., Balazsi, G., Ravasz, E., Daugherty, M.D., Somera, A.L., Kyrpides, N.C., Anderson, I., Gelfand, M.S. *et al.* (2003) Experimental

determination and system level analysis of essential genes in Escherichia coli MG1655. *J. Bacteriol.*, **185**, 5673-5684.
112. Boon, K., Vijgenboom, E., Madsen, L.V., Talens, A., Kraal, B. and Bosch, L. (1992) Isolation and functional-analysis of histidine-tagged Elongation-Factor Tu. *Eur. J. Biochem.*, **210**, 177-183.
113. Kitagawa, M., Ara, T., Arifuzzaman, M., Ioka-Nakamichi, T., Inamoto, E., Toyonaga, H. and Mori, H. (2005) Complete set of ORF clones of *Escherichia coli* ASKA library (A complete Set of E. coli K-12 ORF archive): Unique resources for biological research. *DNA Res.*, **12**, 291-299.
114. Scolnick, E., Tompkins, R., Caskey, T. and Nirenberg, M. (1968) Release factors differing in specificity for terminator codons. *PNAS*, **61**, 768-774.
115. Gasteiger, E., Gattiker, A., Hoogland, C., Ivanyi, I., Appel, R.D. and Bairoch, A. (2003) ExPASy: the proteomics server for in-depth protein knowledge and analysis. *Nucleic Acids Res.*, **31**, 3784-3788.
116. Larkin, M.A., Blackshields, G., Brown, N.P., Chenna, R., McGettigan, P.A., McWilliam, H., Valentin, F., Wallace, I.M., Wilm, A., Lopez, R. *et al.* (2007) Clustal W and clustal X version 2.0. *Bioinformatics*, **23**, 2947-2948.
117. Karl B, N. and Nicholas, H.B.J. (1997) GeneDoc: a tool for editing and annotating multiple sequence alignments.
118. Ozturk, S.B. and Kinzy, T.G. (2008) Guanine nucleotide exchange factor independence of the G-protein eEF1A through novel mutant forms and biochemical properties. *J. Biol. Chem.*, **283**, 23244-23253.
119. Zhang, Y.L., Yu, N.J. and Spremulli, L.L. (1998) Mutational analysis of the roles of residues in *Escherichia coli* elongation factor Ts in the interaction with elongation factor Tu. *J. Biol. Chem.*, **273**, 4556-4562.
120. Doring, G., Conway, S.P., Heijerman, H.G.M., Hodson, M.E., Hoiby, N., Smyth, A., Touw, D.J. and Consensus, C. (2000) Antibiotic therapy against *Pseudomonas aeruginosa* in cystic fibrosis: a European consensus. *Eur. Resp. J.*, **16**, 749-767.
121. de Bentzmann, S. and Plésiat, P. (2011) The *Pseudomonas aeruginosa* opportunistic pathogen and human infections. *Environmental Microbiology*, **13**, 1655-1665.
122. Walsh, C. (2000) Molecular mechanisms that confer antibacterial drug resistance. *Nature*, **406**, 775-781.
123. Cooper, M.A. and Shlaes, D. (2011) Fix the antibiotics pipeline. *Nature*, **472**, 32-32.
124. Ma, D.-L., Chan, D.S.H. and Leung, C.H. (2013) Drug repositioning by structure-based virtual screening. *Chemical Society Reviews*.
125. Munro, J.B., Sanbonmatsu, K.Y., Spahn, C.M.T. and Blanchard, S.C. (2009) Navigating the ribosome's metastable energy landscape. *Trends Biochem.Sci.*, **34**, 390-400.
126. Kaiser, C.M., Chang, H.-C., Agashe, V.R., Lakshmipathy, S.K., Etchells, S.A., Hayer-Hartl, M., Hartl, F.U. and Barral, J.M. (2006) Real-time observation of trigger factor function on translating ribosomes. *Nature*, **444**, 455-460.
127. Kim, Y., Ho, S.O., Gassman, N.R., Korlann, Y., Landorf, E.V., Collart, F.R. and Weiss, S. (2008) Efficient site-specific labeling of proteins via cysteines. *Bioconjugate Chemistry*, **19**, 786-791.
128. Jonak, J., Petersen, T.E., Clark, B.F.C. and Rychlik, I. (1982) "N-Tosyl-L-Phenylalanylchloromethane reacts with Cysteine-81 in the molecule of Elongation Factor-Tu from *Escherichia-coli*. *FEBS Lett.*, **150**, 485-488.
129. Anborgh, P.H., Parmeggiani, A. and Jonak, J. (1992) Site-Directed mutagenesis of Elongation-Factor Tu - The Functional and structureal role of residue Cys 81. *Eur. J. Biochem.*, **208**, 251-257.
130. Blanchard, S.C., Gonzalez, R.L., Kim, H.D., Chu, S. and Puglisi, J.D. (2004) tRNA selection and kinetic proofreading in translation. *Nat. Struct. Mol. Biol.*, **11**, 1008-1014.

131. Perla-Kajan, J., Lin, X., Cooperman, B.S., Goldman, E., Jakubowski, H., Knudsen, C.R. and Mandecki, W. (2010) Properties of *Escherichia coli* EF-Tu mutants designed for fluorescence resonance energy transfer from tRNA molecules. *Protein Eng. Des. Sel.*, **23**, 129-136.
132. Betteridge, T., Liu, H., Gamper, H., Kirillov, S., Cooperman, B.S. and Hou, Y.M. (2007) Fluorescent labeling of tRNAs for dynamics experiments. *RNA-Publ. RNA Soc.*, **13**, 1594-1601.
133. Watve, M.G., Tickoo, R., Jog, M.M. and Bhole, B.D. (2001) How many antibiotics are produced by the genus Streptomyces? *Arch Microbiol*, **176**, 386-390.
134. Sanderson, L.E. and Uhlenbeck, O.C. (2007) Exploring the specificity of bacterial Elongation Factor Tu for different tRNAs. *Biochemistry*, **46**, 6194-6200.
135. Sohmen, D., Harms, J.M., Schlunzen, F. and Wilson, D.N. (2009) SnapShot: Antibiotic Inhibition of Protein Synthesis II. *Cell*, **139**.
136. Noble, C.G. and Song, H. (2008) Structural studies of elongation and release factors. *Cell. Mol. Life Sci.*, **65**, 1335-1346.

Appendix

A.1 LepA

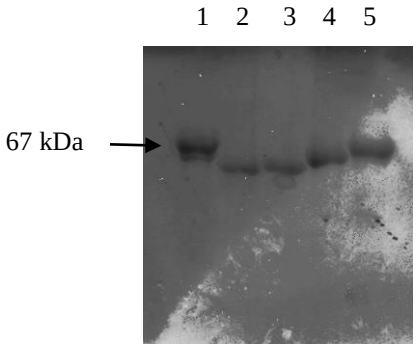

Figure A.1. LepA Protein Preparations. 10% SDS-PAGE of LepA protein preparations where LepA H81A (67 kDa) is shown in lane 1, LepA ΔA494 (55 kDa) is in lane 2, LepA ΔP520 (58 kDa) is in lane 3, LepA ΔG555 (61 kDa) is in lane 4 and wild type LepA (67 kDa) is represented in lane 5.

A.1a Cysteine residues in LepA

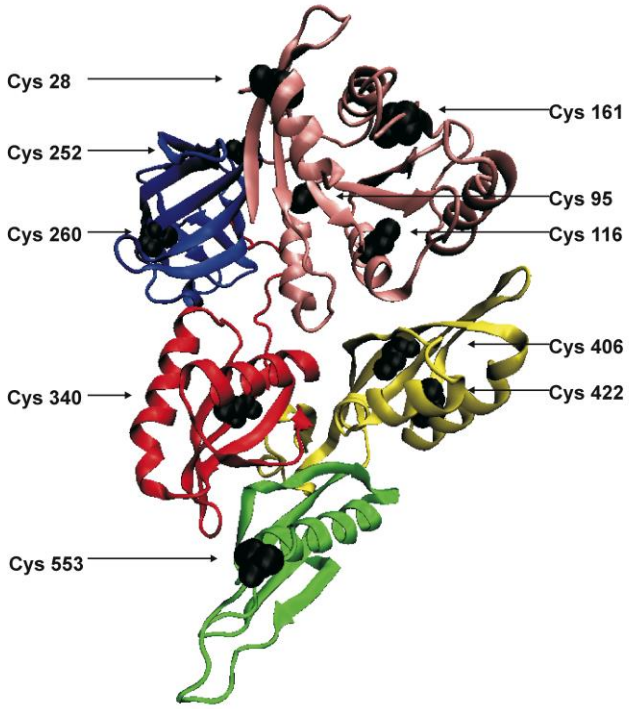

Figure A.2. Overview of cysteine residues in *E. coli* LepA. Structure of *E. coli* LepA represented in cartoon and coloured as figure 2.1. Cysteine residues are represented in spacefill and coloured in black. Coordinates used for this representation are from PDB ID 3CB4 (58).

Table A.1. Identity of Cysteine Composition within Bacterial LepA.

Position of cysteines in *E. coli* LepA and percent identity within bacterial organisms aligned is outlined. The substitution of each cysteine is also shown.

Cysteine Position in *E. coli*	Percent Identity	Substitution Constructed
28	31	Thr
95	97	Ser
116	27	Val
161	21	Val
252	10	Ala
260	12	Ala
340	90	Val
406	12	Ala
422	83	Ala
553	93	Leu

A.1b Alignment of LepA Primary Sequence within Bacteria

Table A.2. Accession Numbers and Organisms used to Align LepA Primary Sequence.

Accession numbers were obtained from the SwissProt Database (115). Percent of cysteine residues within the LepA primary sequence is represented.

Accession Number	Organism	Percent Cysteine Composition	Percent Identity to *E. coli*
P60785	Escherichia coli	17	
Q9X1V8	Thermotoga maritima	6	50
Q72KV2	Thermus thermophilus	3	55
A0RIT7	Bacillus thuringiensis	10	56
C3P8M5	Bacillus anthracis	10	55
P37949	Bacillus subtilis	8	56
Q65H50	Bacillus licheniformis	8	56
A6QHC7	Staphylococcus aureus	8	54
C1CKU6	Streptococcus pneumoniae	9	54
Q5M4M2	Streptococcus thermophilus	9	56
Q831Z0	Enterococcus faecalis	9	56
Q03QU8	Lactobacillus brevis	10	53
Q03FQ4	Pediococcus pentosaceus	3	53
Q14NN1	Spiroplasma citri	10	53
A7FXL9	Clostridium botulinum	8	55
A6L744	Bacteroides vulgatus	15	53
A6LC18	Parabacteroides distasonis	15	52
Q2S5I1	Salinibacter ruber	7	53
A5U598	Mycobacterium tuberculosis	12	52
I7G5I5	Mycobacterium smegmatis	11	48
Q82BZ3	Streptomyces avermitilis	8	48
Q9Z8I4	Chlamydia pneumoniae	13	50
Q823H7	Chlaymydophila caviae	13	49
Q9PKX6	Chlamydia muridarum	13	49
P60788	Shigella flexneri	17	100
P0A1W5	Salmonella typhi	17	96
A4TKY0	Yersinia pestis	17	92
Q6LMS0	Photobacterium profundum	15	83
Q3IDL4	Pseudoalteromonas haloplanktis	12	75
Q0VP16	Alcanivorax borkumensis	13	74
A9KF98	Coxiella burnetii	12	71
Q87C09	Xylella fastidiosa	12	67
A9III9	Bordetella petrii	12	66
B9J716	Agrobacterium radiobacter	10	57
B9JYH0	Agrobacterium vitis	10	55
Q8UIQ2	Agrobacterium tumefaciens	10	57
Q6G1F5	Bartonella quintana	12	56
Q0C5X0	Hyphomonas neptunium	17	56
Q5NLP5	Zymomonas mobilis	12	59
Q5FHQ1	Ehrlichia ruminantium	17	51
A8F140	Rickettsia massiliae	17	56
C4XND4	Desulfovibrio magneticus	12	60

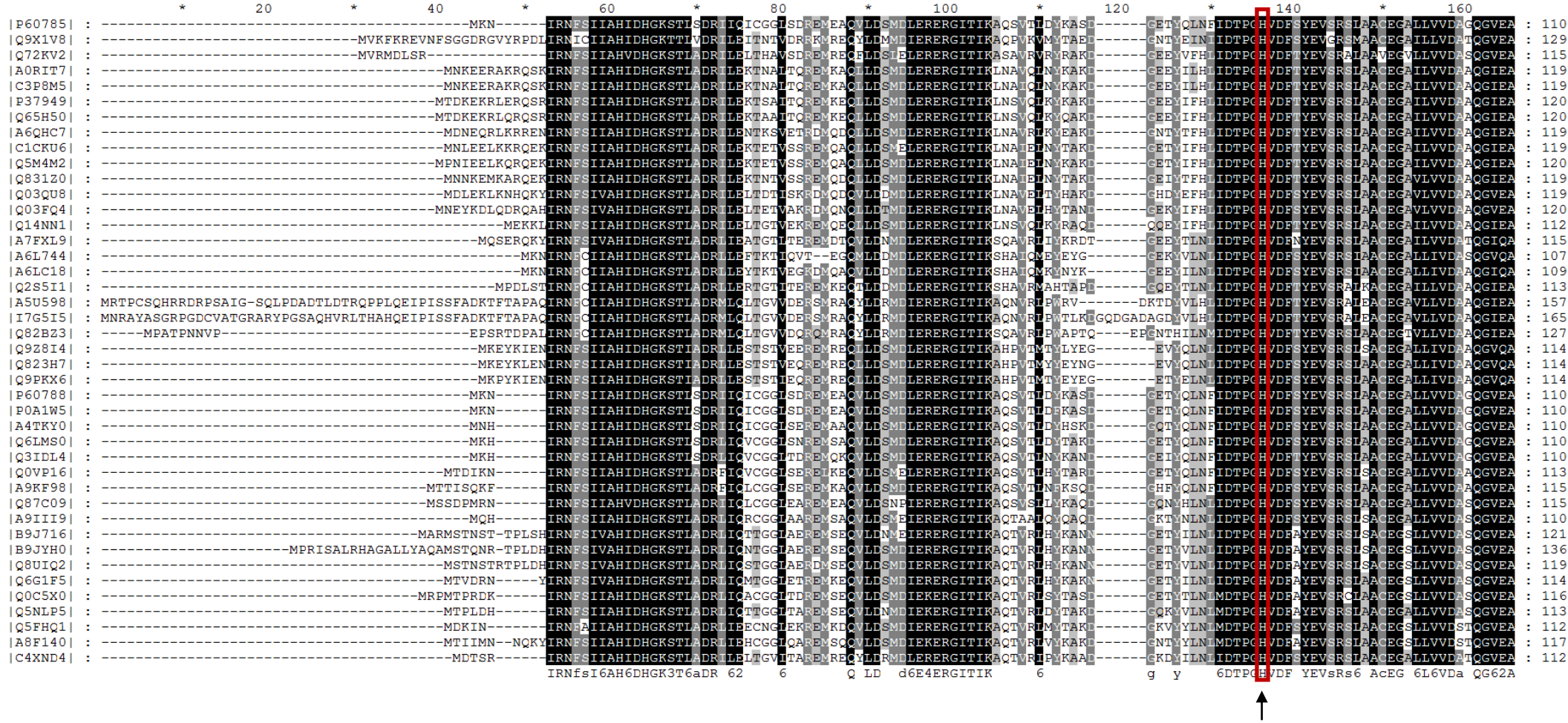

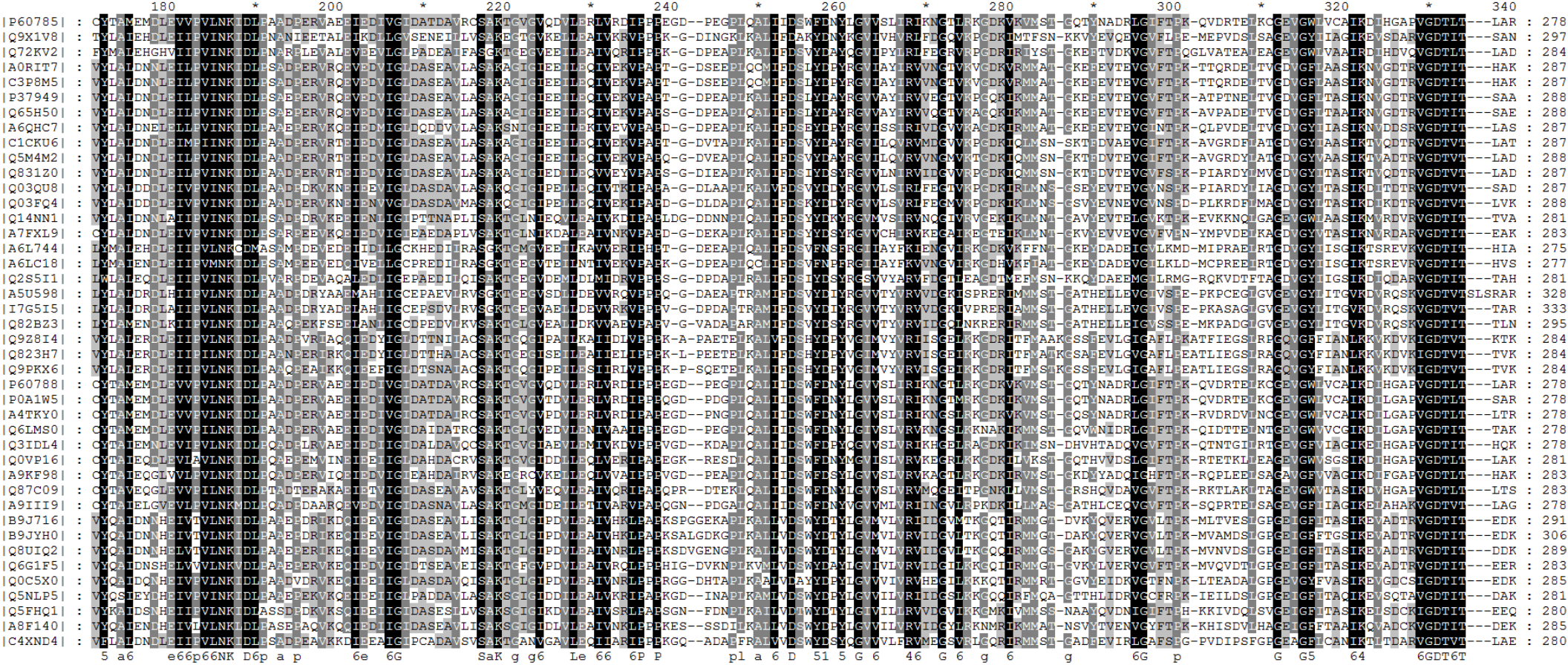

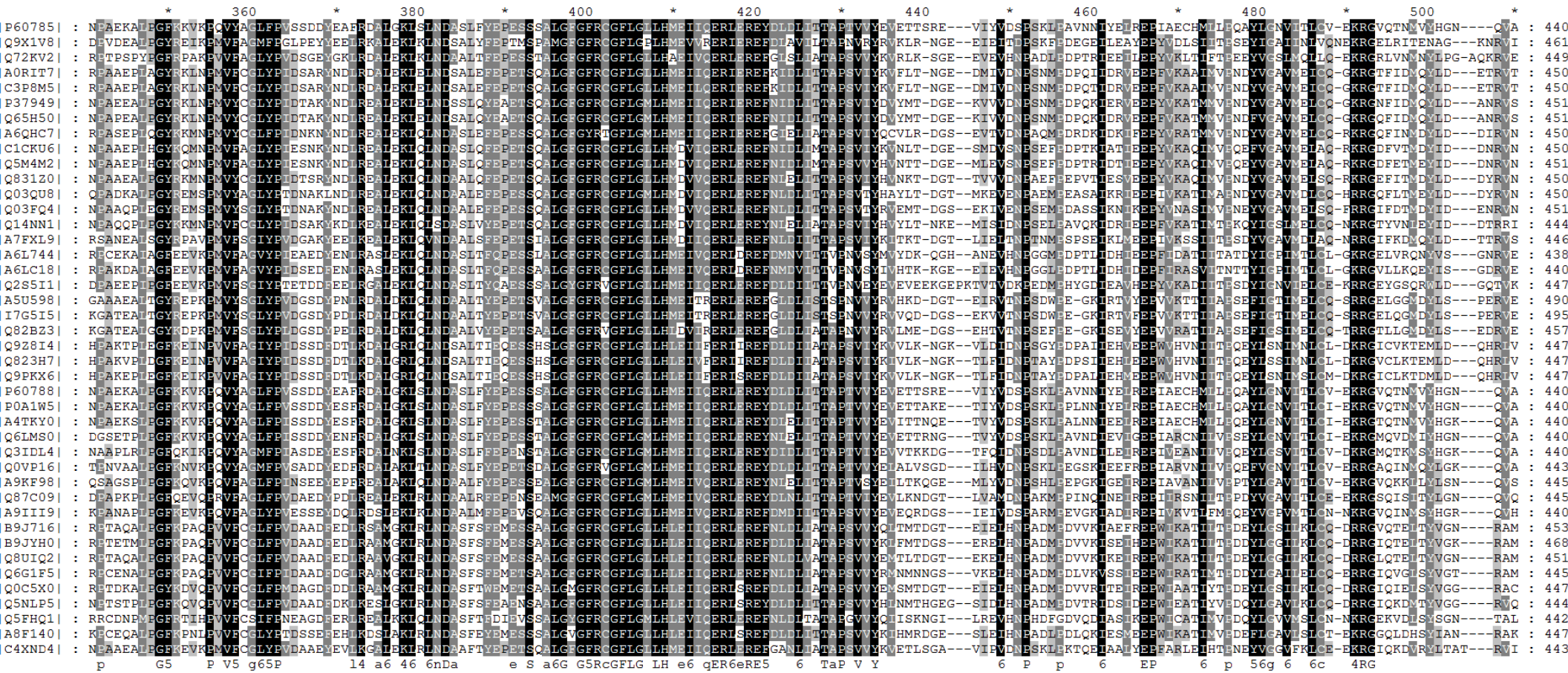

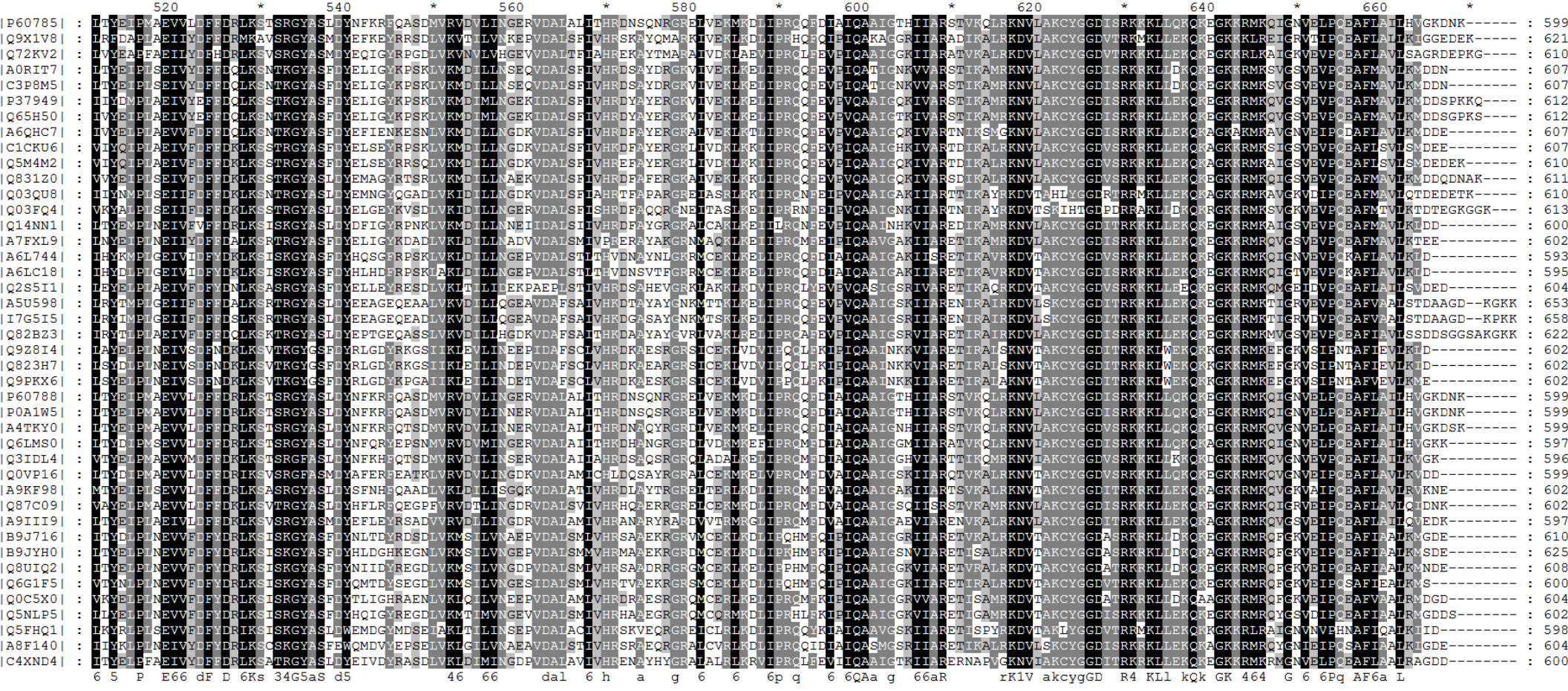

Figure A.3. Primary sequence alignment of LepA within bacteria. Black shows 100% conservation, grey shows 80-100% conservation and white is less than 80% conservation. Conserved catalytic histidine is highlighted in panel 1 a box.

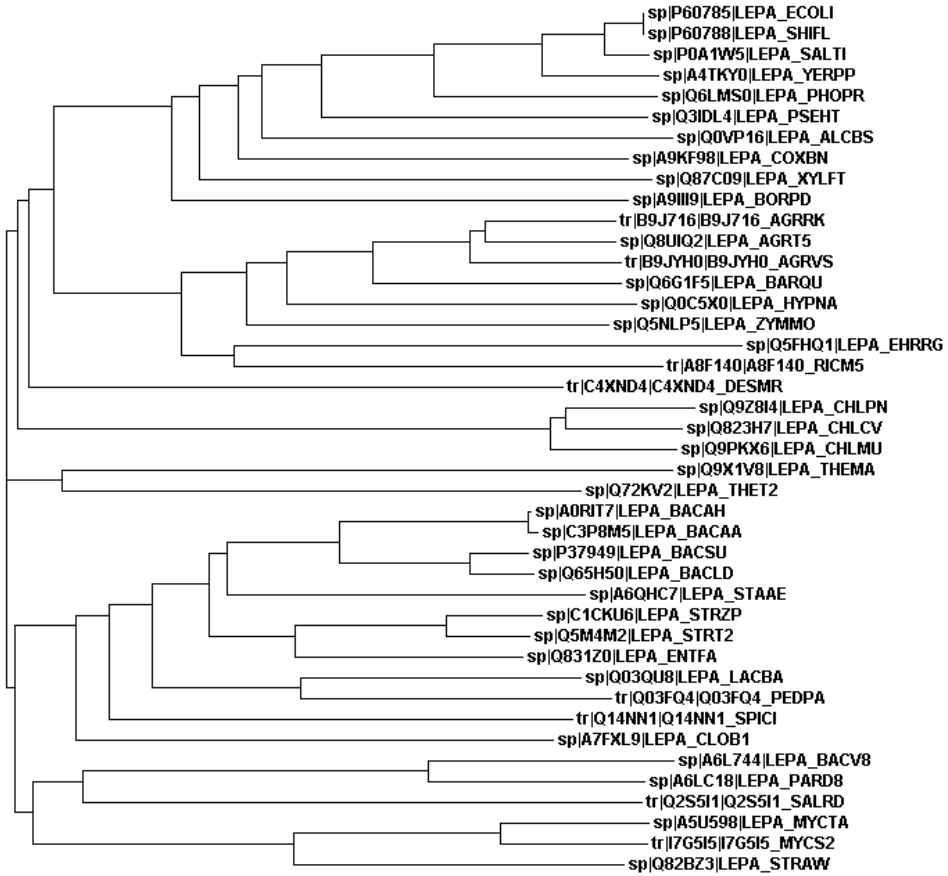

Figure A.4. Phylogenetic Tree of bacterial LepA aligned above. Phylogenetic tree generated by the ClustalW2 program using the LepA bacterial sequences aligned above. The sequence accession code along with the abbreviated species name is shown.

A.2 EF-Tu and EF-Ts

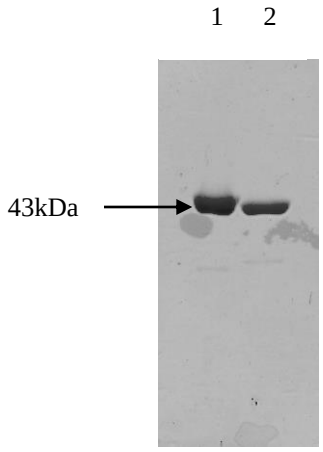

Figure A.5. EF-Tu preparations. 12% SDS-PAGE of EF-Tu protein preparations where EF-Tu from *P. aeruginosa* (43 kDa) is shown in lane 1 and EF-Tu from *E. coli* (43 kDa) is in lane 2.

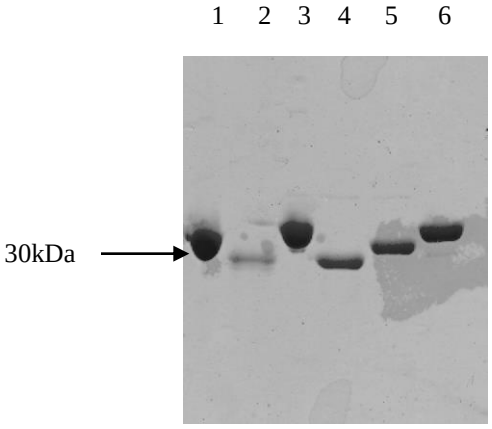

Figure A.6. EF-Ts preparations. 12% SDS-PAGE of EF-Ts protein preparations where EF-Ts from *E. coli* (30 kDa) is shown in lane 1 and 2 and EF-Ts from *P. aeruginosa* (32 kDa) is in lane 3. EF-Ts$_{E.c.}$ Chimera (30 kDa) is shown in lane 4, EF-Ts$_{P.a.}$ C-terminal truncation (31 kDa) is shown in lane 5 and EF-Ts$_{P.a.Q283M}$ (32 kDa) is shown in lane 6.

A.2a Alignment of EF-Ts Primary Sequence within Bacteria

Table A.3. Accession Numbers and Organisms used to Align EF-Ts Primary Sequence.

Accession numbers were obtained from SwissProt Database (115). The presence of a C-terminal module is indicated.

Accession Number	Organism	Contains C-terminal module?	Residue at *E. coli* Met 278	Percent Identity with *E. coli*	Classification
P0A6P1	Escherichia coli	Yes	Met		Gram Negative
O82851	Pseudomonas aeruginosa	Yes	Gln	54	Gram Negative
P43895	Thermus Thermophilus	No		29	Gram Negative
O31213	Streptomyces coelicolor	No		33	Gram Positive
P0A6P4	Shigella flexneri	Yes	Met	98	Gram Negative
P80700	Bacillus subtilis	Yes	Gln	46	Gram Positive
P0A3B7	Streptococcus pneumoniae	Yes	Met	34	Gram Positive
Q65JJ8	Bacillus licheniformis	Yes	Gln	44	Gram Positive
Q9X5U9	Coxiella burnetii	Yes	Gln	48	Gram Negative
A0QVB9	Mycobacterium smegmatis	No		35	Gram Positive
Q10788	Mycobacterium tuberculosis	No		33	Gram Positive
P64053	Salmonella typhi	Yes	Met	90	Gram Negative
Q8ZH65	Yersinia pestis	Yes	Met	69	Gram Negative
A5I4L2	Clostridium botulinum	Yes	Gln	36	Gram Positive
Q81WK9	Bacillus anthracis	Yes	Gln	45	Gram Positive
P71146	Chlamydia muridarum	No		27	Gram Negative
P61330	Pseudoalteromonas haloplanktis	Yes	Gln	62	Gram Negative
Q6LN25	Photobacterium profundum	Yes	Gln	61	Gram Negative
A0RHJ9	Bacillus thuringiensis	Yes	Gln	45	Gram Positive
Q9XCM5	Bartonella quintana	Yes	Ala	42	Gram Negative
P99171	Staphylococcus aureus	Yes	Gln	41	Gram Negative
Q5M1X4	Streptococcus thermophilus	Yes	Met	35	Gram Positive
Q9PAD9	Xylella fastidiosa	Yes	Gln	48	Gram Negative
Q8UFM2	Agrobacterium tumefaciens	Yes	Val	43	Gram Negative
Q0VQF6	Alcanivorax borkumensis	Yes	Ala	50	Gram Negative
P19216	Spiroplasma citri	Yes	Gln	39	No Cell Wall
Q82JX8	Streptomyces avermitilis	No		33	Gram Positive
Q9X5E8	Zymomonas mobilis	Yes	Ala	42	Gram Negative

Q9X5Z9	Streptomyces ramocissimus	No		31	Gram Positive
Q0C1C0	Hyphomonas neptunium	Yes	Leu	44	Gram Negative
Q03QS2	Lactobacillus brevis	Yes	Gln	38	Gram Positive
Q038L3	Lactobacillus casei	Yes	Gln	40	Gram Positive
Q044C9	Lactobacillus gasseri	Yes	Gln	33	Gram Positive
Q04F87	Oenococcus oeni	Yes	Gln	38	Gram Positive
Q03FT5	Pediococcus pentosaceus	Yes	Met	39	Gram Positive
Q2S6J1	Salinibacter ruber	No		35	Gram Negative
Q9X1U1	Thermotoga maritima	No		30	Gram Negative
A6L0V2	Bacteroides vulgatus	No		27	Gram Negative
A9INV9	Bordetella petrii	Yes		47	Gram Negative
C4XMY1	Desulfovibrio magneticus	No		29	Gram Negative
A6LHM8	Parabacteroides distasonis	No		27	Gram Negative
A8F0J0	Rickettsia massiliae	Yes	Ile	41	Gram Negative
B9JEX1	Agrobacterium radiobacter	Yes	Val	43	Gram Negative
B9JX32	Agrobacterium vitis	Yes	Val	41	Gram Negative
Q824U4	Chlamydophila caviae	No		27	Gram Negative
Q831V0	Enterococcus faecalis	Yes	Gln	39	Gram Positive
E1B278	Geobacillus anatolicus	Yes	Gln	41	Gram Negative

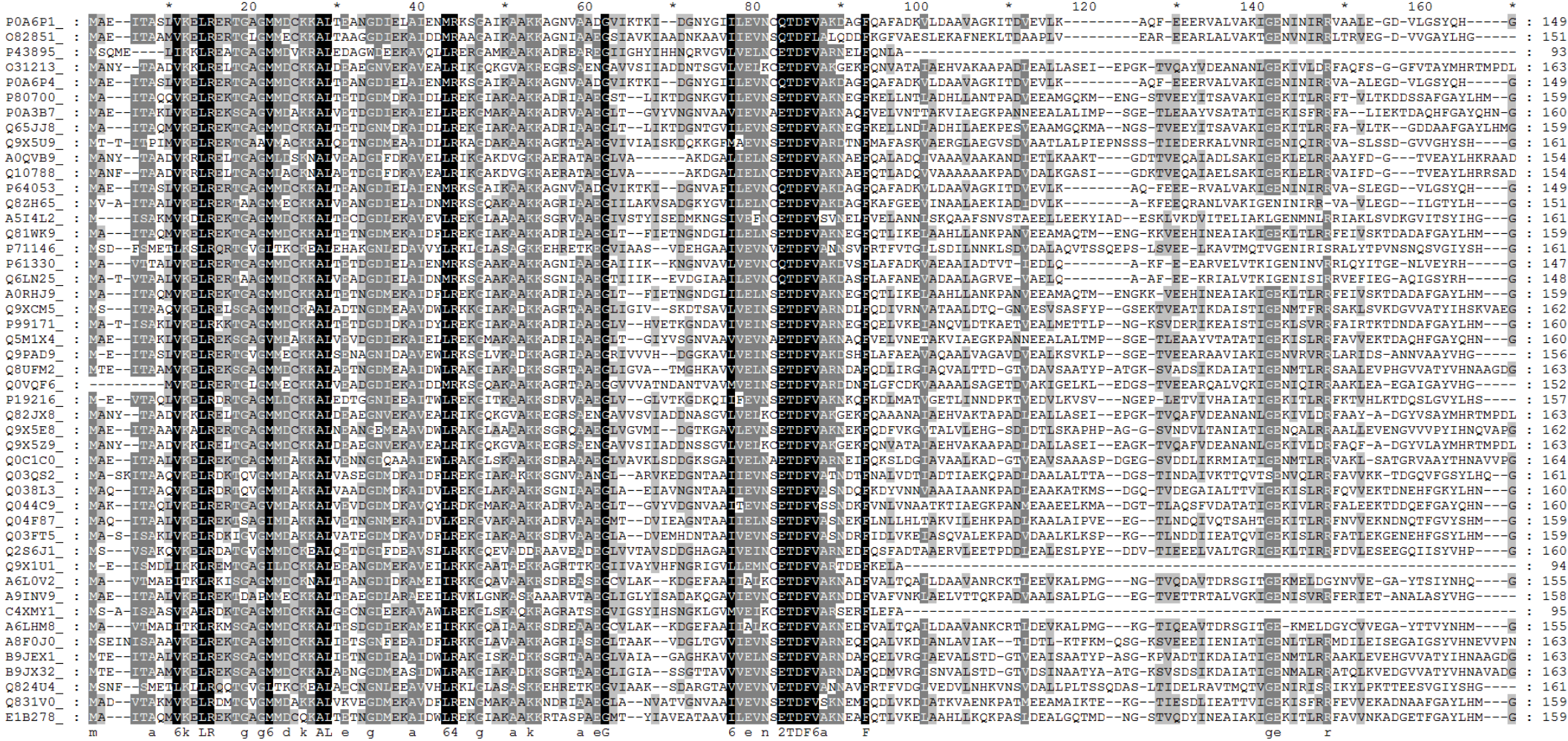

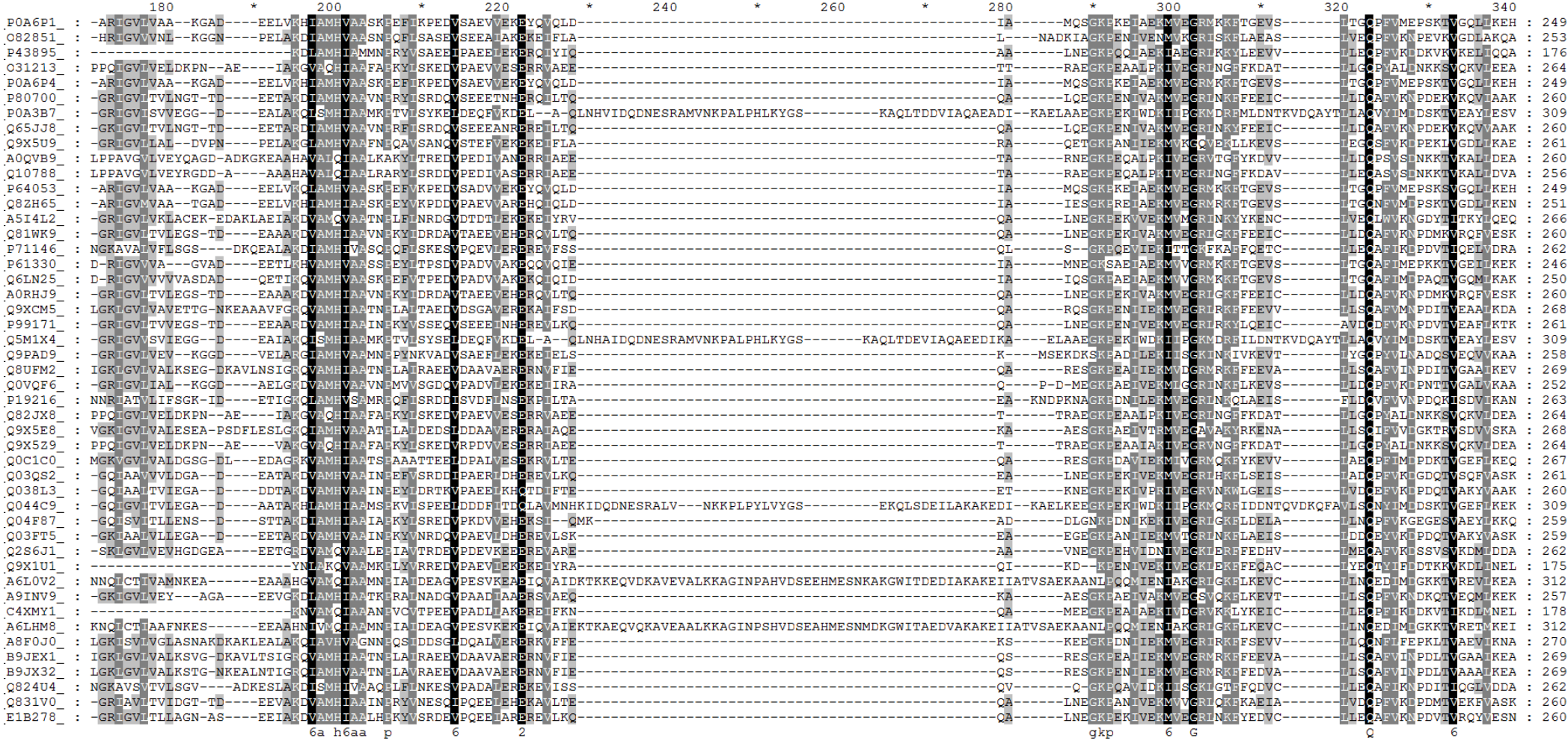

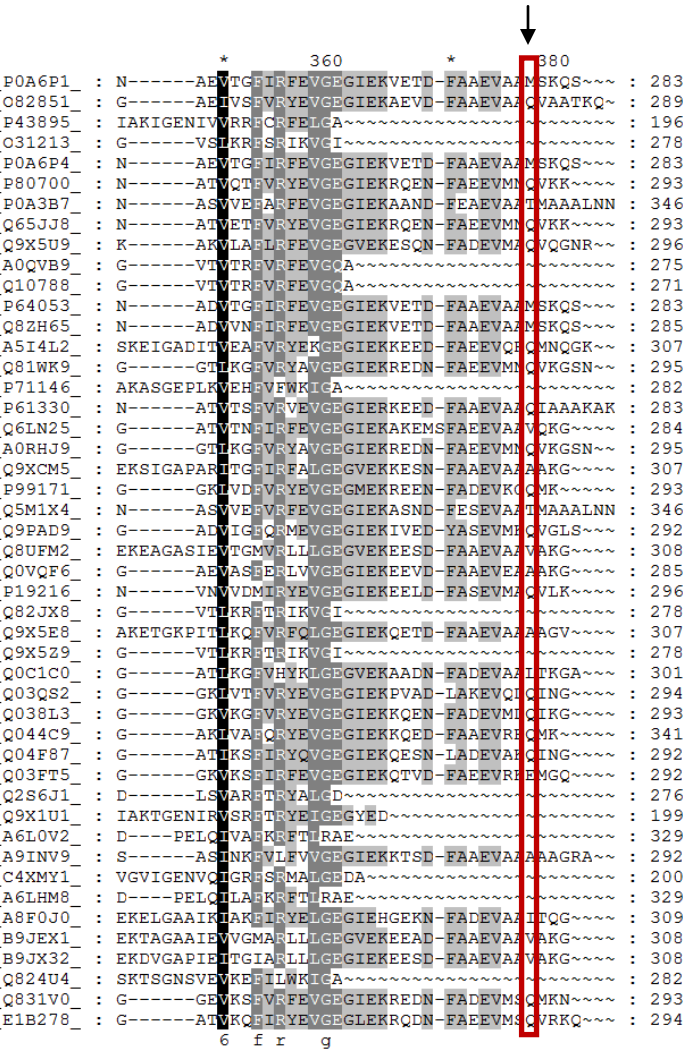

Figure A.7. Primary sequence alignment of EF-Ts within bacteria. Black shows 100% conservation, grey shows 80-100% conservation and white is less than 80% conservation. The conservation of Met 278 from *E. coli* is highlighted in panel 3 by a box.

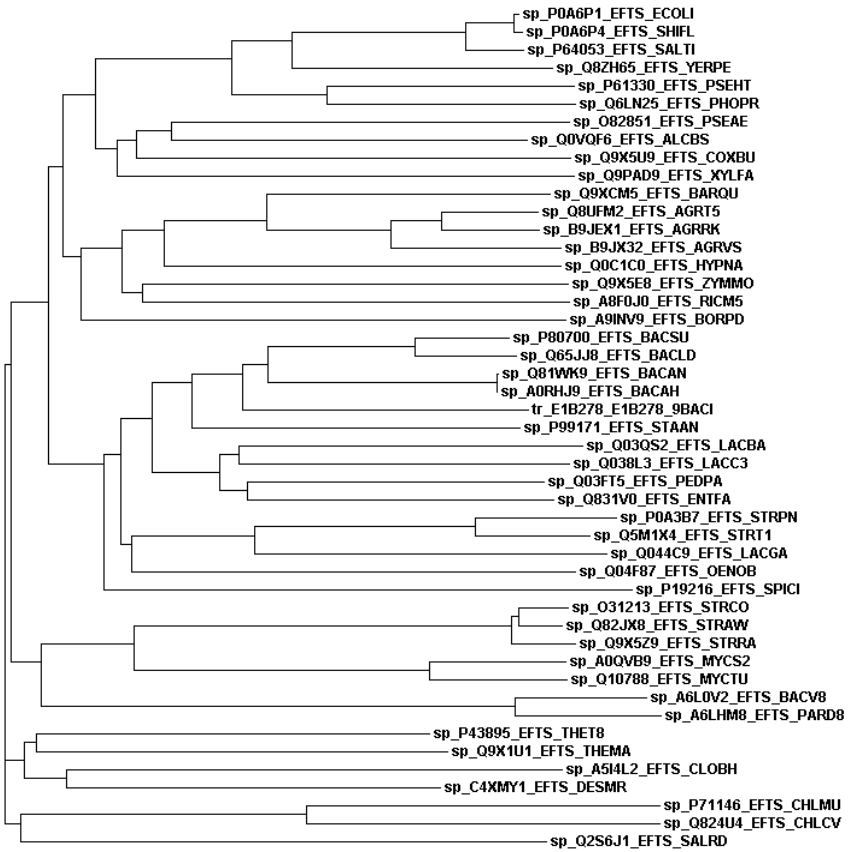

Figure A.8. Phylogenetic Tree of bacterial EF-Ts species aligned above. Phylogenetic tree generated by the ClustalW2 program using the EF-Ts bacterial sequences aligned above. The sequence accession code along with the abbreviated species name is shown.

A.2b Alignment of EF-Tu Primary Sequence within Bacteria

Table A.4. Accession Numbers and Organisms used to Align EF-Tu Primary Sequence.

Accession numbers were obtained from the SwissProt Database (115). The identity with *E. coli* EF-Tu is outlined.

Accession Number	Organism	Identity to *E. coli* EF-Tu
A0QS98	Mycobacterium smegmatis	74
A0R8H8	Bacillus thuringiensis	74
A5I7K8	Clostridium botulinum	73
A6LE88	Parabacteroides distasonis	72
A9IJ05	Bordetella petrii	81
B9JDR0	Agrobacterium radiobacter	73
C4XIP7	Desulfovibrio magneticus	73
C7LCI5	Brucella microti	74
P09591	Pseudomonas aeruginosa	84
P0A1H6	Salmonella typhi	99
P0A558	Mycobacterium tuberculosis	74
P0CE47	Escherichia coli	
P13537	Thermotoga maritima	69
P29542	Streptomyces ramocissimus	74
P33166	Bacillus subtilis	76
P40174	Streptomyces coelicolor	77
P40175	Streptomyces coelicolor	57
P64030	Streptococcus pneumoniae	72
P99152	Staphylococcus aureus	74
Q039K9	Lactobacillus casei	71
Q03F25	Pediococcus pentosaceus	71
Q03QN5	Lactobacillus brevis	69
Q042T5	Lactobacillus gasseri	70
Q04FQ4	Oenococcus oeni	69
Q0C1F4	Hyphomonas neptunium	76
Q0PHN9	Geobacillus anatolicus	75
Q0VSL7	Alcanivorax borkumensis	82
Q14QA4	Spiroplasma citri	72
Q2S1P8	Salinibacter ruber	70
Q3ILP4	Pseudoalteromonas haloplanktis	84
Q5HAS0	Ehrlichia ruminantium	66
Q5M101	Streptococcus thermophilus	72
Q5NQ65	Zymomonas mobilis	75
Q5SHN6	Thermus thermophilus	70
Q65PA9	Bacillus licheniformis	75
Q6FZC0	Bartonella quintana	74
Q6LVC0	Photobacterium profundum	85
Q81VT2	Bacillus anthracis	74
Q822I4	Chlamydophila caviae	68
Q82DQ0	Streptomyces avermitilis	74
Q839G8	Enterococcus faecalis	76
Q83ES6	Coxiella burnetii	78
Q83JC4	Shigella flexneri	100

Q8UE16	Agrobacterium tumefaciens	73
Q8ZJB2	Yersinia pestis	95
Q9P9Q9	Xylella fastidiosa	77
Q9PK73	Chlamydia muridarum	68
Q9Z9A7	Chlamydia pneumoniae	68

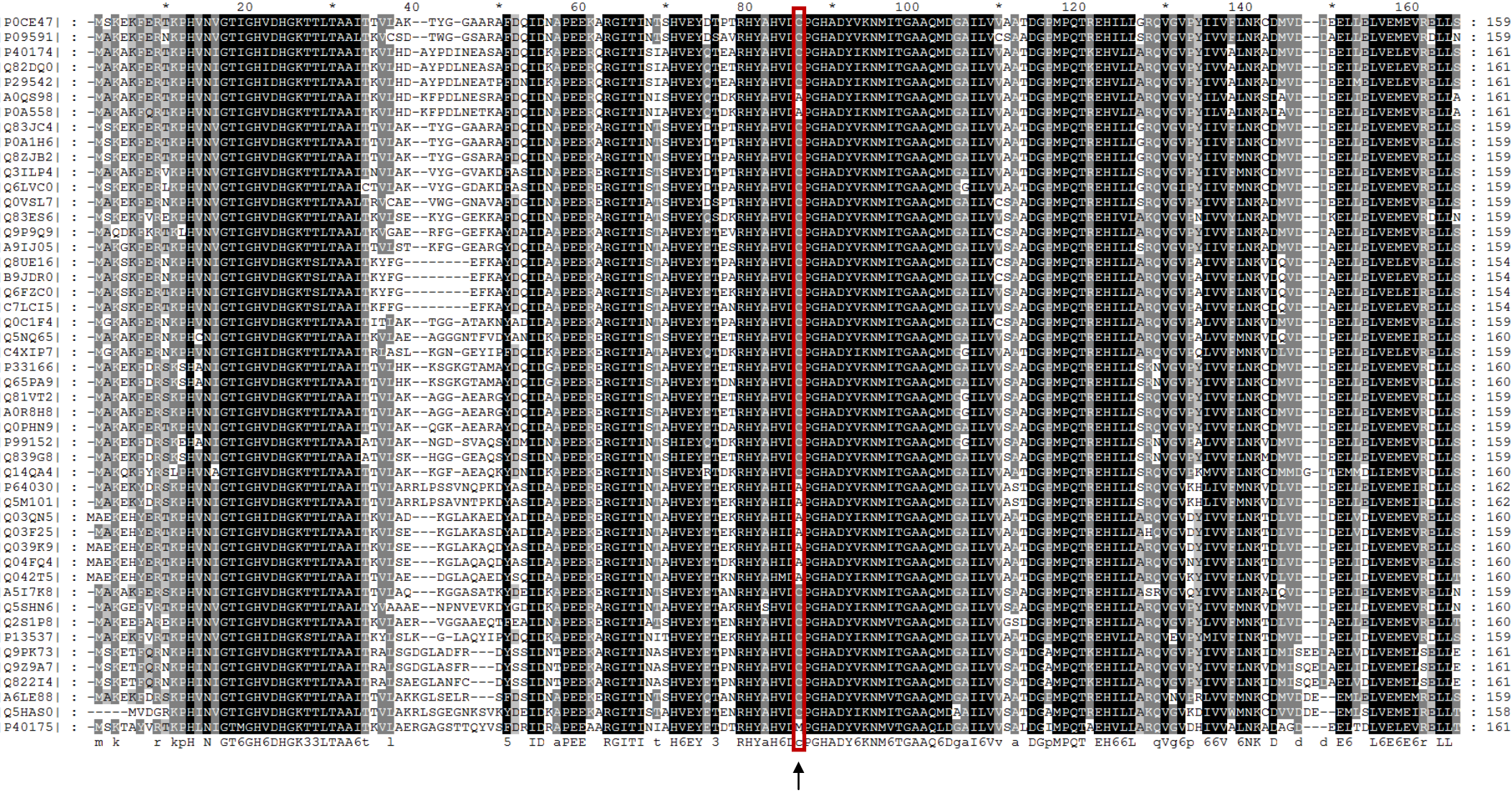

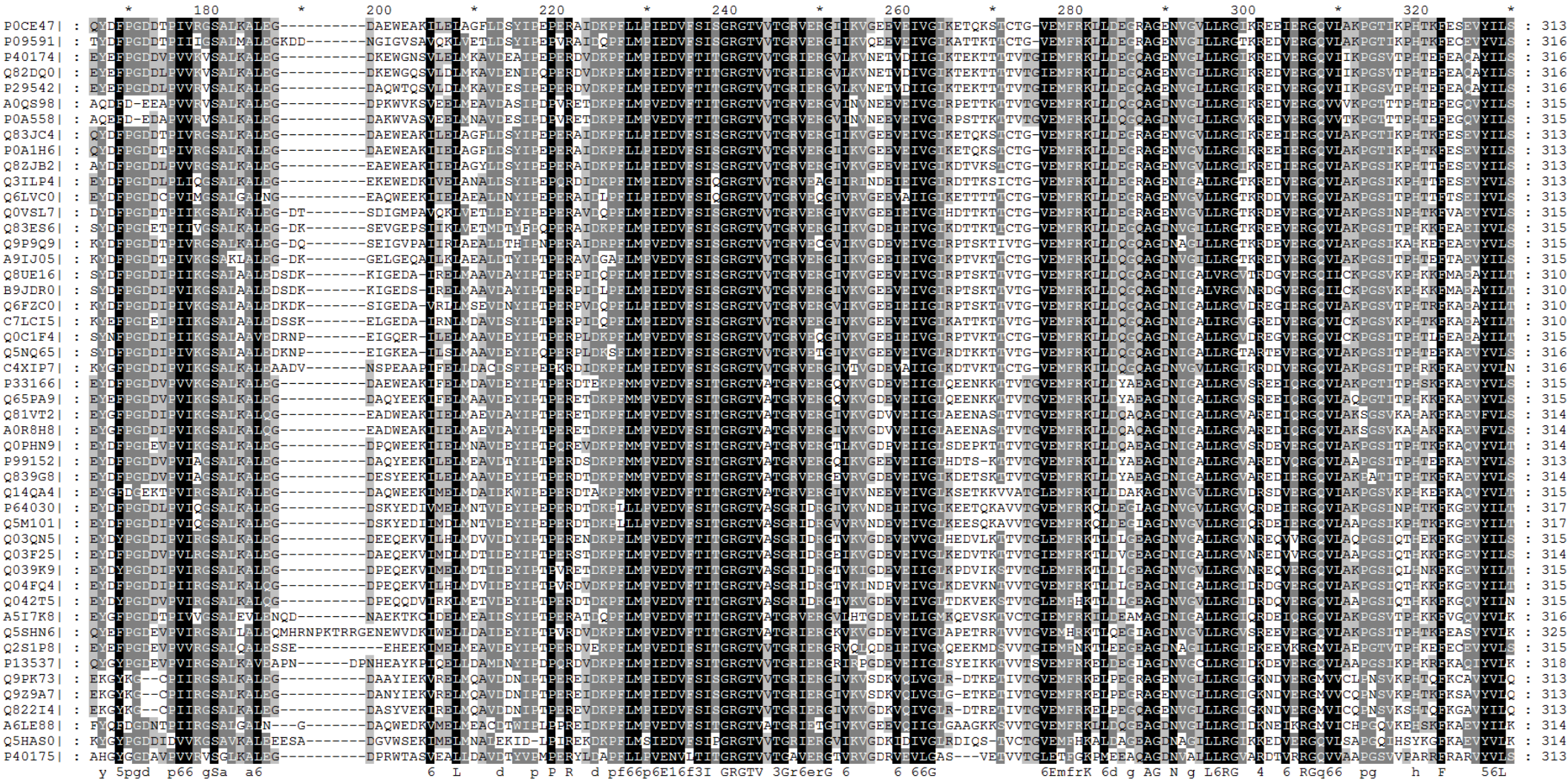

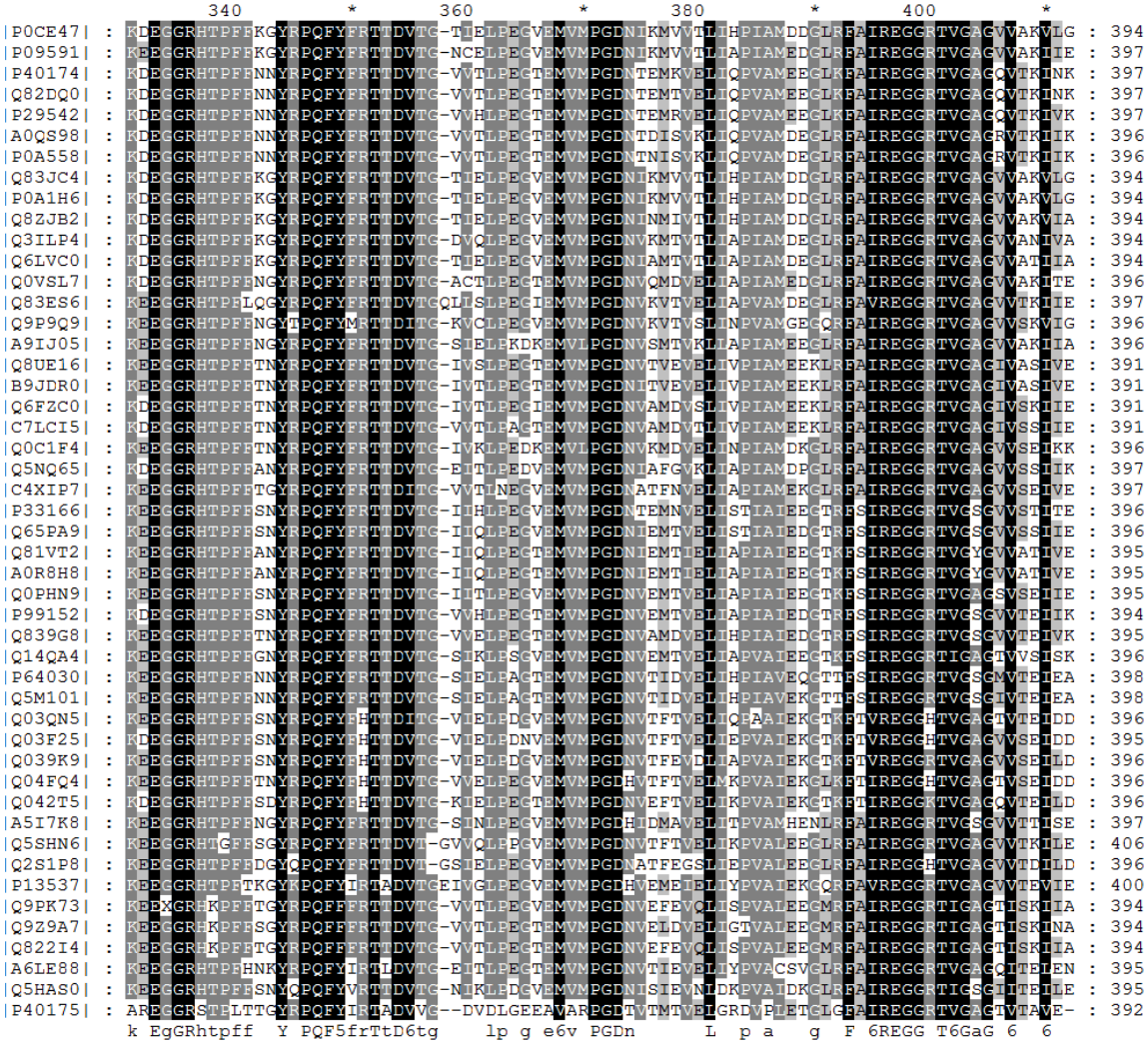

Figure A.9. Primary sequence alignment of EF-Tu within bacteria. Black shows 100% conservation, grey shows 80-100% conservation and white is less than 80% conervation. The conservation of Cys 81 from *E. coli* is highlighted in panel 1 by a box.

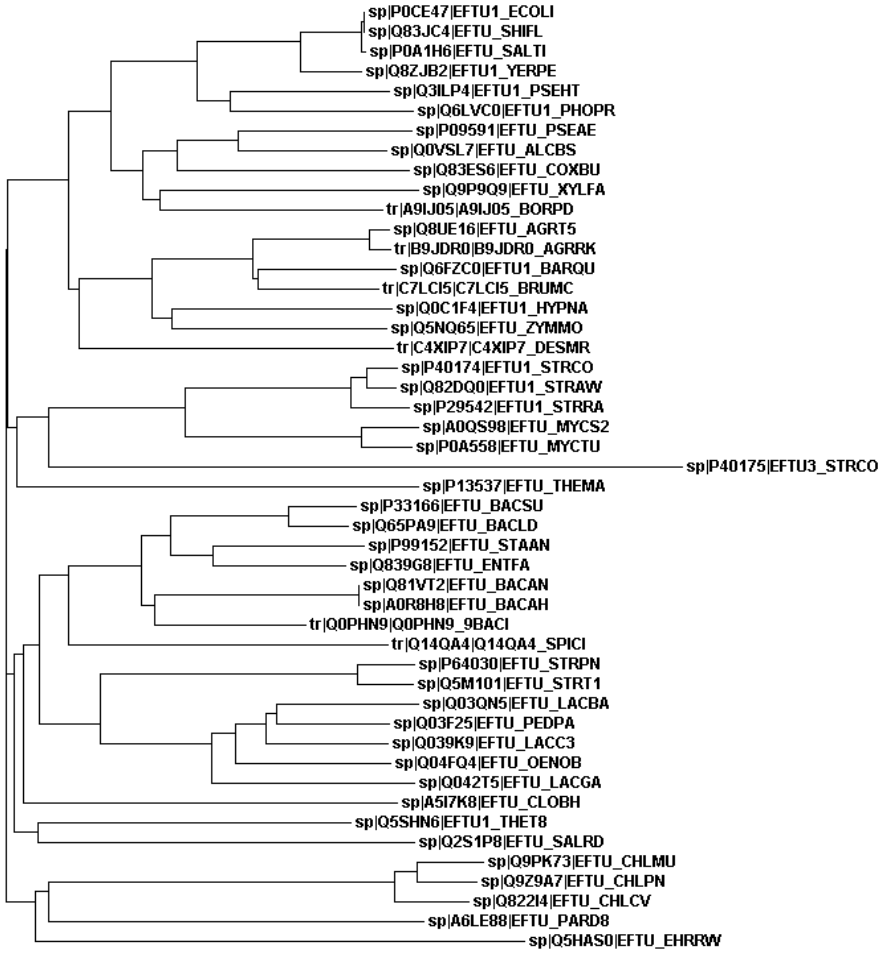

Figure A.10. Phylogenetic Tree of bacterial EF-Tu species aligned above. Phylogenetic tree generated by the ClustalW2 program using the EF-Tu bacterial sequences aligned above. The sequence accession code along with the abbreviated species name is shown.

A.3 Fluorescent labelling of EF-Tu

5-((((2-iodoacetyl)amino)ethyl)amino)naphthalene-1-sulfonic acid (1,5-IAEDANS (Invitrogen)), 7-diethylamino-3-(4-maleimidylphenyl)4-Methylcoumarin (CPM (Biotium)), Fluorescein-5-maleimide (F5M (Biotium)) or Rhodamine Red Maleimide (RRM (Invitrogen)) were used as thiol specific fluorescent dyes (Figure A.11).

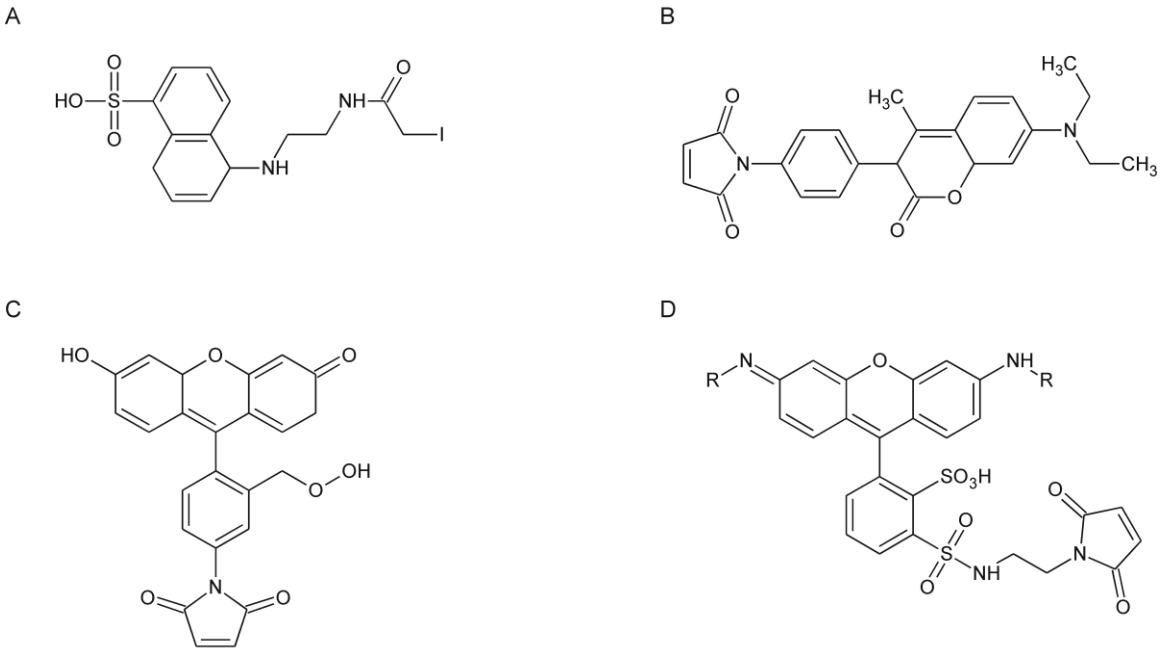

Figure A.11. Structures of thiol reactive fluorescent dyes. (A) 1,5-IAEDANS: Peak excitation 336 nm, peak emission 490 nm. (B) CPM: Peak excitation 384 nm, peak emission 470 nm. (C) F5M: Peak excitation 494 nm, peak emission 515 nm. (D) RRM: Peak excitation 560 nm, peak emission 580 nm. R represents $(CH_2CH_3)_2$.

A.3a Fluorescently Labelling EF-Tu Containing a Single Cysteine (L264C)

15 000 pmol of highly purified EF-Tu was diluted 5-fold in buffer A.1 (25 mM Tris-Cl pH 7.5 (4 °C), 7 mM $MgCl_2$, 30 mM KCl, 20% glycerol). A 20-fold molar excess of 1,5-IAEDANS , CPM or F5M was added to the solution and incubated at 4°C in the dark for 3 hrs with periodic mixing. After incubation, the solution was centrifuged at 13 000 x *g* for 5 min. Labelled protein was purified away from excess free dye using a

26 mL size exclusion column (Sephadex G25, GE Healthcare) (set to a 1 mL/min flow rate) equilibrated in buffer A.2 (25 mM Tris-Cl pH 7.5 (4 °C), 7 mM $MgCl_2$, 30 mM KCl). Fractions (500 μL) were collected and analyzed via 12% SDS-PAGE. Fractions containing EF-Tu were pooled and concentrated using ultrafiltration (MWCO 30 000 (Sartorious)). Aliquots were stored at -80°C. Efficiency of labelling EF-Tu using the above method is represented in Table A.5, where yields for each step were determined based on the amount of EF-Tu present as observed by SDS-PAGE and absorbance values at 280 nm. Quantification of the protein concentration was achieved using silver stained SDS-PAGE and analysis using Image J software.

Table A.5. Protein Yield Following Fluorescent Labelling of a Single Cysteine Containing EF-Tu.

Step	Protein Recovered with 1,5-IAEDANS	Protein Recovered with F5M	Protein Recovered with CPM
Post incubation with fluorescent dye	75%	75%	60%
Final Labelled Protein	30%	30%	30%

A.3b Intramolecular Hetero-Fluorescent Labelling of EF-Tu Containing Two Cysteine Residues

Purified EF-Tu (70 000 pmol) was diluted 5-fold in buffer A.1 supplemented with 20 μM GDP. A 20-fold molar excess of CPM was added dropwise and the reaction was quenched after 30-50 sec with 10 mM BME. The sample was centrifuged at 13 000 x *g* for 5 min. CPM labelled EF-Tu was separated from excess dye using SEC

chromatography (Sephadex G25 (GE Healthcare)) equilibrated in buffer A.1. Fractions (500 µL) were analyzed by 12% SDS-PAGE and those containing EF-Tu were pooled and incubated on a 5 mL activated thiol sepharose 4B resin (GE Healthcare) for 9 hrs. Any unbound protein was collected by centrifugation at 500 x *g* for 2 min. All following washes and elutions were collected in this manner. The thiol sepharose resin was washed with 20 mL of buffer A.1 until absorbance values after washes were close to zero at 280 nm (protein) and 384 nm (CPM). Protein covalently linked to the thiol sepharose resin was eluted with 5 mL of buffer A.3 (buffer A.1 supplemented with 100 mM DTT (Biobasic)). All washes and elutions were analyzed for EF-Tu content by 12% SDS-PAGE, and the elutions containing EF-Tu were pooled and concentrated using ultrafiltration as above. Excess DTT was removed using dialysis (10 000 MWCO tubing (Sigma-Aldrich)) against buffer A.1 so that DTT was diluted at least 500-fold. The sample was incubated with a 35-fold molar excess of F5M at 4°C with periodic mixing for 2 hrs. The sample was centrifuged at 13 000 x *g* for 5 min. Excess free dye was removed by SEC chromatography (Sephadex G25) equilibrated in buffer A.2 as described above. Fractions were analyzed by 12% SDS-PAGE and those containing EF-Tu were pooled and concentrated using ultrafiltration as above. Efficiency of labelling using the above method is represented in Table A.6 and was determined based on the amount of EF-Tu present as observed by SDS-PAGE and absorbance values at 280 nm as described above in section A.3a.

Table A.6. Protein Yield Following Intramolecular Double-Labelling an EF-Tu Containing Two Cysteine Residues.

Step	Overall Protein Recovered
Post CPM incubation	80-90%
Post affinity chromatography (thiol column)	40-50%
Removal of DTT by dialysis	20-30%
Post F5M incubation	15-20%
Final labelled proteins	10%

A.3c Intramolecular Hetero-Fluorescent Labelling of EF-Tu Containing Two Cysteine Residues using a "Shotgun" Method

Purified EF-Tu (100 000 pmol) was diluted 5-fold in buffer A.1 supplemented with 7 mM BME. Excess BME was diluted at least 1000-fold by dialyzing against buffer A.1 at 4°C overnight. The retained solution was centrifuged at 5000 x *g* for 2 min. 10-fold molar excess of dyes (F5M and RRM) was added simultaneously. The mixture was incubated at 4°C for 3 hrs with mixing. To separate excess free dye away from labelled EF-Tu the mixture was purified using SEC chromatography (Sephadex G25), equilibrated in buffer A.2, at 1 mL/min. Fractions (500 µL) were analyzed via absorbance at 280 nm (protein), 493 nm (F5M) and 560 nm (RRM) to determine which fractions contained all three components. The fractions containing both dyes and EF-Tu were pooled and concentrated before being flash frozen and stored at -80°C. Efficiency of labelling using the above method is represented in Table A.7 and was determined based on the amount of EF-Tu present as observed by absorbance measurements at 280 nm.

Table A.7. Protein Yield Following Intramolecular Double-Labelling an EF-Tu Containing Two Cysteine Residues via "Shotgun" Method.

Step	Overall Protein Recovered
Post Dialysis	40%
Post incubate with dyes	30%
Final labelled proteins	15%

A.3d Absorbance and Fluorescence Emission Analysis

Samples of identical concentration were prepared by dilution in buffer A.2.

Absorbance scans were performed on a UV/Visible Spectrophotometer (Varian Eclipse). Fluorescence emission scans were performed on a fluorescence spectrometer (PTI) set to 3 nm slit widths. EF-Tu fluorescently labelled with either 1,5-IAEDANS, CPM or F5M was examined by direct excitation of tryptophan at 280 nm (Figure A.12). EF-Tu labelled with two different fluorescent dyes (CPM and F5M or F5M and RRM) was analyzed by excitation of the tryptophan (280 nm) (Figure A.13a) or excitation of F5M (493 nm) (Figure A.13b).

Trypsin digestion of F5M and RRM labelled EF-Tu was performed to ensure fluorescence emission observed was indeed FRET and not direct excitation of the acceptor dye RRM. Trypsin (BioBasic) was added to a final concentration of 40 mg/mL to labelled EF-Tu and incubated for 1 hr. This was then analyzed and compared to labelled EF-Tu not treated with trypsin (Figure A.13b).

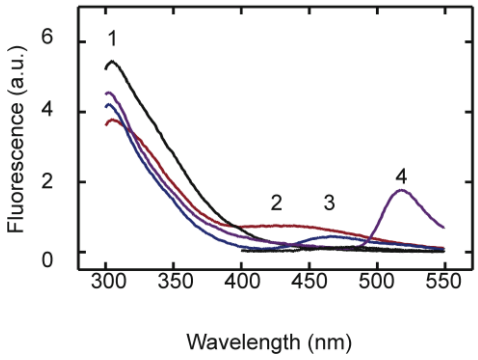

Figure A.12. Fluorescence emission scans of single labelled EF-Tu. Samples were excited at 280 nm and fluorescence emission was scanned from 300 – 550 nm. EF-Tu labelled with 1,5-IAEDANS (red), or CPM (blue), or F5M (purple) is shown. Fluorescence emission of (1) EF-Tu at 325 nm, (2) blue shifted fluorescence emission of 1,5-IAEDANS at 450 nm, (3) CPM at 470 nm and (4) F5M at 515 nm can be observed. Unlabelled EF-Tu is also shown in black with one emission peak at 325 nm.

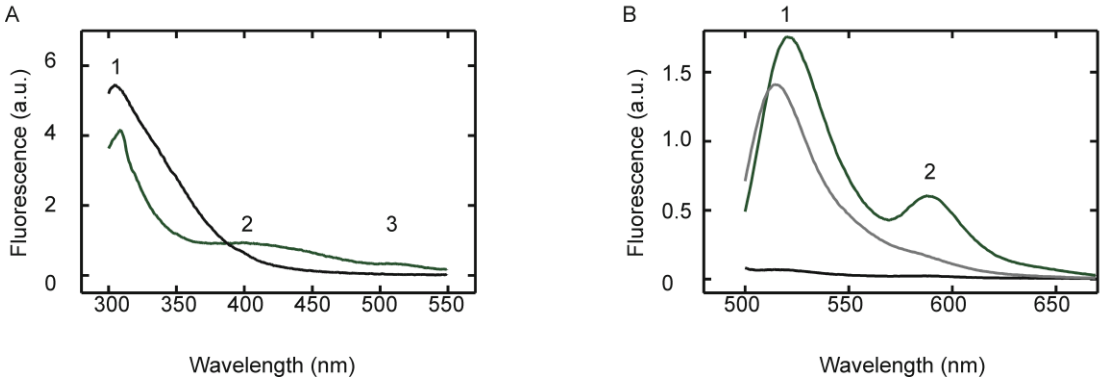

Figure A.13. Emission scans of EF-Tu fluorescently labelled with two different dyes. (A) Samples were excited at 280 nm and fluorescence emission was scanned from 300 – 550 nm. EF-Tu labelled with CPM and F5M (green) is shown. Fluorescence emission of (1) EF-Tu at 325 nm, (2) blue shifted fluorescence emission of CPM at 430 nm and (3) F5M at 515 nm can be observed. Unlabelled EF-Tu is also shown in black with one emission peak at 325 nm. (B) Samples were excited at 493 nm and fluorescence emission was scanned from 500 – 700 nm. EF-Tu labelled with F5M and RRM (green) is shown. Fluorescence emission of (1) red shifted F5M at 530 nm and (2) RRM at 580 nm can be observed. Unlabelled EF-Tu is also shown in black and trypsin digested fluorescently labelled EF-Tu is shown (grey) with one emission for F5M at 515 nm.

Fluorescence emission analyses of F5M-RRM labelled samples were analyzed on SDS-PAGE and imaged on a Typhoon 9400 Variable Mode Imager (GE). F5M was imaged using a blue 488 nm laser and RRM was imaged with a Green 532 nm laser (Figure A.14).

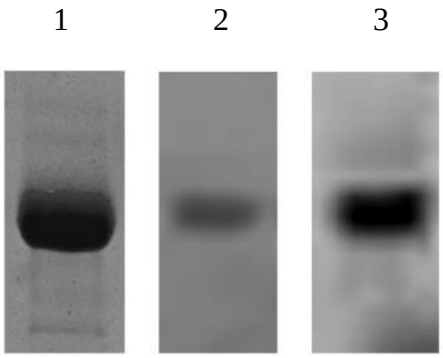

Figure A.14. EF-Tu labelled with F5M and RRM. Fluorescent imaging was performed on a Typhoon 9400 scanner to confirm labelling. (1) Protein was imaged using coomassie brilliant blue. (2) F5M was imaged using a blue 488 nm laser. (3) RRM was imaged using a green 532 nm laser.